INTRINSIC ANTIBIOTIC RESISTANCE IN GRAM-NEGATIVE BACTERIA

COMBATING INTRINSIC ANTIBIOTIC RESISTANCE IN GRAM-NEGATIVE BACTERIA

By

PATRICIA LYN TAYLOR, B.Sc.

A Thesis

Submitted to the School of Graduate Studies

in Partial Fulfillment of the Requirements

for the Degree

Doctor of Philosophy

McMaster University

DOCTOR OF PHILOSOPHY (2011) McMaster University

(Biochemistry and Biomedical Sciences) Hamilton, ON

TITLE:	Combating Intrinsic Antibiotic Resistance in Gram-Negative Bacteria
AUTHOR:	Patricia Lyn Taylor, B.Sc. (University of Guelph)
SUPERVISOR:	Dr. Gerard D. Wright
NUMBER OF PAGES:	x, 115

ABSTRACT

The current rise in multi-drug resistant Gram-negative bacterial infections is of particular concern. Gram-negative pathogens are difficult to treat due to their intrinsic resistome. The outer membrane (OM) of Gram-negative bacteria serves as a permeability barrier to many antibiotics, due in large part to the lipopolysaccharide (LPS) component that is unique to these organisms, and in addition to, the OM is lined with a number of multi-drug resistant efflux pumps. As the clinical effectiveness of first line therapies declines in the face of this resistance, novel strategies to discover new antibiotics are required. The identification of new antibiotic targets is one method currently being applied to meet this challenge. This work examines the permeability barrier of *Escherichia coli* as a possible target for antibiotic adjuvants. A structure-function analysis of GmhA and GmhB, which catalyze the first and third conserved steps in LPS ADP-heptose biosynthesis, was performed. The active site residues of each of these enzymes were identified via crystallographic, mutagenic, and kinetic analyses. Potential mechanisms have been proposed, offering insight into the function of these potential adjuvant targets. In addition, a whole screen of *E. coli* was performed to identify compounds that potentiate novobiocin, an antibiotic with limited activity against Gram-negative pathogens due to OM permeability. Four small molecules were found that were able to synergize with novobiocin. One of these, A22, is known to alter bacterial cell shape, suggesting a new pathway for antibiotic adjuvants to combat Gram-negative infection. Together, these studies highlight the varied targets available for novel therapeutic strategies.

ACKNOWLEDGMENTS

I would like to start off by thanking my supervisor, Dr. Gerard Wright, for giving me the opportunity to work in such a fantastic environment. I will always be grateful for his guidance and support throughout my time at McMaster. In the same vein, I would like to thank my committee members, Dr. Lori Burrows and Dr. Eric Brown, for many thought-provoking conversations and pushing me to be a better scientist. I would also like to acknowledge the personal funding support of Cystic Fibrosis Canada and the Canadian Institutes of Health Research.

Much of the work presented in this thesis results from the cumulative efforts of a lot of people. I am tremendously grateful for the efforts of all of my collaborators: Kim Blakely, Gladys De Leon, Dr. John Walker, Fiona McArthur, Elena Evidokimova, Kun Zhang, Seiji Suigiman-Marangos, and Dr. Miguel Valvano. These talented individuals worked tirelessly on the crystal structures of GmhA and GmhB, and the resulting manuscripts, work that is critical to the presentation of this thesis. In addition, I must acknowledge the received technical guidance I received from Raquel Epand, the late Dr. Don Hughes, and the staff of the high-throughput screening facility. Most especially, I would like to thank Dr. Murray Junop, who could never be classified as just collaborator, for his guidance and advice, and always treating me as an equal partner in our publishing efforts.

I could not have enjoyed my experience at McMaster without the camaraderie of the Wright lab. I am honoured to have worked with and learned from such a terrific group of scientists. Specifically, I would like to thank Dr. Kalinka Koteva, Linda Ejim, and Laura Rossi for years of guidance, both scientific and personal. My love and gratitude for the continued support of Dr. Tushar Shakya, my benchmate and partner, cannot be adequately expressed in this space.

Finally, I would like to thank my family for allowing me to achieve my goals and always supporting me no matter what: my sister, Kris, for providing much needed retail-therapy; my brother, Jordy, for always making me laugh; and my parents, Jim and Marilyn, whose unconditional love and constant faith convinced me that I can do anything. Thank-you.

TABLE OF CONTENTS

LIST OF FIGURES

PAGE

CHAPTER ONE

CHAPTER TWO

CHAPTER THREE

CHAPTER FOUR

LIST OF TABLES

LIST OF ABBREVIATIONS

ADP	adenosine diphoshate
ATP	adenosine triphosphate
DMSO	dimethyl sulfoxide
DTT	dithiohreitol
EDTA	ethylenediaminetetraactetic acid
ESBL	extended spectrum β-lactamase
FIC	fractional inhibitory concentraion
HAD	haloacid dehydrogenase
HBP	D-*glycero*-D-*manno*-heptose 1,7-bisphosphate
HEPES	4-(2-hydroxyethyl)-1-piperazineethanesulfonic acid
ICU	intensive care unit
IPTG	isopropyl β-D-1-thiogalactopyranoside
Kdo	2-keto-3-deoxy-D-*manno*-octulosonic acid
KPC	carbapenemase-producing *Klebsiella pneumoneae*
LB	Luria-Bertani
LPS	lipopolysaccharide
MDR	multi-drug resistant
MFP	membrane fusion protein
MIC	minimum inhibitory concentration
MRSA	methicillin-resistant *Staphylococcus aureus*
OM	outer membrane
OMF	outer membrane factor
OS	oligosaccharide
RND	resistance-nodulation division
S7P	sedoheptulose 7-phosphate
VRE	vancomycin-resistant *Enterococci*

CHAPTER ONE
INTRODUCTION

The Antibiotic Era

The discovery and development of antimicrobial agents is arguably one of the most important advances of the last century. Alexander Fleming is credited with the discovery of the β-lactam penicillin, the first natural product antibiotic, in 1928, though this drug was not available for use until 1944. In 1932, Gerhard Domagk synthesized an active sulphonamide that became available in 1938 (Bentley, 2009). Over the next fifty years, a number of new antibiotic classes, both synthetic and from natural sources, were discovered: aminoglycosides, aminocoumarins, glycopeptides, macrolides, fluoroquinolones, rifamycins, and tetracyclines, amongst others.

The introduction of antibiotics reduced the severity of many bacterial infections from mortal wound to minor nuisance almost instantly. The success of antibiotic therapy has not only curbed the spread of diseases such as tuberculosis, syphilis, and bacterial pneumonia, it has also led to major advances in surgery and medicine that would not have been possible under constant threat of infection. The impacts of this discovery are vast, and often taken for granted. Unfortunately, like many things that seem too-good-to-be true, it was soon realized that antibiotic discovery came with a caveat: bacteria have evolved resistance mechanisms that can render even the most powerful antibiotic useless.

Almost as soon as penicillin was discovered, resistant bacteria were isolated. As early as the 1940s, it was observed that not only could bacteria be simultaneously resistant to multiple classes of antibiotics, but resistance was transferable to sensitive strains (Davies, 2007). The result is selection of a growing population of bacteria that are now resistant to most of the commonly used drugs. To make matters worse, the rate of discovery of new antibiotics has rapidly declined over the past 30 years, offering little support to the diminishing usefulness of current first-line therapies. It is difficult to believe that less than 100 years after the discovery of antibiotics, the human race is facing the possibility of a return to the pre-antibiotic era. Novel strategies to combat multidrug resistant (MDR) bacteria are needed in order to overcome this threat for the next century and beyond .

The Gram-negative problem

There are four main categories of antibiotic resistance (Figure 1-1): 1) alteration of the antibiotic via modifying enzymes to abolish activity; 2) modification of the antibiotic target, via modified biosynthesis or mutation, to prevent drug binding; 3) active efflux of the antibiotic using membrane spanning pumps; and 4) physical barriers to entry into the cell due to specialized membranes, capsules, and biofilms. The former two mechanisms can be found in most resistant bacteria and represent resistance that can be acquired over time in response to environmental exposure (Alekshun and Levy, 2007). The latter two mechanisms are most often associated with Gram-negative bacteria, and demonstrate the intrinsic resistance these bacteria have to a number of antibiotics (Zgurskaya and Nikaido, 2000) (Cos et al., 2010) (Delcour, 2009).

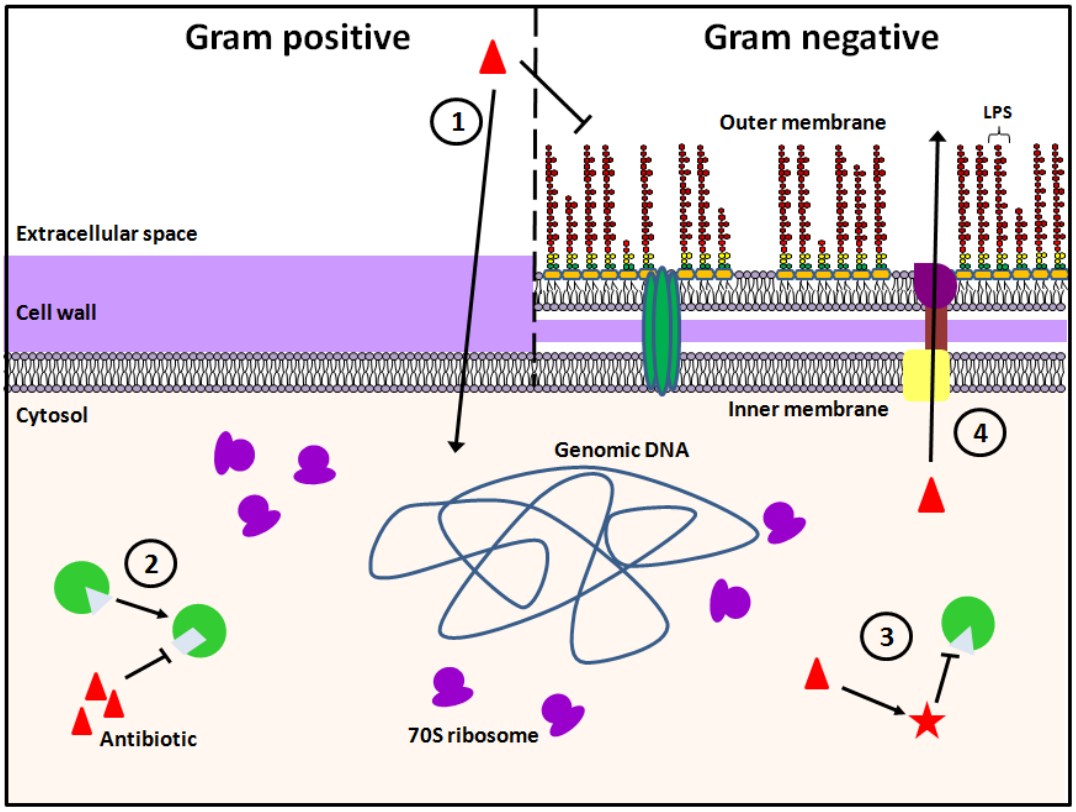

Figure 1-1 General antibiotic resistance profile of Gram-positive and Gram-negative bacteria. 1 – The outer membrane of Gram-negative bacteria creates a permeability barrier, excluding entry to some antibiotics; 2 – Target modification prevents antibiotic binding and activity; 3- Antibiotic modification reduces or eliminates affinity for the target; 4 – Efflux pumps actively remove antibiotics from the cell.

The emergence of methicillin-resistant *Staphylococcus aureus* (MRSA) and vancomycin-resistant *enterococci* (VRE), both clinically and community acquired, has stimulated a great deal of antimicrobial research toward the treatment of infections caused by these Gram-positive pathogens. In both cases, resistance is acquired via alteration of the antibiotic target (de Lencastre et al., 2007) (Courvalin, 2006). However, novel therapeutics to combat these bacteria will not necessarily be broad spectrum in application. Drug therapies for Gram-negative pathogens must be designed to combat the intrinsic resistance as well as the acquired resistance. Figure 1-2 depicts the fraction of commonly used antibiotic classes that are available for use against Gram-negative bacteria.

The emerging threat of MDR Gram-negative bacteria rivals that of MRSA and VRE. Indeed, the Infectious Diseases Society of America classifies three Gram-negative species, extended spectrum β-lactamase(ESBL)-producing Enterobacteriaceae, *Acinetobacter baumannii,* and *Pseudomonas aeruginosa*, among its top six priorities. Indeed, the Infectious Diseases Society of America classifies three Gram-negative species, extended spectrum β-lactamase(ESBL)-producing Enterobacteriaceae, *Acinetobacter baumannii,* and *Pseudomonas aeruginosa*, amoung its top six priority pathogens (the others being MRSA, VRE, and *Aspergillus* sp.) (Lee et al., 2009). ESBL-producing Enterobacteriaceae carry β-lactamases that are able to hydrolyze multiple classes of β-lactams, including penicillins, cephalosporins, and monobactams. As such, the first line treatment for these infections is now carbapenems or fluoroquinolones. With such limited treatment options, development of resistance to either or both of these classes of antibiotics will render ESBL-producing Enterobacteriaceae infections untreatable. Carbapenemase-producing Enterobacteriaceae (Gupta et al., 2011), which includes carbapenemase-producing *Klebsiella pneumonia* (KPC) (Walsh, 2010), has already been found in the clinics, further highlighting this need for new treatment options against these organisms. Most recently, New Delhi metallo-β-lactamase 1 (NDM-1)-producing Enterobacteriaceae has been identified in India and the United Kingdom, with the potential to spread globally (Kumarasamy et al., 2010). These organisms were shown to be resistant to all antibiotics, excepting colistin and tigecycline. Hospitalized patients, especially those in intensive care units (ICUs) are most at risk for contracting these infections, most commonly in the urinary or gastrointestinal tract, but also as bloodstream infections or pneumonia (Kunz and Brook, 2010). Such infections often increase mortality and delay recovery for these patients.

P. aeruginosa is one of the most difficult to treat Gram-negative bacteria due to its outer membrane and effective system of efflux pumps (Ho et al., 2010). This pathogen plagues immune-compromised individuals including burn victims and cancer patients, and it is the number one cause of death in cystic fibrosis patients. MDR *P. aeruginosa* infections are resistant to three or more antibiotics from a list so varied as to include almost all known treatment options: penicillins, cephalosporins, aminoglycosides, fluoroquinolones, and carbapenems (Kunz and Brook, 2010). Some pan-resistant strains are not susceptible to anything but polymyxins. The ability of this organism to form

biofilms allows it to exist on surfaces and resist cursory sanitization efforts, increasing the likelihood of spread between patients.

A. baumannii are environmental organisms that are now a clinical concern due to MDR capacities. Resistance to β-lactams, carapenems, and fluoroquinolones, represent the worst threat from these organisms (Kunz and Brook, 2010). Recent outbreaks of MDR-*A. baumannii* in American overseas military hospitals has contributed to the spread of these infections, where injured soldiers are infected in the field or in field hospitals and carry the pathogen to base and non-military hospitals (Petersen et al., 2011). With resistance seen to virtually all available antibiotics, it is clear that MDR Gram-negative bacterial infections require new treatment options, such as polymyxins, cationic peptides and inhibitors of LPS biosynthesis.

Gram-negative and Gram-positive bacteria differ substantially in cell envelope composition. Gram-positive bacteria are protected by a phospholipid membrane surrounded by a thick (40-200 nm) multilayered peptidoglycan component with covalently bound polysaccharides. Though the peptidoglycan layer is believed to maintain the integrity of the cell and act as a barrier to environmental influences, it provides little barrier to diffusion (Yethon and Whitfield, 2001) (Schaffer and Messner, 2005). Conversely, Gram-negative pathogens are notorious for being resistant to hydrophobic antibiotics, such as rifampin, erythromycin, and novobiocin, due to a low permeable outer membrane (OM), which surrounds an inner phospholipid membrane and a thin (~8 nm thick) peptidoglycan layer (Ruiz et al., 2006) (Savage, 2001) (Hancock, 1984) (Nikaido, 2003) .

The OM contains a phospholipid inner leaflet and a lipopolysaccharide (LPS) outer leaflet. LPS is comprised of three components: lipid A, a conserved core polysaccharide (3-deoxy-D-*manno*-oct-2-ulosonic acid (Kdo) and one or more heptose residues), and a polysaccharide comprised of a variety of sugars (Figure 1-3) (Raetz and Whitfield, 2002; Vaara, 1992) (Hancock, 1984; Yethon and Whitfield, 2001). The permeability barrier of the OM is believed to be greatly influenced by the structure of LPS. Both lipid A and heptose molecules are phosphorylated, imparting an overall negative charge that is neutralized through intra-strand binding of divalent cations, such as Ca^{2+} and Mg^{2+}. This results in a tightly packed, cross-linked network of LPS units that resist hydrophobic antibiotics reflected in the asymmetry of drug susceptibility shown in Figure 1-2 (Yethon and Whitfield, 2001) (Hancock, 1984).

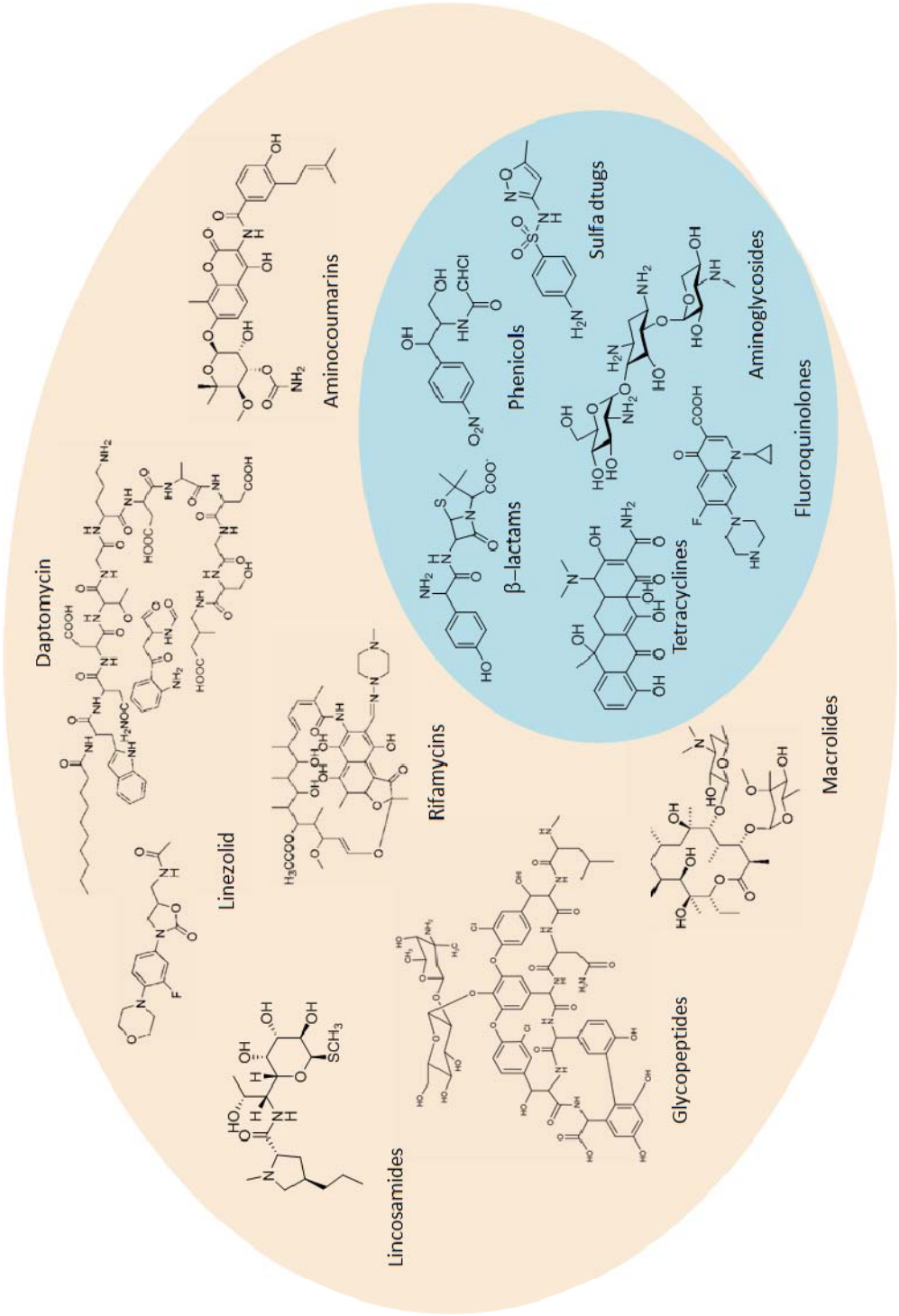

Figure 1-2 The treatment limitations of Gram-negative bacteria. All antibiotic classes depicted (pink) have demonstrated use in Gram-positive bacteria, while only a fraction of these (blue) are useful in treating Gram-negative infections.

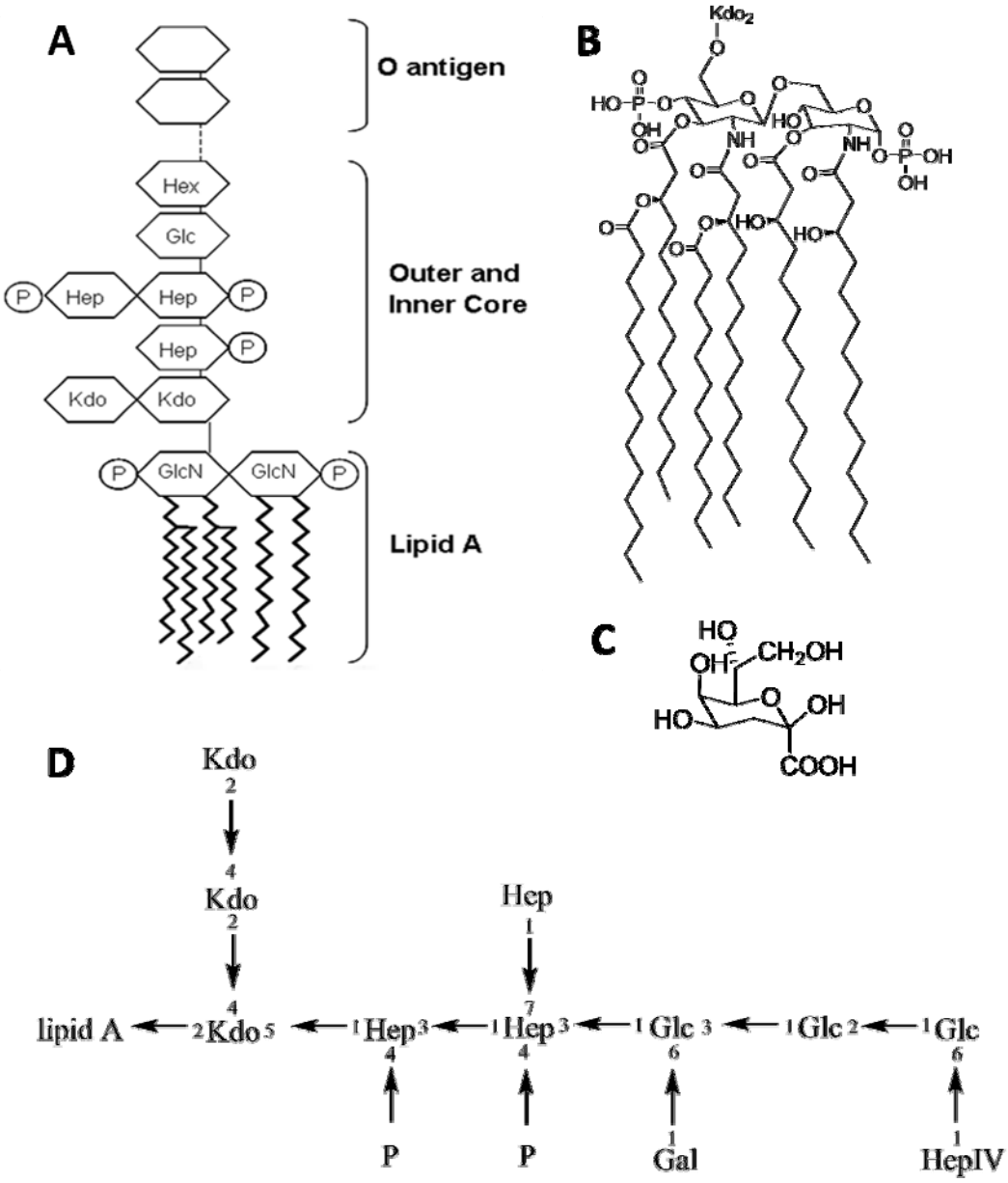

Figure 1-3 LPS structure. (A) Schematic representation of general LPS structure. Number of heptose, glucose and hexose residues varies by organism, as does the number and type of O antigen oligosaccharide repeats. (B) *E. coli* Lipid A structure. (C) Kdo structure. (D) Specific composition of *E. coli* K-12 LPS. GlcN – glucosamine; P – phosphate; Kdo - 3-deoxy-D-*manno*-oct-2-ulosonic acid; Hep - L-*glycero*-D-*manno*-heptose; Glc – glucose; Hex - hexose. Adapted from (Raetz and Whitfield, 2002).

Outer membrane permeabilization

Strategies that permeabilize the OM should increase the arsenal of antibiotics available to treat Gram-negative infections by enabling access to drugs that are currently limited to Gram-positive treatment, such as vancomycin, erythromycin, and rifampicin. These antibiotics, when used in synergy with OM permeabilizers, would find new efficacy against Gram-negatives in such a strategy. In addition, since these pathogens have largely escaped exposure to such antibiotics in the past, resistance mechanisms might be expected to be more limited than those seen in Gram-positive bacteria. Indeed several compounds have already been identified as OM permeability agents with demonstrated clinical efficacy as described below.

Polymyxins. Polymyxins are cyclic cationic lipopeptides that were discovered over 50 years ago and have shown antimicrobial activity both alone and in synergy with hydrophobic antibiotics (Vaara, 1992) (Savage, 2001). In particular, polymyxin B nonapeptide (PMBN) and colistin (polymyxin E) have seen clinical use. Polymyxins function by binding to the OM by an unknown mechanism, resulting in permeabilization. In addition to granting access to antibiotics, the binding of polymyxins also allows cellular components to diffuse out, resulting in cell death (Yuan and Tam, 2008) (Zavascki et al., 2007). Due to potential toxicity compared to other antibiotics, polymyxin use was discontinued in the 1970s. However, as MDR bacteria have emerged, polymyxins have been reintroduced into the clinical setting, and were found to be effective treatment for MDR *P. aeruginosa, A. baumannii*, and more recently, *K. pneumoniae,* as a "salvage" therapy (Lim et al., 2010) (Molina et al., 2009) (Tsubery et al., 2005). The reemergence of polymyxins in antimicrobial therapy has led to increased study on their pharmacodynamic and toxicity properties. Not surprisingly, the increased frequency of use of polymyxins as a last resort against MDR pathogens has led to the emergence of resistance apparently from an altered LPS, which reduces the binding efficiency of polymyxins (Cunha, 2006) (Falagas et al., 2006) (Falagas et al., 2005). The rapid emergence of such resistance highlights the need for new compounds to permeabilize the membrane, rather than relying entirely on old discoveries.

Cationic peptides. Other cationic peptides, including defensins, magainins, and bacteriocidal/permeability-increasing protein (BPI), function similarly to polymyxins in that they bind LPS resulting in permeabilization. The overall positive charge of the peptide allows it to displace the divalent cations cross-linking the LPS, while the size of the peptide induces permeabilization (Hancock, 1984) (Hancock and Sahl, 2006). Problems with cationic peptides include the potential for toxicity and susceptibility to proteases (Hancock and Sahl, 2006) (Papo and Shai, 2005). "Designer peptides," where peptides components are chosen specifically for the ability to resist protease action or less toxic attribute, are currently being explored as an option to alleviate these issues (Sitaram and Nagaraj, 2002). While drug potential is still under review for this class of compound, cationic peptides represent an exciting new class of antimicrobial agents.

LPS targets. Recent advances in determining the structure and biosynthesis of LPS molecules have led researchers to pursue LPS, specifically lipid A and ADP-heptose biosynthetic enzymes, as potential drug targets. The lipid A molecule consists of two β,1'-6 linked glucosamine residues, phosphorylated at the 1 and 4' positions. In *E. coli,* this disaccharide is acylated at the 2, 3, 2' and 3' positions with 3-hydroxymyristate. Following linkage to two Kdo molecules at the 6' position, laurate and myristate are added to complete the LPS-Kdo compound essential for *E. coli* survival under standard conditions (Yethon and Whitfield, 2001). It is important to note that structure of LPS varies between species, and even within a species. In *E. coli* K-12, the organism used throughout this work, two more Kdo residues are then added to core lipidA-Kdo molecule, at the 4 and subsequent 2 positions, respectively, followed by three heptose residues, linked sequentially 1,5-, 1,3-, and 1,7- respectively (residues 1 and 2 are also phosphorylated at the 4 position) to form the inner core. The outer core is then comprised of three sequentially linked glucose residues (1,3-, 1,3-, and 1,2-), with a 1,6- linked galactose on glucose 1 and a 1,6- linked heptose on glucose 3. K-12 is lacking an O-antigen, which would otherwise follow to complete the LPS molecule (Raetz and Whitfield, 2002).

The presence of lipid A in the outer membrane is necessary for survival and the biosynthetic pathway of lipid A is well characterized (Yethon and Whitfield, 2001) (Raetz and Whitfield, 2002). Lipid A biosynthetic enzymes make ideal drug targets as they are both essential and absent from eukaryotic cells. For example, CHIR-90 is an inhibitor of LpxC, a zinc-dependent amidase that catalyzes the first conserved step in lipid A biosynthesis. This compound has shown antimicrobial activity against both *P. aeruginosa* and *E. coli.* (Barb et al., 2007) (McClerren et al., 2005) (Mdluli et al., 2006). Several other, essential enzymes in the lipid A biosynthesis pathway remain unexplored targets for novel antimicrobials.

A second, unexploited target within LPS is heptose biosynthesis. The biosynthetic pathway of ADP-heptose, the precursor to the LPS heptose molecule, has been elucidated and involves five steps performed by four enzymes: GmhA, HldE, GmhB, HldD (Figure 1-4) (Valvano et al., 2002) (Kneidinger et al., 2002). Unlike lipid A, LPS heptoses are apparently not essential for the survival of many bacterial species, for instance, among Enterobacteriacea organisms. It has been shown however, that a truncated LPS deficient in heptose molecules, results in increased permeability toward hydrophobic antibiotics (Yethon and Whitfield, 2001) (Valvano et al., 2002) (Loutet et al., 2006). Thus compounds that inhibit the function of any of the four pathway enzymes could be used to potentiate hydrophobic antibiotics. An *in vitro* screen of the ADP-heptose pathway successfully identified *in vitro* inhibitors of this pathway (De Leon et al., 2006). Several recent studies have contributed to the mechanistic knowledge of these enzymes, including those discussed in this thesis; however, further screening on both the lipid A and ADP-heptose biosynthetic pathways has the potential to deliver novel antibiotics and membrane permeabilizers.

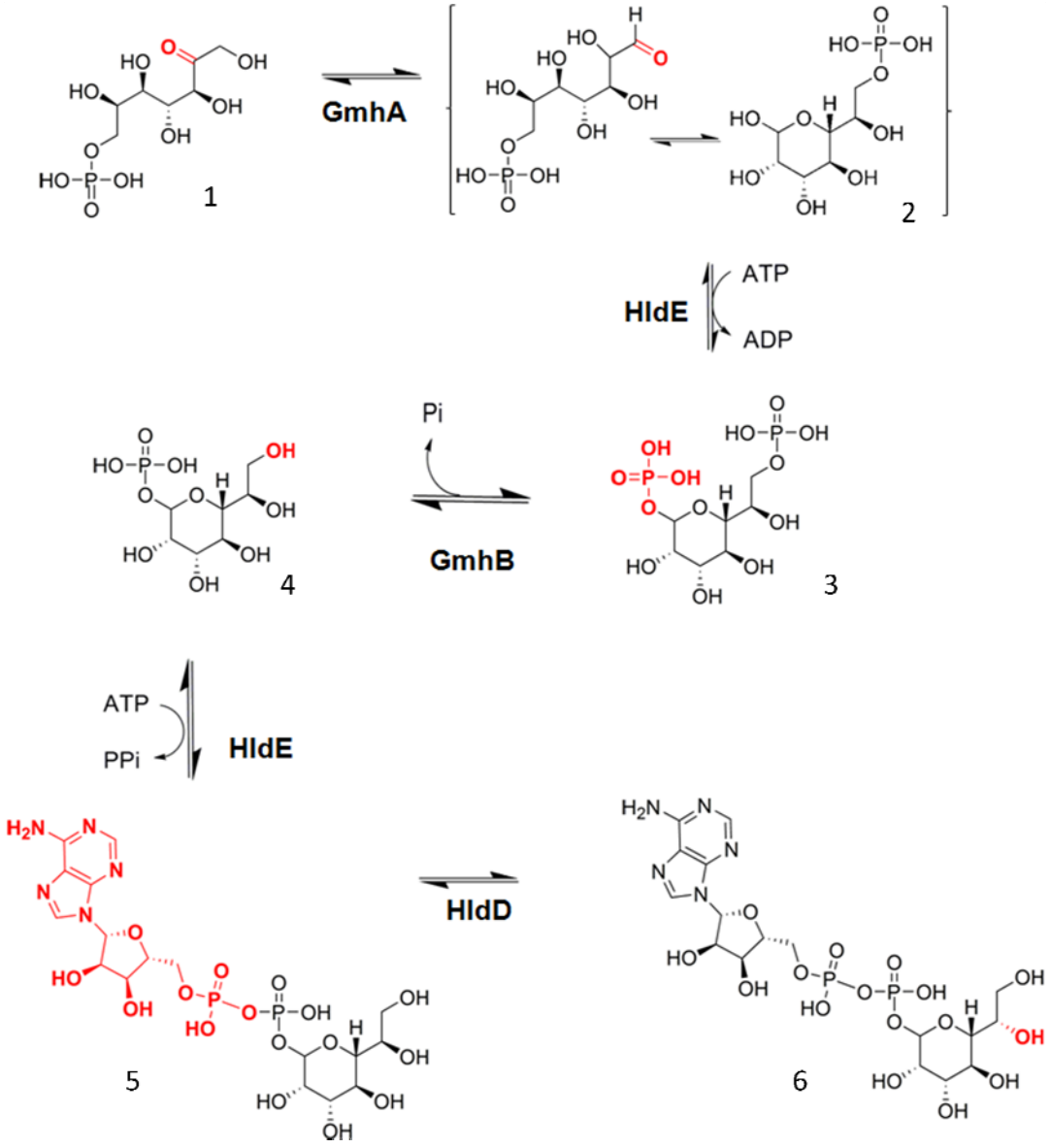

Figure 1-4 The biosynthetic pathway of ADP-heptose in *E. coli*. 1– sedoheptulose 7-phosphate; 2 - D-*glycero*-D-*manno*-heptose 7-phosphate; 3 - D-*glycero*-D-*manno*-heptose 1,7-bisphosphate; 4 - D-*glycero*-D-*manno*-heptose 1-phosphate; 5 - ADP-D-*glycero*-D-*manno*-heptose; 6 - ADP-L-*glycero*-D-*manno*-heptose.

Efflux pump inhibitors

Efflux proteins span the bacterial membrane and actively transport toxins, including antibiotics, from the cell. There are five families of efflux proteins related to MDR: the ATP binding cassette superfamily (ABC), the major facilitator superfamily (MFS), the multidrug and toxic-compound extrusion family (MATE), the small multidrug resistance family (SMR), and the resistance-nodulation-division family (RND) (Pages et al., 2005; Piddock, 2006; Taylor and Wright, 2008). The RND family of pumps is responsible for most Gram-negative pump-associated bacterial resistance (Marquez, 2005). *P. aeruginosa* has six known active RND pumps: five of these are regulated in response to specific antibiotics, while the sixth (MexAB-OprM) is contitutively expressed. The MexAB-OprM pump is of particular concern as it contributed to resistance against β-lactams and fluoroquinolones (Rice, 2006). The major RND pump in *E. coli* is ArcAB-TolC. This pump has broad transport specificity, resulting in intrinsic resistance to macrolides, β-lactams, fluoroquinolones, and tetracyclines(Piddock, 2006). Due to the cross species contribution to antibiotic resistance, efflux pumps are an obvious target for novel antibacterial agents.

The RND tripartite pump system is generically comprised of three distinct components: the RND transporter that spans the inner membrane, a membrane-fusion protein (MFP) that crosses the periplasm, and an outer membrane protein factor (OMF) that connects the MFP to the extracellular space (Poole, 2004). Three monomers comprised of twelve individual helices that fold together to form the pore of the RND transporter. Alternate conformations of these monomers create the pump action of this unit. Efflux is driven by proton motive force across three charged conserved residues (two aspartic acids and a lysine) (Blair and Piddock, 2009). The MFP is comprised of three domains: a 6-strand β-barrel, a central lipoyl domain, and an α-helical hairpin. Meanwhile, the OMF have similar, but unconserved, structures comprised of a β-barrel that forms a pore in the OM, and an α-helical tunnel that extends into the periplasm. Studies suggest the MFP and OMF interact via the periplasmic domain of the MFP (Misra and Bavro, 2009).

Several options exist to disrupt RND efflux pump activity: blocking the OMF or MFP protein channel, inhibiting the inner-membrane pump, eliminating the energy source driving pump action, or altering pump conformation (Pages et al., 2005). Recent efforts have led to the discovery of varied efflux pump inhibitors (EPI). For example, tetracycline derivatives are able to effectively inhibit the TetB efflux pump and L-Phe-L-Arg-β-naphthalamide (PAβN) has been shown to potentiate fluoroquinolones in *P. aeruginosa* and *E. coli.* Similarly, arylpiperazines can potentiate antibiotics in *E. coli* (Piddock, 2006) (Marquez, 2005) (Mahamoud et al., 2007). Natural product screening initiatives have also identified extracts from *Streptomyce*s that are able to inhibit MexAB-OprM in *P. aeruginosa* (Stavri et al., 2007).

There are a number of challenges associated with EPIs (Lomovskaya and Bostian, 2006). Given the substrate specificity of the majority of pumps (previous examples excluded), most inhibitors are likely to have limited range. Additionally, while EPIs would be effective in combination with the pump-associated antibiotic, these compounds are unlikely to have independent antimicrobial action.

Unpredicted targets

Less obvious unique targets may also exist to be exploited. A recent study by Liu *et al.* screened a collection of 4 000 non-essential gene deletions in *E. coli* to examine the sensitivity of these strains to 22 different antibiotics, including a number with limited efficacy in Gram-negative organisms (Liu et al., 2010). Many of the mutants showed increased susceptibility to more than one antibiotic. Individual genes from pathways involved in all major cellular functions, including transport, cell wall synthesis, protein synthesis, central metabolism, and proteins of unknown function, were implicated. This study serves as a guide to the possible targets available to potentiators and highlights the interconnectedness of all cellular pathways in maintaining the integrity of the cell.

A similar study by Alvarez-Ortega *et al.* screened a *P. aeruginosa* deletion library to identify mutants with increased sensitivity to three different β-lactams: ceftazidime, imipenem, and meropenem (Alvarez-Ortega et al., 2010). Again, different genetic profiles were observed for each of the antibiotics tested, suggesting the specificity each antibiotic has in its interactions with the cell. Together, the results of these two studies confirm that the number of potential targets for antibiotic adjuvants is only limited by the number of genes encoded by each organism.

Novel approaches to antibiotic discovery

There are two approaches to the discovery of new antibacterial therapies. A reverse chemical-genetics approach focuses on a specific target, such as a single enzyme, and looks for compounds that inhibit this target. The challenge with this method is that a fantastic inhibitor in an *in vitro* system does not necessarily translate into *in vivo* activity. The alternative would be a forward chemical-genetics approach, where compounds are applied to the whole cell of interest and hits are defined by a desired phenotype, such as decreased growth. The benefit of this approach is that bioactivity of a compound is determined immediately. The drawback is that the cellular target, or possibly targets, is unknown and must be elucidated.

Recent studies have shown that whole-cell screens can successfully identify combination therapies. One study screened a collection of previously approved drugs to identify compounds that improve minocycline activity in *P. aeruginosa*. Surprisingly, loperamide, an antidiarrheal drug, was found to improve minocycline activity by facilitating uptake (Ejim et al., 2011). Another synergy-based whole-cell screen demonstrated that the natural product cyslabdan increases the potency of imipenem

against MRSA (Fukumoto et al., 2008b) (Fukumoto et al., 2008a). Finally, erythromycin, an antibiotic with limited Gram-negative activity, has been shown to synergize with ceragenin, a synthetic cholic acid derivative able to permeabilize the OM (Saha et al., 2008).

A number of combination therapies have set a precedent for efficacy against bacterial infections. Arguably, the most famous synergistic therapy is Augmentin®, which combines amoxicillin, a semisynthetic β-lactam, with clavulanic acid, a weak β-lactam that is able to bind and inhibit β-lactamases (Ball, 2007; White et al., 2004). As individual drugs, amoxicillin is susceptible to inactivation and clavulanic acid has no clinically relevant antibacterial action, but together, this combination provides a potent, broad-spectrum treatment option. Unfortunately, even Augmentin® is susceptible to resistance, as documented by the isolation of resistant clinical strains (Oteo et al., 2008).

For the past 30 years, the combination of trimethoprim and sulfamethoxazole has seen clinical success. Both drugs act via different mechanisms to inhibit folate synthesis in bacteria. Sulfamethoxazome, a sulfonamide drug, inhibits the production of the precursor dihydrofolic acid, while trimethoprim inhibits the conversion of dihydrofolic acid into tetrahydrofolic acid (Masters et al., 2003). This combination remains clinically relevant, especially as new resistance patterns against other antibiotics continue to emerge.

There is little doubt that the discovery of novel antimicrobial therapies will be followed just as rapidly by the emergence of corresponding resistance mechanisms. One way to circumvent this cycle is to change the way antibiotics are applied. Combination therapies that remove intrinsic resistance barriers are one step toward combating Gram-negative bacterial infection.

Objectives

The objective of the research in this thesis was to probe the OM of Gram-negative bacteria for novel targets in combating antibiotic resistance. Structural differences in the composition of the cellular envelope exist between Gram-negative and Gram-positive organisms, resulting in the development and use of antimicrobial agents to treat respective infections. As a result, Gram-negative pathogens may have less exposure to Gram-positive specific antimicrobials, and theoretically, are less likely to have acquired resistance mechanisms. Based on this theory, my hypothesis is that compounds that permeate the outer membrane of Gram-negative organisms, granting access to Gram-positive specific antimicrobials, would increase the arsenal of treatments available to fight Gram-negative infection. The specific aims of this research were two-fold. First, a target specific approach was applied. The lipopolysaccharide component of the outer membrane, specifically the heptose biosynthesis pathway, has been identified as a potential target for permeabilization. Two of the proteins in this pathway, GmhA and GmhB, were selected for characterization, to gain a better understanding of the function

of these potential novel targets. The kinetic characterization of GmhA and GmhB are described here. Second, a forward chemical genetic approach was applied in the development of a small molecule and phenotype-based screen to identify compounds that synergize *E. coli* to hydrophobic antibiotics, such as novobiocin. Such a screen would highlight new targets involved in maintaining the outer membrane permeability barrier and identify small molecules with promising clinical value.

REFERENCES

Alekshun, M.N., and Levy, S.B. (2007). Molecular mechanisms of antibacterial multidrug resistance. Cell *128*, 1037-1050.

Alvarez-Ortega, C., Wiegand, I., Olivares, J., Hancock, R.E., and Martinez, J.L. (2010). Genetic determinants involved in the susceptibility of *Pseudomonas aeruginosa* to beta-lactam antibiotics. Antimicrob Agents Chemother *54*, 4159-4167.

Ball, P. (2007). Conclusions: the future of antimicrobial therapy - Augmentin and beyond. Int J Antimicrob Agents *30 Suppl 2*, S139-141.

Barb, A.W., McClerren, A.L., Snehelatha, K., Reynolds, C.M., Zhou, P., and Raetz, C.R. (2007). Inhibition of lipid A biosynthesis as the primary mechanism of CHIR-090 antibiotic activity in *Escherichia coli*. Biochemistry *46*, 3793-3802.

Bentley, R. (2009). Different roads to discovery; Prontosil (hence sulfa drugs) and penicillin (hence beta-lactams). J Ind Microbiol Biotechnol *36*, 775-786.

Blair, J.M., and Piddock, L.J. (2009). Structure, function and inhibition of RND efflux pumps in Gram-negative bacteria: an update. Curr Opin Microbiol *12*, 512-519.

Cos, P., Tote, K., Horemans, T., and Maes, L. (2010). Biofilms: an extra hurdle for effective antimicrobial therapy. Curr Pharm Des *16*, 2279-2295.

Courvalin, P. (2006). Vancomycin resistance in gram-positive cocci. Clin Infect Dis *42 Suppl 1*, S25-34.

Cunha, B.A. (2006). New uses for older antibiotics: nitrofurantoin, amikacin, colistin, polymyxin B, doxycycline, and minocycline revisited. Med Clin North Am *90*, 1089-1107.

Davies, J. (2007). Microbes have the last word. A drastic re-evaluation of antimicrobial treatment is needed to overcome the threat of antibiotic-resistant bacteria. EMBO Rep *8*, 616-621.

de Lencastre, H., Oliveira, D., and Tomasz, A. (2007). Antibiotic resistant *Staphylococcus aureus*: a paradigm of adaptive power. Curr Opin Microbiol *10*, 428-435.

De Leon, G.P., Elowe, N.H., Koteva, K.P., Valvano, M.A., and Wright, G.D. (2006). An in vitro screen of bacterial lipopolysaccharide biosynthetic enzymes identifies an inhibitor of ADP-heptose biosynthesis. Chem Biol *13*, 437-441.

Delcour, A.H. (2009). Outer membrane permeability and antibiotic resistance. Biochim Biophys Acta *1794*, 808-816.

Ejim, L., Farha, M.A., Falconer, S.B., Wildenhain, J., Coombes, B.K., Tyers, M., Brown, E.D., and Wright, G.D. (2011). Combinations of antibiotics and nonantibiotic drugs enhance antimicrobial efficacy. Nat Chem Biol *7*, 348-350.

Falagas, M.E., Bliziotis, I.A., Kasiakou, S.K., Samonis, G., Athanassopoulou, P., and Michalopoulos, A. (2005). Outcome of infections due to pandrug-resistant (PDR) Gram-negative bacteria. BMC Infect Dis *5*, 24.

Falagas, M.E., Kasiakou, S.K., and Michalopoulos, A. (2006). Polymyxins: a word of caution for prudent use of valuable "old antibiotics". Infect Control Hosp Epidemiol *27*, 995.

Fukumoto, A., Kim, Y.P., Hanaki, H., Shiomi, K., Tomoda, H., and Omura, S. (2008a). Cyslabdan, a new potentiator of imipenem activity against methicillin-resistant *Staphylococcus aureus*, produced by Streptomyces sp. K04-0144. II. Biological activities. J Antibiot (Tokyo) *61*, 7-10.

Fukumoto, A., Kim, Y.P., Matsumoto, A., Takahashi, Y., Shiomi, K., Tomoda, H., and Omura, S. (2008b). Cyslabdan, a new potentiator of imipenem activity against methicillin-resistant *Staphylococcus aureus*, produced by *Streptomyces* sp. K04-0144. I. Taxonomy, fermentation, isolation and structural elucidation. J Antibiot (Tokyo) *61*, 1-6.

Gupta, N., Limbago, B.M., Patel, J.B., and Kallen, A.J. (2011). Carbapenem-resistant enterobacteriaceae: epidemiology and prevention. Clin Infect Dis *53*, 60-67.

Hancock, R.E. (1984). Alterations in outer membrane permeability. Annu Rev Microbiol *38*, 237-264.

Hancock, R.E., and Sahl, H.G. (2006). Antimicrobial and host-defense peptides as new anti-infective therapeutic strategies. Nat Biotechnol *24*, 1551-1557.

Ho, J., Tambyah, P.A., and Paterson, D.L. (2010). Multiresistant Gram-negative infections: a global perspective. Curr Opin Infect Dis *23*, 546-553.

Kneidinger, B., Marolda, C., Graninger, M., Zamyatina, A., McArthur, F., Kosma, P., Valvano, M.A., and Messner, P. (2002). Biosynthesis pathway of ADP-L-glycero-beta-D-manno-heptose in Escherichia coli. J Bacteriol *184*, 363-369.

Kumarasamy, K.K., Toleman, M.A., Walsh, T.R., Bagaria, J., Butt, F., Balakrishnan, R., Chaudhary, U., Doumith, M., Giske, C.G., Irfan, S., *et al.* (2010). Emergence of a new antibiotic resistance mechanism in India, Pakistan, and the UK: a molecular, biological, and epidemiological study. Lancet Infect Dis *10*, 597-602.

Kunz, A.N., and Brook, I. (2010). Emerging resistant Gram-negative aerobic bacilli in hospital-acquired infections. Chemotherapy *56*, 492-500.

Lee, J.H., Jeong, S.H., Cha, S.S., and Lee, S.H. (2009). New disturbing trend in antimicrobial resistance of gram-negative pathogens. PLoS Pathog *5*, e1000221.

Lim, L.M., Ly, N., Anderson, D., Yang, J.C., Macander, L., Jarkowski, A., 3rd, Forrest, A., Bulitta, J.B., and Tsuji, B.T. (2010). Resurgence of colistin: a review of resistance, toxicity, pharmacodynamics, and dosing. Pharmacotherapy *30*, 1279-1291.

Liu, A., Tran, L., Becket, E., Lee, K., Chinn, L., Park, E., Tran, K., and Miller, J.H. (2010). Antibiotic sensitivity profiles determined with an *Escherichia coli* gene knockout

collection: generating an antibiotic bar code. Antimicrob Agents Chemother *54*, 1393-1403.

Lomovskaya, O., and Bostian, K.A. (2006). Practical applications and feasibility of efflux pump inhibitors in the clinic--a vision for applied use. Biochem Pharmacol *71*, 910-918.

Loutet, S.A., Flannagan, R.S., Kooi, C., Sokol, P.A., and Valvano, M.A. (2006). A complete lipopolysaccharide inner core oligosaccharide is required for resistance of *Burkholderia cenocepacia* to antimicrobial peptides and bacterial survival in vivo. J Bacteriol *188*, 2073-2080.

Mahamoud, A., Chevalier, J., Alibert-Franco, S., Kern, W.V., and Pages, J.M. (2007). Antibiotic efflux pumps in Gram-negative bacteria: the inhibitor response strategy. J Antimicrob Chemother *59*, 1223-1229.

Marquez, B. (2005). Bacterial efflux systems and efflux pumps inhibitors. Biochimie *87*, 1137-1147.

Masters, P.A., O'Bryan, T.A., Zurlo, J., Miller, D.Q., and Joshi, N. (2003). Trimethoprim-sulfamethoxazole revisited. Arch Intern Med *163*, 402-410.

McClerren, A.L., Endsley, S., Bowman, J.L., Andersen, N.H., Guan, Z., Rudolph, J., and Raetz, C.R. (2005). A slow, tight-binding inhibitor of the zinc-dependent deacetylase LpxC of lipid A biosynthesis with antibiotic activity comparable to ciprofloxacin. Biochemistry *44*, 16574-16583.

Mdluli, K.E., Witte, P.R., Kline, T., Barb, A.W., Erwin, A.L., Mansfield, B.E., McClerren, A.L., Pirrung, M.C., Tumey, L.N., Warrener, P.*, et al.* (2006). Molecular validation of LpxC as an antibacterial drug target in Pseudomonas aeruginosa. Antimicrob Agents Chemother *50*, 2178-2184.

Misra, R., and Bavro, V.N. (2009). Assembly and transport mechanism of tripartite drug efflux systems. Biochim Biophys Acta *1794*, 817-825.

Molina, J., Cordero, E., and Pachon, J. (2009). New information about the polymyxin/colistin class of antibiotics. Expert Opin Pharmacother *10*, 2811-2828.

Nikaido, H. (2003). Molecular basis of bacterial outer membrane permeability revisited. Microbiol Mol Biol Rev *67*, 593-656.

Oteo, J., Campos, J., Lazaro, E., Cuevas, O., Garcia-Cobos, S., Perez-Vazquez, M., and de Abajo, F.J. (2008). Increased amoxicillin-clavulanic acid resistance in *Escherichia coli* blood isolates, Spain. Emerg Infect Dis *14*, 1259-1262.

Pages, J.M., Masi, M., and Barbe, J. (2005). Inhibitors of efflux pumps in Gram-negative bacteria. Trends Mol Med *11*, 382-389.

Papo, N., and Shai, Y. (2005). A molecular mechanism for lipopolysaccharide protection of Gram-negative bacteria from antimicrobial peptides. J Biol Chem *280*, 10378-10387.

Petersen, K., Cannegieter, S.C., van der Reijden, T.J., van Strijen, B., You, D.M., Babel, B.S., Philip, A.I., and Dijkshoorn, L. (2011). Diversity and clinical impact of

Acinetobacter baumannii colonization and infection at a military medical center. J Clin Microbiol *49*, 159-166.

Piddock, L.J. (2006). Multidrug-resistance efflux pumps - not just for resistance. Nat Rev Microbiol *4*, 629-636.

Poole, K. (2004). Efflux-mediated multiresistance in Gram-negative bacteria. Clin Microbiol Infect *10*, 12-26.

Raetz, C.R., and Whitfield, C. (2002). Lipopolysaccharide endotoxins. Annu Rev Biochem *71*, 635-700.

Rice, L.B. (2006). Challenges in identifying new antimicrobial agents effective for treating infections with *Acinetobacter baumannii* and *Pseudomonas aeruginosa*. Clin Infect Dis *43 Suppl 2*, S100-105.

Ruiz, N., Kahne, D., and Silhavy, T.J. (2006). Advances in understanding bacterial outer-membrane biogenesis. Nat Rev Microbiol *4*, 57-66.

Saha, S., Savage, P.B., and Bal, M. (2008). Enhancement of the efficacy of erythromycin in multiple antibiotic-resistant gram-negative bacterial pathogens. J Appl Microbiol *105*, 822-828.

Savage, P.B. (2001). Multidrug-resistant bacteria: overcoming antibiotic permeability barriers of gram-negative bacteria. Ann Med *33*, 167-171.

Schaffer, C., and Messner, P. (2005). The structure of secondary cell wall polymers: how Gram-positive bacteria stick their cell walls together. Microbiology *151*, 643-651.

Sitaram, N., and Nagaraj, R. (2002). The therapeutic potential of host-defense antimicrobial peptides. Curr Drug Targets *3*, 259-267.

Stavri, M., Piddock, L.J., and Gibbons, S. (2007). Bacterial efflux pump inhibitors from natural sources. J Antimicrob Chemother *59*, 1247-1260.

Taylor, P.L., and Wright, G.D. (2008). Novel approaches to discovery of antibacterial agents. Anim Health Res Rev *9*, 237-246.

Tsubery, H., Yaakov, H., Cohen, S., Giterman, T., Matityahou, A., Fridkin, M., and Ofek, I. (2005). Neopeptide antibiotics that function as opsonins and membrane-permeabilizing agents for gram-negative bacteria. Antimicrob Agents Chemother *49*, 3122-3128.

Vaara, M. (1992). Agents that increase the permeability of the outer membrane. Microbiol Rev *56*, 395-411.

Valvano, M.A., Messner, P., and Kosma, P. (2002). Novel pathways for biosynthesis of nucleotide-activated glycero-manno-heptose precursors of bacterial glycoproteins and cell surface polysaccharides. Microbiology *148*, 1979-1989.

Walsh, T.R. (2010). Emerging carbapenemases: a global perspective. Int J Antimicrob Agents *36 Suppl 3*, S8-14.

White, A.R., Kaye, C., Poupard, J., Pypstra, R., Woodnutt, G., and Wynne, B. (2004). Augmentin (amoxicillin/clavulanate) in the treatment of community-acquired respiratory tract infection: a review of the continuing development of an innovative antimicrobial agent. J Antimicrob Chemother *53 Suppl 1*, i3-20.

Yethon, J.A., and Whitfield, C. (2001). Lipopolysaccharide as a target for the development of novel therapeutics in gram-negative bacteria. Curr Drug Targets Infect Disord *1*, 91-106.

Yuan, Z., and Tam, V.H. (2008). Polymyxin B: a new strategy for multidrug-resistant Gram-negative organisms. Expert Opin Investig Drugs *17*, 661-668.

Zavascki, A.P., Goldani, L.Z., Li, J., and Nation, R.L. (2007). Polymyxin B for the treatment of multidrug-resistant pathogens: a critical review. J Antimicrob Chemother *60*, 1206-1215.

Zgurskaya, H.I., and Nikaido, H. (2000). Multidrug resistance mechanisms: drug efflux across two membranes. Mol Microbiol *37*, 219-225.

CHAPTER TWO

STRUCTURE AND FUNCTION OF GMHA (SEDOHEPTULOSE 7-PHOSPHATE ISOMERASE): A CRITICAL ENZYME FOR LIPOPOLYSACCHARIDE BIOSYNTHESIS AND A TARGET FOR ANTIBIOTIC ADJUVANT

CHAPTER TWO PREFACE:

The work presented in this chapter was previously published in:

Taylor, PL, Blakely, KM, de Leon, GP, Walker, JR, McArthur, F, Evidokimova, E, Zhang, K, Valvano, MA, Wright, GD, and Junop, MS. (2008) Structure and function of sedoheptulose 7-phosphate isomerase, a critical enzyme for lipopolysaccharide biosynthesis and a target for antibiotic adjuvants. *J Biol Chem,* **283**:2835-2845.

I co-authored this work with Dr. M. Junop and Dr. G. Wright. I conducted all substrate synthesis, the enzymatic characterization and mutational analysis of GmhA, and all *in vivo* experimentation.

Acknowledgements:

We would like to thank Kalinka Koteva and Don Hughes for assistance with substrate synthesis and J. Osipuik of the Midwest Center for Structural Genomics for collecting the selenomethionine *P. aeruginosa* diffraction data.

ABSTRACT

The barrier imposed by lipopolysaccharide (LPS) in the outer membrane of Gram-negative bacteria presents a significant challenge in treatment of these organisms with otherwise effective hydrophobic antibiotics. The absence of L-*glycero*-D-*manno*-heptose in the LPS molecule is associated with a dramatically increased bacterial susceptibility to hydrophobic antibiotics and thus enzymes in the ADP-heptose biosynthesis pathway are of significant interest. GmhA catalyzes the isomerization of D-sedoheptulose 7-phosphate into D-*glycero*-D-*manno*-heptose 7-phosphate, the first committed step in the formation of ADP-heptose. Here we report structures of GmhA from *Escherichia coli* and *Pseudomonas aeruginosa* in apo, substrate and product-bound forms, which together suggest that GmhA adopts two distinct conformations during iosmerization through reorganization of quaternary structure. Biochemical characterization of GmhA mutants, combined with *in vivo* analysis of LPS biosynthesis and novobiocin susceptibility, identifies key catalytic residues. We postulate GmhA acts through an enediol-intermediate isomerase mechanism.

INTRODUCTION

Lipopolysaccharide (LPS) is an essential component of the outer membrane (OM) in Gram-negative bacteria (Raetz and Whitfield, 2002). LPS not only functions as a protective barrier preventing cell entry of hydrophobic molecules, including bile salts, detergents, and lipophilic antibiotics, but also helps maintain the structural integrity of the outer membrane. Thus, LPS is vital for bacterial virulence and antibiotic sensitivity in pathogenic Gram-negative bacteria.

Gram-negative pathogens are increasingly becoming a serious clinical threat. Multidrug resistant hospital acquired infections caused by enteric bacteria such as *Escherichia coli* and *Klebsiella pneumoniae* and by emerging pathogens of environmental origin such as *Acinetobacter baumannii* and *Pseudomonas aeruginosa* as the next big problem facing the infectious disease community. Furthermore, Gram-negative pathogens of animal origin such as *E. coli* O157-H7 are ongoing threats to agriculture and water quality. New chemotherapeutic strategies against Gram-negative bacteria are therefore required. LPS biosynthesis represents a unique Gram-negative target for new antimicrobial intervention.

LPS comprises lipid A, a core oligosaccharide, and in some bacteria, an O-specific polysaccharide chain. The core oligosaccharide has an inner core region consisting of 3-deoxy-D-*manno*-oct-2-ulosonic acid (Kdo) and one or more heptose units, and an outer core, consisting of additional sugar residues. (Figure 2-1A) (reviewed in refs (Nikaido, 2003; Nikaido and Vaara, 1985; Raetz and Whitfield, 2002; Yethon and Whitfield, 2001). Lipid A and Kdo are highly conserved in Gram-negative bacteria and essential for cell viability. The biosynthesis of these molecules is therefore a target for traditional antibiotic discovery efforts. Indeed, small molecule inhibitors of lipid A biosynthesis have been reported to have anti-Gram-negative activity (Onishi et al., 1996).

Most Gram-negatives also contain one or more L-*glycero*-D-*manno*-heptose molecules attached to the Kdo. Mutants in heptose metabolism, which are viable in laboratory conditions, are avirulent and highly susceptible to antibiotics (reviewed in Valvano et al., 2002). Heptose biosynthesis is thus a non-traditional target for Gram-negative selective antimicrobial agents. Inhibitors of heptose biosynthesis could be used as anti-virulence drugs or could be co-administered with antibiotics that do not normally cross the outer membrane barrier (e.g. novobiocin, erythromycin) to sensitize bacteria to these agents. We have termed such molecules antibiotic adjuvants (Wright and Sutherland, 2007).

The outer-core carbohydrates and the O-specific polysaccharide side chains, also known as O antigens, comprise the remainder of the LPS polymer. These components vary significantly by organism (Raetz and Whitfield, 2002). They are not essential for cell growth, but do mediate host-microbe interactions and play a significant role in virulence. Inhibitors of outer core and O-antigen biosynthesis could therefore be strategically deployed as organism-specific anti-virulence compounds.

All levels of LPS biosynthesis represent underexploited targets for new anti-microbial agents. The heptose biosynthetic pathway in Gram-negative bacteria, in particular, is highly attractive being essential for virulence and antibiotic sensitivity. Heptoses targeted to the inner core LPS are synthesized within the cytosol as ADP activated L-*glycero*-β-D-*manno*-heptose molecules (Eidels and Osborn, 1971; Kneidinger et al., 2001; Kneidinger et al., 2002). Biosynthesis is initiated from D-sedoheptulose 7-phosphate (S7P). Sedoheptulose 7-phosphate isomerase (GmhA) catalyzes the first committed step in the pathway (Figure 2-1B) (Brooke and Valvano, 1996a, b; Eidels and Osborn, 1974). In *E. coli,* phosphorylation at the 1 position of the resulting D-*glycero*-α,β-D-*manno*- heptose 7-phosphate is then catalyzed by the kinase moiety of the bifunctional D-*β*-D-heptose phosphate kinase/ D-β-D-heptose 1-phosphate adenyltransferase (HldE) (McArthur et al., 2005). A bifunctional HldE is also predicted in the opportunistic pathogen *P. aeruginosa* based on genomic sequence comparisons. However, in other pathogenic organisms, such as *Burkholderia cenocepacia*, this bifunctional enzyme is replaced by two distinct enzymes, HldA and HldC, which accomplish the respective functions (Loutet et al., 2006; Valvano et al., 2002). D-α,β-D-heptose-1,7-bisphosphate phosphatase (GmhB) catalyzes the removal of the phosphate at the 7 position, while the adenyltransferase action of HldE (or mono-functional HldC) transfers the AMP moiety from ATP to give ADP-D-*glycero*-ß-D-*manno*-heptose (Valvano et al., 2000; Valvano et al., 2002). Finally, ADP-D-β-D heptose epimerase (HldD) catalyzes the formation of ADP-L-*glycero*-β-D-*manno*-heptose, the precursor for the incorporation of heptose into the inner core, which is mediated by specific heptosyltransferases (Morrison and Tanner, 2007; Sirisena et al., 1994).

A key step in ADP-heptose biosynthesis is S7P isomerization catalyzed by GmhA. Previous studies of GmhA predicted its function using gene deletion and product analysis (Brooke and Valvano, 1996a; Eidels and Osborn, 1974). Mutation of *gmhA* also results in a compromised OM, effectively removing the protective barrier normally afforded by LPS, therefore greatly increasing susceptibility to antibiotics (Brooke and Valvano, 1996b). Understanding the structure-function of GmhA could aid in the future development of inhibitors that would increase the permeability of Gram-negative pathogens and act synergistically with known antibiotics as a novel treatment for Gram-negative infections.

We report crystal structures of *E. coli* and *P. aeruginosa* GmhA in apo, substrate and product-bound forms and the use of this structural data to guide site-directed mutagenesis studies that enable prediction of the molecular mechanism of S7P isomerization, a potential target for new antimicrobial agents.

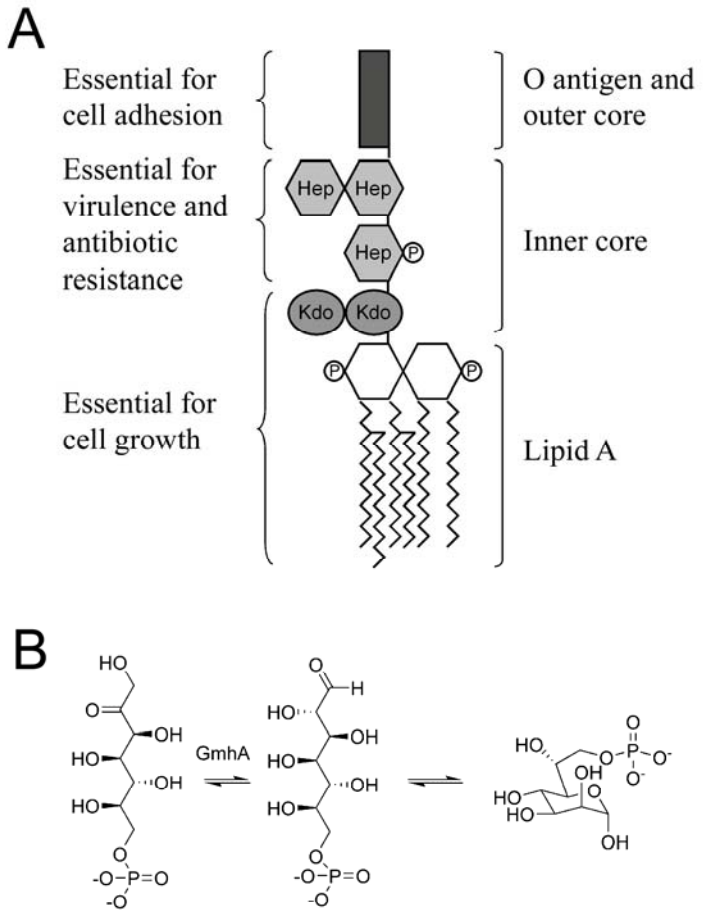

Figure 2-1. LPS structure and activity of GmhA. (A) General structure of LPS in Gram-negative bacteria. Kdo, 3-deoxy-D-*manno*-oct-2-ulosonic acid; Hep, Heptose; P, phosphate. **(B)** Schematic of the isomerase reaction catalyzed by GmhA, where D-sedoheptulose 7-phosphate is converted into D-*glycero*-D-*manno*-heptose 7-phosphate.

MATERIALS AND METHODS

Purification of GmhA. Purification of *E. coli* GmhA followed a previously described protocol (De Leon et al., 2006). An additional purification step was performed for GmhA protein used in crystallization and analytical ultracentrifugation studies. For these studies, GmhA was applied to a Q-Sepharose column (Amersham Bioscience) and eluted using a linear KCl gradient (GmhA buffer A – 20 mM HEPES pH 8.0, 1 mM EDTA, 5 mM dithiothreitol (DTT); GmhA Buffer B - 20 mM HEPES pH 8.0, 1 mM EDTA, 5 mM DTT, 500 mM KCl). Fractions containing only GmhA were pooled and dialyzed extensively against 20 mM HEPES pH 8.0 and 4 mM DTT. *P. aeruginosa* GmhA was over-expressed in *E. coli* BL21-Gold (DE3) (Stratagene), harboring an extra plasmid encoding three rare tRNAs (AGG and AGA for Arg, ATA for Ile). Cells were grown in auto-inducible media (Grossman et al., 1998) for 4-5 h at 37 °C and 12-15 h at 20 °C. Cells were sonicated in binding buffer (5 mM imidazole, 5% glycerol, 50 mM HEPES Na pH 7.5, 0.5 M NaCl), supplemented with 1 mM of PMSF and benzamidine and 0.5% IGEPAL CA-630 (Sigma). Clarified lysate was passed in series through DE52 and Ni NTA (Qiagen) columns. GmhA was dialyzed in 10 mM HEPES Na pH 7.5, 0.5 M NaCl, and concentrated using a BioMax concentrator (Millipore). Selenomethionine (SeMet) enriched protein was produced according to a previously described procedure (O'Gara et al., 1997; Qoronfleh et al., 1995). TCEP (0.5 mM) was added to all purification buffers.

Structure Determination of GmhA. All GmhA crystals were grown at 20 ºC using the hanging drop/vapor diffusion method. *E. coli* GmhA (10 mg/ml) was mixed with an equal volume of crystallization solution (3% (w/v) polyethylene glycol PEG-8000, 0.1 M imidazole pH 7.3 and 3% (v/v) ethylene glycol) and dehydrated against 1.5 M $(NH_4)_2SO_4$. For crystallization of substrate bound GmhA, S7P (see below) was added at a final concentration of 1 mM and ethylene glycol was replaced with 1,6-hexandiol. Prior to flash freezing in liquid nitrogen, apo and substrate-bound GmhA crystals were soaked (~30-60 sec) in a cryo-protecting solution (10 mM HEPES pH 7.3, 2 mM DTT, 1.5% PEG-8000, 50 mM imidazole, 3% ethylene glycol, 30% glycerol; or 0.5 mM S7P, 15.45 mM HEPES pH 7.3, 3.1 mM DTT, 2.31% PEG-8000, 77.27 mM imidazole, 4.67% 1,6-hexandiol, 30% glycerol, respectively). *P. aeruginosa* apo-GmhA SeMet crystals grew in a solution of 25% PEG3350, 0.1M Ammonium Sulfate and 0.1 M Bis-Tris pH 5.5 and were cryoprotected with a mixture of 8% glycerol, 8% ethylene glycol, and 8% sucrose. Product-bound GmhA crystallized in a solution of 2.5 mM S7P (Sigma), 2 M Ammonium Sulfate, 0.2 M K/Na Tartrate and 0.1 M Na Citrate pH 5.6, and were cryoprotected with 25% ethylene glycol. All X-ray diffraction data sets were collected at 100 K. *E. coli* apo and substrate-bound GmhA data were collected with an R-AXIS IV image-plate detector mounted on an RU300 rotating-anode X-ray generator (Rigaku/MSC Ltd, TX). Data sets were processed and scaled using d*TREK (Pflugrath, 1999). An initial search model for molecular replacement using *MOLREP* (Vagin and Teplyakov, 1997) was generated from *V. cholerae* GmhA (Seetharaman et al., 2006), PDB code 1X94. Substrate-bound GmhA was solved by molecular replacement using the refined *E. coli* apo-GmhA structure as a search model. *P. aeruginosa* SeMet GmhA SAD data was collected at the 19ID beamline

of the Structural Biology Center, Advanced Photon Source (APS), Argonne National Laboratory, while product-bound GmhA data was collected at the 17ID beamline of the Industrial Macromolecular Crystallography Association Collaborative Access Team. These data were processed with HKL2000 (Otwinoski and Minor, 1997). Using SOLVE (Terwilliger and Berendzen, 1999), all 20 expected selenium sites in the asymmetric unit were located. Resolve (Terwilliger, 2000) was then used to build an initial model. To determine the structure of product bound *P. aeruginosa* GmhA, the structure of the SeMet *P. aeruginosa* GmhA was used as a search model. Model building and refinement for all GmhA structures were carried out using *O* (Jones et al., 1991), *Coot* (Emsley and Cowtan, 2004), *REFMAC5* (Murshudov et al., 1996) or *CNS* (Brunger et al., 1998), until R values and model geometry statistics fell within acceptable ranges (Table 2-1, Results). Surface area calculations were performed using *POPSCOMP* (http://zeus.cs.vu.nl/programs/popscompwww) (Fraternali and Cavallo, 2002). Structural illustrations were generated using PyMOL Molecular Graphics System (DeLano Scientific).

GmhA Mutagenesis. Site mutations in *E. coli gmhA* were generated in both pET28a(+)*gmhA* and pBAD30*gmhA* inserts using the QuikChange Site-Directed Mutagenesis protocol (Stratagene). Sequences of mutagenic oligonucleotide primers are described in Appendix 1. Mutations were verified by DNA sequence analysis (MOBIX, McMaster University) using vector-specific sequencing primers (Appendix 1).

Sedimentation equilibrium. *E. coli* GmhA and GmhA-D94N molecular weights in solution were determined by sedimentation equilibrium analysis using a Beckman-Coulter XL-1 analytical ultracentrifuge (Palo Alto, CA). Protein concentrations corresponding to 0.1, 0.2 and 0.4 of absorbance at 280 nm (A_{280}) values, respectively, were loaded into a 6-channel epon-charcoal cell with a 1.2 cm path length. Equilibrium was allowed to develop for 12 – 14 hrs at rotor speeds of 20 000 and 25 000 rpm. The reference solvent contained 20 mM HEPES pH 8.0, 150 mM KCl, 5 mM DTT (ρ = 1.006 g/mL). Absorbance data were collected at A_{280} and analyzed using the Beckman-Coulter Optima XL-1 Analytical Ultracentrifuge Origin Data Analysis Package (version 60-4) and Microcoal Origin 6.0. GmhA partial specific volume (0.739 mL/g) and solvent densities were determined using SEDNTERP, a public domain program developed by Hayes, Laue, and Philo (http://www.rasmb.bbri.org). Resulting gradients were then fit to a self-association model using the above software. Due to the poor absorption of GmhA, high protein concentrations were required for detection, prohibiting accurate K_d determination.

Sedoheptulose 7-phosphate synthesis. S7P was synthesized enzymatically from D-serine and ribose 5-phosphate based on the protocol by Lee and colleagues, with minor modifications (Lee, 1999). *E. coli* transketolase (TktA) was purified as previously described (De Leon et al., 2006). Porcine D-amino acid oxidase (gift of V. Massey) was purified from *E. coli* BL21(DE3)/pET28a(+)DAO cells by anion exchange using a Q Sepharose column. Purified protein was analyzed using 12% SDS-polyacrylamide gel

electrophoresis and activity was confirmed using a lactate dehydrogenase coupled enzyme assay (Fukui et al., 1988). DAO was stored in the presence of 5 mM FAD. S7P synthesis and purity was determined using LC/ES-MS and ^{1}H, ^{13}C, and ^{31}P NMR.

E. coli GmhA Steady State Kinetic Analysis. GmhA activity was monitored by coupling product formation to HldE and GmhB and monitoring Pi release, as previously described (De Leon et al., 2006) with the following modifications. Reaction mixture consisted of 20 mM HEPES pH 8.0, 10 mM MgCl, 10 mM KCl, 6 mM ATP, 0.4% Tween-20, 0.214 nmol GmhA, 0.375 nmol GmhB, 0.094 nmol HldE, and 0.2 U pyrophosphatase in a total volume of 90 µL. Reactions were initiated with 10 µL of S7P for final concentrations ranging from 0 to 2 mM. Initial rates were fit to (eq 1) describing Michaelis-Menten kinetics using Grafit 4 software (Erithacus Software, Staines, U.K.).

$$\upsilon = k_{cat}E_t[S]/(K_m + [S]) \quad \text{(eq. 1)}$$

GmhA in vivo complementation studies . pBAD30*gmhA* wild type and mutant vectors were used to transform *E. coli* BW25113Δ*gmhA* cells (Baba et al., 2006) to create complement strains. Positive and negative control strains were created by transforming the pBAD30 vector into *E. coli* BW25113 and *E. coli* BW25113Δ*gmhA* cells respectively. Cells were cultured overnight at 37 ºC, 250 rpm in M9 minimal media, 0.2% arabinose, 100 µg/mL ampicillin. To confirm GmhA expression, 1 mL overnight culture was harvested, resuspended in 50 µL 10 mM Tris pH 7.5, 1mM EDTA buffer, 50 µL 2x SDS loading dye. Cells were lysed by boiling 30 min and analyzed by 15% SDS polyacrylamide gel electrophoresis. For immunoblot analysis, gel contents were transferred to a polyvinylidene fluoride membrane. GmhA was detected using mouse IgG anti-histidine primary antibody (Amersham) and peroxidase-conjugated Affini-pure donkey anti-mouse IgG secondary antibody (Jackson Immunoresearch). Perkin-Elmer Western lighting chemiluminescence reagent was used in detection. Minimal inhibitory concentrations (MIC) of novobiocin were determined as follows: Overnight cultures, as described above, were diluted to an optical density of 600 nm (OD_{600}) 0.11 and further diluted 1 in 200. Strains were grown at 37 ºC in 96 well plates in the presence of varying concentrations of DMSO dissolved novobiocin (2 to 1024 µg/mL). OD_{600} was measured after 20 hours to assay growth. MIC was determined as the concentration of novobiocin required to reduce the OD_{600} of each strain to 90 % of the OD_{600} in the absence of drug.

LPS analysis. *E. coli* BW25113Δ*gmhA* /pBAD30*gmhA* wild type and mutant strains were grown at 37 ºC for 24 h on M9 minimal media, 0.2% arabinose, 100 µg/mL ampicillin agar plates. LPS was extracted from these cells as previously described (Marolda et al., 2006). LPS samples were analyzed by 10% SDS polyacrylamide gel electrophoresis in the Tricine buffer system and detected by silver staining (Marolda et al., 2006; Tsai and Frasch, 1982). Gels were fixed overnight in 250 mL fixing solution (60% MeOH, 10% acetic acid). Gels were washed, in order, using 200 mL 7.5% acetic acid for 30 min, 200 mL 0.7% periodic acid for 30 min, mQ H_2O for 3 x 15 min, 200 mL staining solution (42 mL 0.36% NaOH, 2.8 mL conc. NH_4OH, 8 mL 19.4% silver nitrate,

148 mL H_2O) for 25 min, mQ H_2O for 2 x 15 min, and 200 mL developing solution (50 mg citric acid, 0.5 mL 37% formaldehyde in H_2O) until bands appeared. Stain development was stopped by repeated washing in H_2O.

RESULTS

Structural analysis of GmhA. The crystal structures of apo-GmhA from *E. coli* and *P. aeruginosa* were determined to 1.95 Å (PDB 2I2W) and 2.4 Å (PDB not yet released), respectively (Table 2-1). The structure from *E. coli* was solved via molecular replacement using an initial model based on the GmhA structure from *V. cholerae* (PDB 1X94). *E. coli* apo-GmhA crystals grew in the space group $P2_12_12_1$ with four molecules of GmhA in each asymmetric unit as shown in Figure 2-2 (subunits A, B, C and D). Predication of oligomerization using the program *PISA* (Krissinel and Henrick, 2007) strongly suggested that GmhA would exist in solution as a tetramer. This was further verified by sedimentation equilibrium studies (Appendix 2). No electron density was observed for residues 83-97 in chains B or D, and therefore these regions are represented as dotted lines in Figure 2-2. Three intersubunit Cys-Cys disulphide linkages were observed in the asymmetric unit, one at C90 linking chain A-C, and two others linking Chains A-B and C-D at C57, respectively. These linkages are likely artifacts as addition of reducing agent or substitution of Cys to Ser resulted in increased GmhA activity (discussed below). The A-D and B-C dimer interfaces are extensive (2680 $Å^2$), each resulting from reciprocal interactions between helices H1, H3 and H6. A-B and C-D interfaces are less extensive (1515 $Å^2$) and are formed primarily through H4 and reciprocal interactions with loop regions joining H3-β2 or β2-H4. The final model was refined to R and R_{free} values of 19.2 and 22.4, respectively. Apo-GmhA from *P. aeruginosa* was crystallized in space group $P2_12_12$ and the structure determined to 2.4 Å using SeMet substituted protein and single-wavelength anomalous diffraction. The final model was refined to R and R_{free} values of 19.7 and 27.4, respectively. As with the apo-GmhA structure from *E. coli,* a tetramer of GmhA was observed in the asymmetric unit and residues 83-96 in each chain were disordered. The Cα traces of these monomers could be superimposed with an rms deviation of 1.1 Å (Appendix 3).

Each GmhA monomer consists of a central five-stranded parallel β-sheet, flanked by five alpha helices (Figure 2-2A) forming a three-layered HβH sandwich. Helical layers are comprised of H2, H3, H6 on one side and H4, H5 on the opposing side of the central β-sheet with topology β2,1,3,4,5. The overall fold is quite similar to the flavodoxin-type nucleotide-binding motif, and is essentially identical to GmhA structures from *V. cholerae* (PDB 1X94) and *Campylobacter jejuni* (PDB 1TK9) (Seetharaman et al., 2006).

In addition to apo-structures of GmhA, we also determined structures of GmhA in the presence of substrate and product. The structure of *E. coli* GmhA in complex with S7P was determined to 2.79 Å (PDB 2I22). This complex crystallized in a different space group ($P2_1$) compared to apo protein. The final model was refined to R and R_{free} values of 20.3 and 25.7, respectively. The major difference observed between the apoprotein and substrate-bound complex, aside from the presence of S7P, centers on the loop connecting β2 and H4, which becomes disordered in the presence of substrate (Figure 2-3A). Since wild type GmhA isomerase was used to generate these crystals, and crystals took several days to grow, a mixture of product and substrate is expected to have been present during

Table 2-1. GmhA data collection and model refinement statistics.

Data Collection				
Data Set	Apo_{EC}	Sub-$bound_{EC}$	Apo_{PA}	Product-$bound_{PA}$
Space group	$P2_12_12_1$	$P2_1$	$P2_12_12$	$P6_522$
Cell parameters				
a,b,c (Å)	83.9, 89.6, 106.9	73.0, 76.5, 78.3	123.8, 131.6, 48.8	126.3, 126.3, 113.2
α, β, γ (°)	90, 90, 90	90, 106.1, 90	90, 90, 90	90, 90, 120
Molecules in ASU	4	4	4	2
Resolution (Å)[a]	45.93 – 1.95 (2.02 – 1.95)	47.39 – 2.79 (2.89 – 2.79)	40.0 – 2.40 (2.46 – 2.40)	40.0 – 2.30 (2.38 – 2.30)
Unique reflections	59,294	20,533	30,927	24,669
Redundancy[a]	4.27 (4.18)	2.63 (2.68)	7.6 (6.8)	12.4 (12.6)
Completeness (%)[a]	99.8 (100.0)	98.6 (99.4)	99.9 (100.0)	99.9 (100.0)
I/σ(I)[a]	10.9 (3.4)	6.7 (2.6)	29.1 (4.2)	25.0 (6.2)
R_{merge} (%)[a]	7.5 (39.8)	11.1 (36.0)	7.0 (40.0)	12.5 (40.4)
Model and refinement				
Resolution (Å)[a]	45.93 – 1.95	25.0 – 2.80	39.19 – 2.40	39.3 – 2.30
R_{work} (%)	19.2	20.3	19.7	17.6
R_{free} (%)	22.4	25.7	27.4	22.1
Reflections (observed)	56,213	18,807	29,349	24,221
Reflections (Rfree)	2,996	1,478	1,578	1,222
No. residues/atoms	737/5630	707/5436	715/5535	391/2969
No. of waters	634	226	148	178
Rmsd Bond:				
lengths (Å)	0.013	0.024	0.010	0.019
angles (°)	1.27	2.05	1.28	1.80
Mean *B* factor (Å^2)	36.7	45.6	35.1	29.1
PDB ID Code	2I2W	2I22		1X92

[a]Statistics for the highest resolution shell are shown in parentheses.

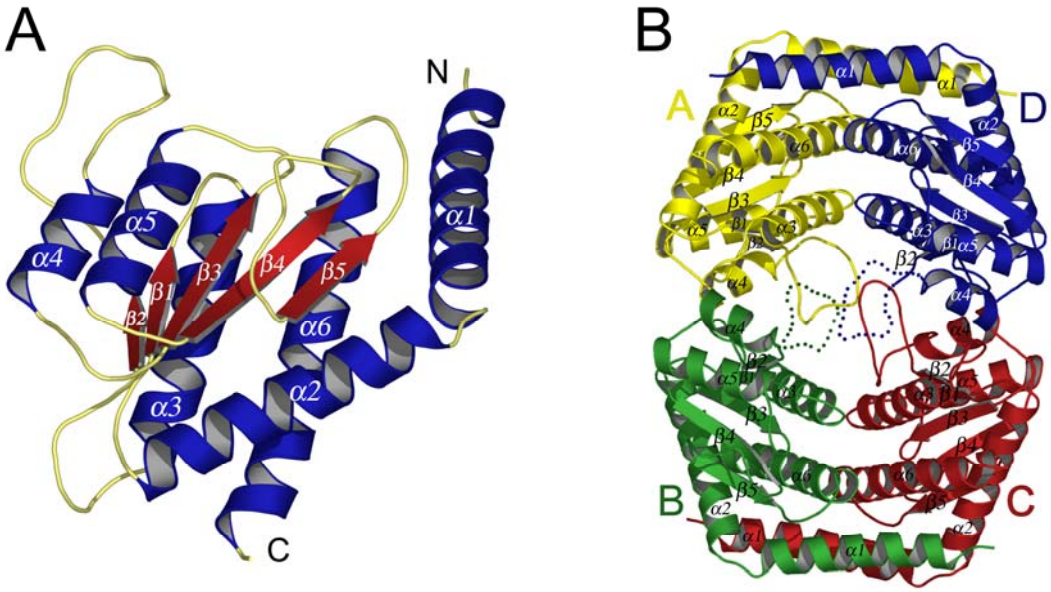

Figure 2-2. Structure of the *E. coli* GmhA apoprotein. (A) GmhA monomer. β-strand and α-helix in red and blue, respectively **(B)** GmhA tetramer. Dashed lines in subunits B and D represent disordered regions of GmhA not observed in the final model.

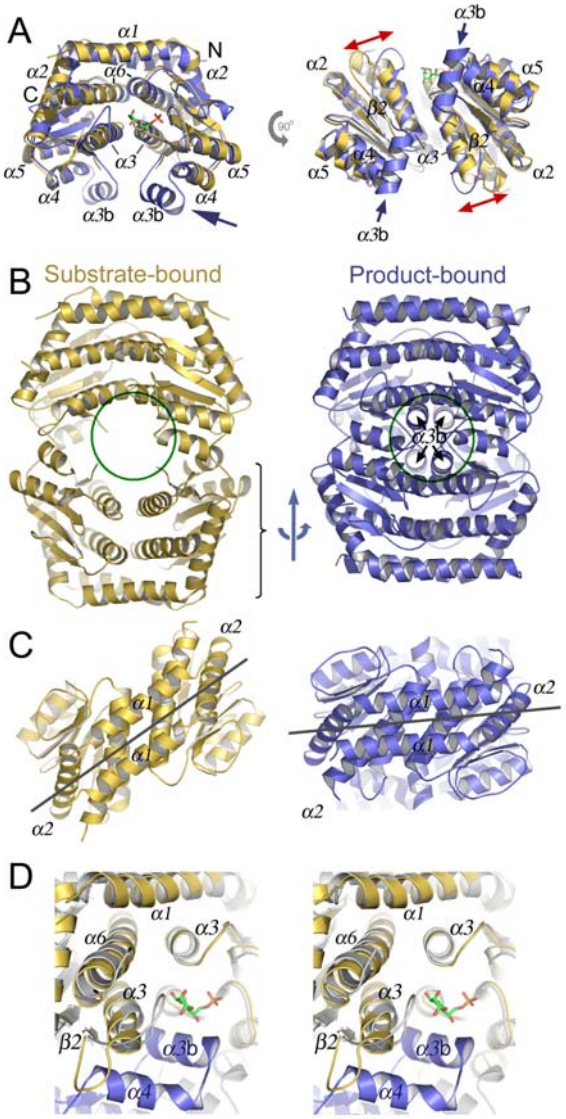

Figure 2-3. Structural comparison of substrate and product-bound GmhA. *E. coli* GmhA complexed with S7P (purple) and *P. aeruginosa* GmhA compexed with D-*glycero*-D-*manno*-heptose 7-phosphate (gray). **(A)** Two orthogonal views of the A-D dimer are presented. Purple and red arrows illustrate formation of new H3' helix and repositioning of the H3-β2 loop, respectively. **(B)** Comparison of change in quaternary structure between substrate and product-bound GmhA tetrameric forms. Green circle highlights relative position of four H3' helices formed in presence of product. Blue arrows illustrate the translational and rotational differences of the dimer-dimer interface between substrate and product-bound forms. **(C)** Same illustration as presented in (B), but from the bottom of the structure. Light grey lines illustrate the relative rotational difference between equivalent BC dimers of the substrate- an product-bound structures. **(D)** Close-up stereo view comparing the relative positions of H3 and H3-β2 loop regions of substrate and product-bound GmhA. Blue, subunit B of product-bound structure.

crystal formation. Clear additional electron density was observed at only one of the four potential active sites within the GmhA tetramer. As shown in Figure 2-5, this density is consistent with the presence of substrate; however, given the relatively low resolution to which this structure was determined, further structural and functional analysis was required to fully characterize the active site of GmhA.

The product-bound structure of GmhA from *P. aeruginosa* was determined in space group $P6_522$ to 2.3 Å (PDB 1X92). These crystals were generated following incubation of GmhA with substrate (see Experimental Procedures). In this case, clear electron density corresponding to product was observed in each active site region (Figure 2-5). In contrast to the apo and substrate-bound structures of *E. coli* GmhA, the product-bound protein crystallized as a dimer in the asymmetric unit (Figure 2-3A). However, by combining two dimers from crystallographic related symmetry mates, a tetramer could be generated (Figure 2-3B).

Since wild type GmhA was used in all of these studies, it would appear that crystallization conditions (as opposed to an inactive GmhA) were responsible for selecting distinct conformations of GmhA capable of binding either substrate or product.

To date, six structures of GmhA have been determined: apo and substrate bound *E. coli* GmhA, apo and product bound *P. aeruginosa* GmhA, *V. cholera* GmhA, and *C. jejuni* GmhA. As shown in Figure 2-4, these structures can be categorized into two distinct conformations, designated open and closed. The *E. coli* structures, as well as the apo *P. aeruginosa* and the *V. cholerae* structures adopt an open conformation, while the *P. aeruginosa* and *C. jejuni* exist in the closed state. Three major differences between the open and closed conformations are apparent. First, a new helix (H3') in the product-bound structure is present in place of the disordered loop located between β2-H4 in the apo and substrate-bound structures (Figure 2-3A, purple arrow). A second difference is the overall positioning of the loop joining H3 and β2. In the closed state this loop is rotated inward towards the opposing subunit by ~ 20 Å relative to the open conformation (Figure 2-3A, red arrow), with the exception of apo *P. aeruginosa*, where the H3-β2 loop is in line with the closed conformation rather than the open. Finally, compared to the open conformation structures, the tetramer formed in the closed conformation structures are more compact and bury substantially more dimer-dimer surface area (2500 vs. 1250 $Å^2$) due to the packing of H3'. Figures 2-3B and 2-3C illustrate the difference between these two tetrameric forms, highlighting a large reorganization of the dimer-dimer interface. Bringing dimers of product-bound GmhA together involves a corkscrew-like movement with concerted translational (5 Å) and rotational (25^o) movements between A-D and B-C dimers (see supplemental data for a movie illustrating the structural transition between open and closed conformations). As shown in Figure 2-3D, the formation of H3' in the closed conformation of GmhA is responsible for repositioning the H3-β2 loop due to steric hindrance.

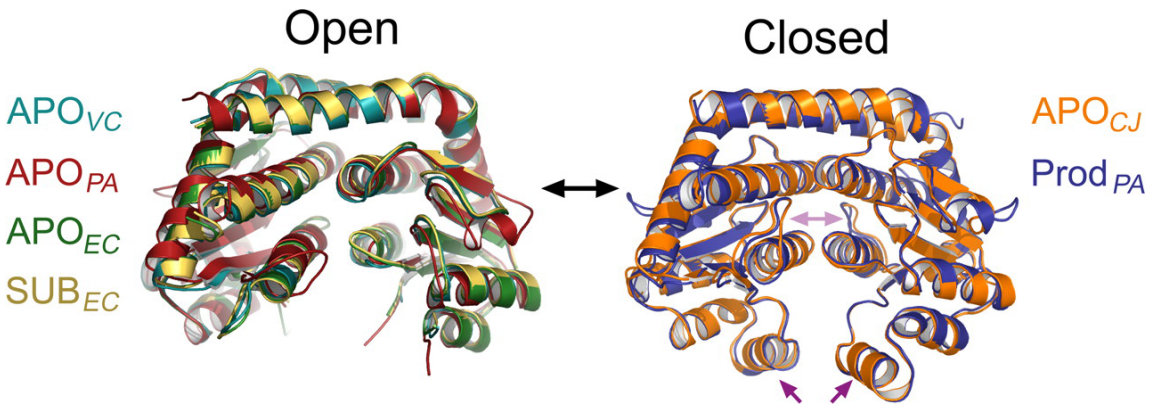

Figure 2-4. Structural comparison of all known GmhA structures. Aligned structures were grouped into either the open or closed conformation. Light and dark purple arrows highlight structural transitions involving the H3-β2 loop and H3' helix, respectively. *VC – V. cholerae*; *PA – P. aeruginosa*; *EC – E. coli*; *CJ – C. jejuni*.

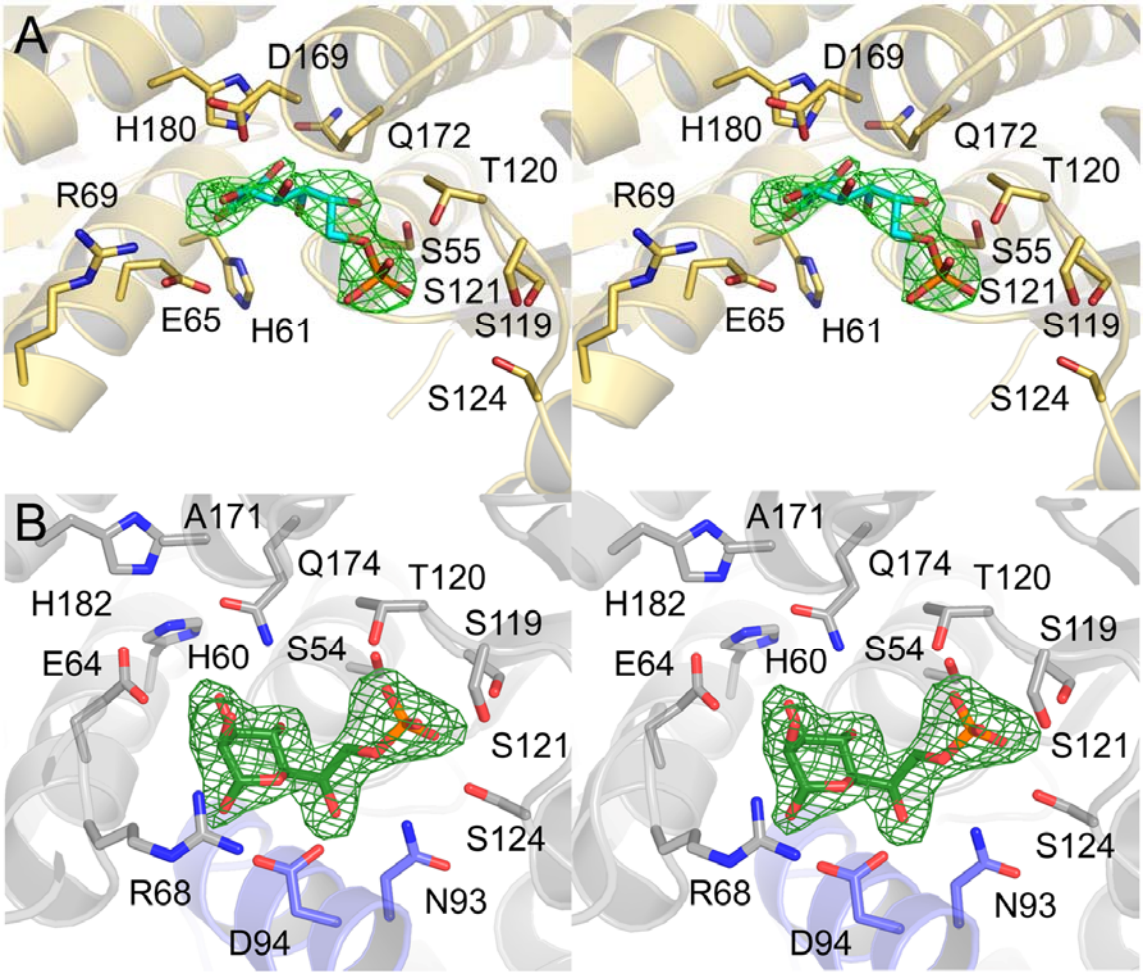

Figure 2-5. Stereo view of active site structures of substrate and product-bound GmhA. (A) *E. coli* GmhA in complex with S7P. **(B)** *P. aeruginosa* GmhA in complex with D-*glycero*-D-*manno*-heptose 7-phosphate. All amino acid side chains making direct interaction with either substrate (A) or product (B) are shown. Product and substrate Fo-Fc omit maps ($\sigma = 3.0$) are presented.

Both substrate and product are found at the interface formed between subunits A and D. As discussed above, only one of the four active sites within GmhA contained substrate, whereas the structure of product-bound GmhA contained fully occupied active sites. In the S7P-bound structure numerous contacts are observed between substrate and the following amino acid side chains (Appendix 4): S55, T120, D169, and Q172 of chain D, and H61, E65 and H180 of chain A. In general, the active sites observed for both the substrate and product-bound structures are comparable (Figure 2-5). Several residues from both structures remain unchanged, in particular: S55 (S54), S119, T120, S121, S124, and H180 (H182) (residues in parentheses correspond to product-bound *P. aeruginosa* GmhA). While not perfectly superimposible, side chains from residues E65 (E64) and Q172 (Q174) did not differ significantly in their overall position between the two structures. In contrast, residues H61 (H60) and R69 (R68) adopt different positions largely due to the dramatic change of position in the H3-β2 loop. The most striking difference, however, occurs in the product-bound form, by additional contacts made with residues N93 and D94 of chain B (Figure 2-5B). The finding that residues from three chains (A, B and D) are involved in binding product suggests that assembly of a GmhA tetramer may be required for function.

Rationale for site directed mutagenesis. Potential GmhA active site residues were chosen for analysis based on crystallographic active site data of both the substrate bound *E. coli* enzyme and product bound *P. aeruginosa* enzyme (Figure 2-5). A total of eight residues were selected for analysis and are described by *E. coli* residue number. Equivalent residues of E65, T120, and Q172 show direct contact in both substrate and product bound crystal structures. The highly conserved S55, S119, T120, S121, S124 pocket was hypothesized to bind the S7P phosphate, rather than play a direct role in catalysis. As such, only one residue from this pocket, T120, was chosen for mutagenesis. H61, D169, and H180 contacts are unique to the *E. coli* substrate bound structure, while R69 and D94 contacts are unique to the *P. aeruginosa* product bound structure. As shown in Figure 2-6, all mutated residues are conserved across species, with the exception of D169. D169 was examined even without conservation due to its prominent position depicted in the *E. coli* active site.

In vitro mutational analysis. The ability of purified *E. coli* GmhA wild type and mutant proteins to convert enzymatically synthesized S7P into product was assessed using a coupled assay monitoring P_i release. Initial studies, using wild type GmhA, determined that synthesized S7P was indeed a substrate of GmhA, and that the reaction was linear for at least 10 min in the presence of 0.214 nmol protein. Purified mutant GmhA proteins were then assayed for activity against S7P (Table 2-2). Of the eight mutants tested, only H61Q and R69Q demonstrated measurable *in vitro* activity. R69Q turnover (0.45 +/- 0.1 sec^{-1}) was equal to that of wild type GmhA (0.44 +/- 0.07 sec^{-1}), while the turnover of H61Q (0.23 +/- 0.07 sec^{-1}) was roughly half that of wild type. The remaining GmhA mutants, E65N/Q, D94N, T120A, D169N, Q172E, and H180Q showed undetectable in vitro activity (limit of detection 0.003 sec^{-1} at 2 mM S7P).

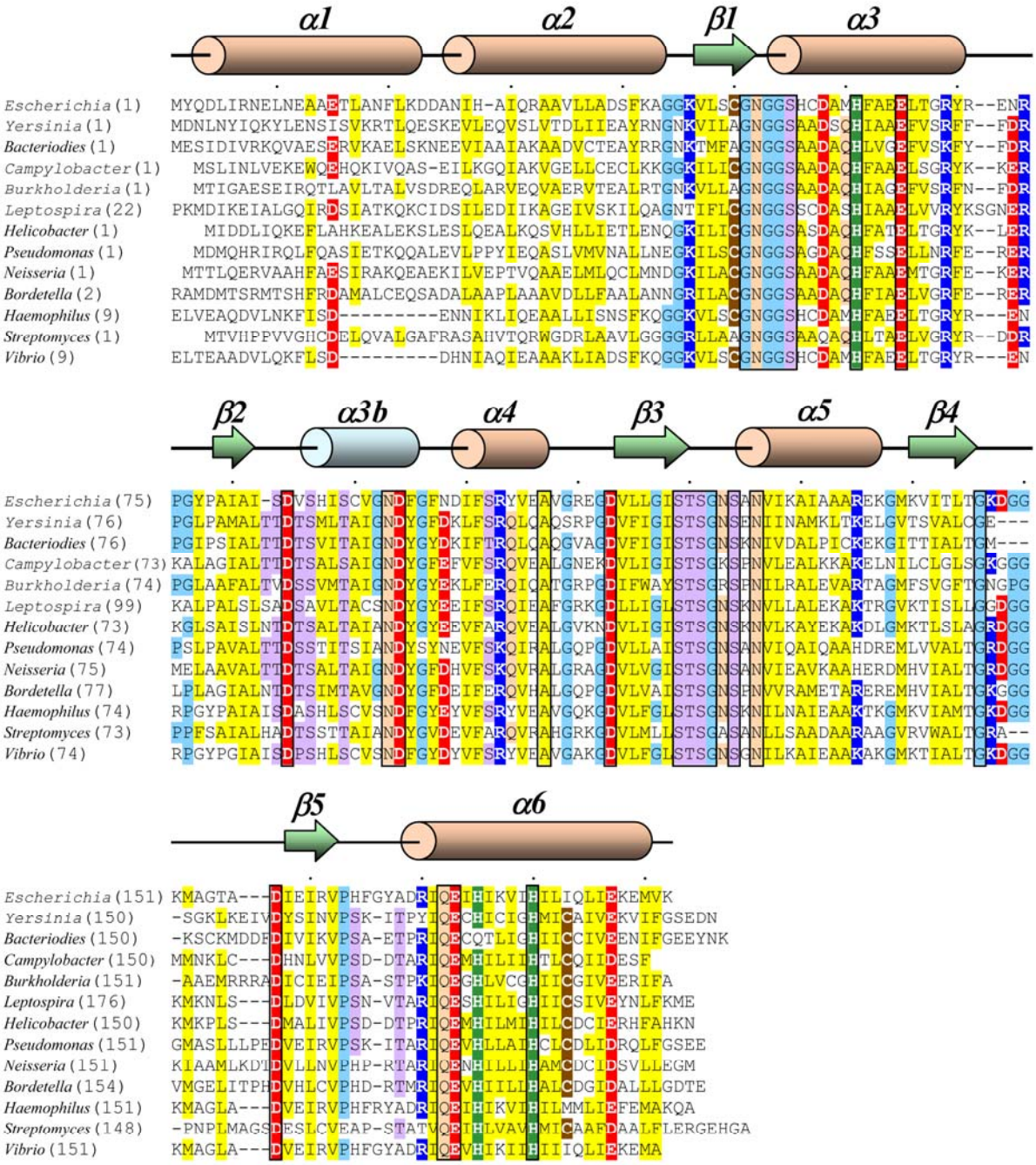

Figure 2-6. Sequence alignment of GmhA from various bacterial pathogens. Boxed residues are completely conserved between organisms. Colors indicate properties of conserved residues: Yellow – partial conservation; Red – acidic; Dark blue - basic; Pale blue – Gly/Pro; Pink – Asn/Gln; Green - His; Brown - Cys; Purple – Ser/Thr.

Table 2-2. GmhA kinetic parameters. Summary of kinetic parameters of wild type and mutant *E. coli* GmhA purified proteins. GmhA activity was determined using the malachite green phosphate detection assay by coupling product formation to HldE and GmhB and monitoring the release of inorganic phosphate spectrophotometrically at 660 nm. Reactions were initiated with S7P to final concentrations of 0 to 2 mM. A detection limit of 0.003 sec^{-1} was determined for this assay.

GmhA mutant	k_{cat} (sec^{-1})	K_m (mM)	k_{cat}/K_m (mM^{-1} sec^{-1})
Wild-type	0.44 ± 0.7	0.9 ± 0.3	0.5
H61Q	0.23 ± .07	1.2 ± 0.7	0.2
E65N	< 0.003	-	-
E65Q	< 0.003	-	-
R69Q	0.45 ± 0.1	0.5 ± 0.3	0.9
D94N	< 0.003	-	-
T120A	< 0.003	-	-
D169N	< 0.003	-	-
Q172E	< 0.003	-	-
H180Q	< 0.003	-	-

In vivo mutational analysis. To further explore the role of each residue in the active site, *in vivo* complementation studies were performed using *E. coli* BW25113Δ*gmhA*/pBAD30*gmhA* wild type and mutant expressing strains. A positive control strain, *E. coli* BW25113/pBAD30 (wild type + vector only), and negative control strain, *E. coli* BW25113Δ*gmhA*/pBAD30 (*gmhA* deletion + vector only), were also generated. Equivalent amounts of GmhA expression, and therefore complementation to the chromosomal deletion, were confirmed in each mutant strain by anti-histidine immunoblot (Appendix 5).

The growth of each *gmhA* expressing strain was analyzed to ensure the over-expression of *gmhA* did not have adverse effects. For the first 20 h, growth of all strains was consistent, as measured by OD_{600}. After 20 h growth, the OD_{600} of E65N, E65Q, Q172E, H180Q, and D94N expressing strains, as well as the negative control strain, reached a maximum of approximately 0.6, and actually began to decrease with time. Conversely, the remaining strains continued to increase in OD_{600} after 18 hours growth. By 48 hours, however, the OD_{600} of all strains reached a consistent level, suggesting the presence or absence of GmhA, whether present in basal or over-expressed levels, has little effect on the growth of *E. coli* cells.

The susceptibility of these mutant *gmhA* complemented strains to the antibiotic novobiocin was then examined (Figure 2-7A). Under normal wild type conditions with an intact LPS, *E. coli* is insensitive to novobiocin. In contrast, *E. coli* exhibiting a deep-rough phenotype where only lipid A and Kdo are synthesized, display increased sensitivity to novobiocin (Tamaki et al., 1971). This property was confirmed in the control strains, with the positive control exhibiting a novobiocin MIC of 1024 μg/mL, compared to an MIC of 64 μg/mL determined for the negative control (*gmhA* deletion, heptoseless) strain. The H61Q, R69Q, T120A and D169N complement strains were able to completely restore novobiocin resistance to positive control levels (Figure 2-7A). The D94N strain, showed increased sensitivity to drug within one dilution. The E65 mutant expressing strains, as well as Q172E and H180Q mutational strains, exhibited reduced MIC values. MIC values in each case approximated, within one drug dilution that of the negative control strain. The strain expressing H180Q demonstrated a slightly higher MIC value, while the strain expressing E65N/Q had slightly lower values. This represents a 10-fold decrease in MIC when compared to wild type levels.

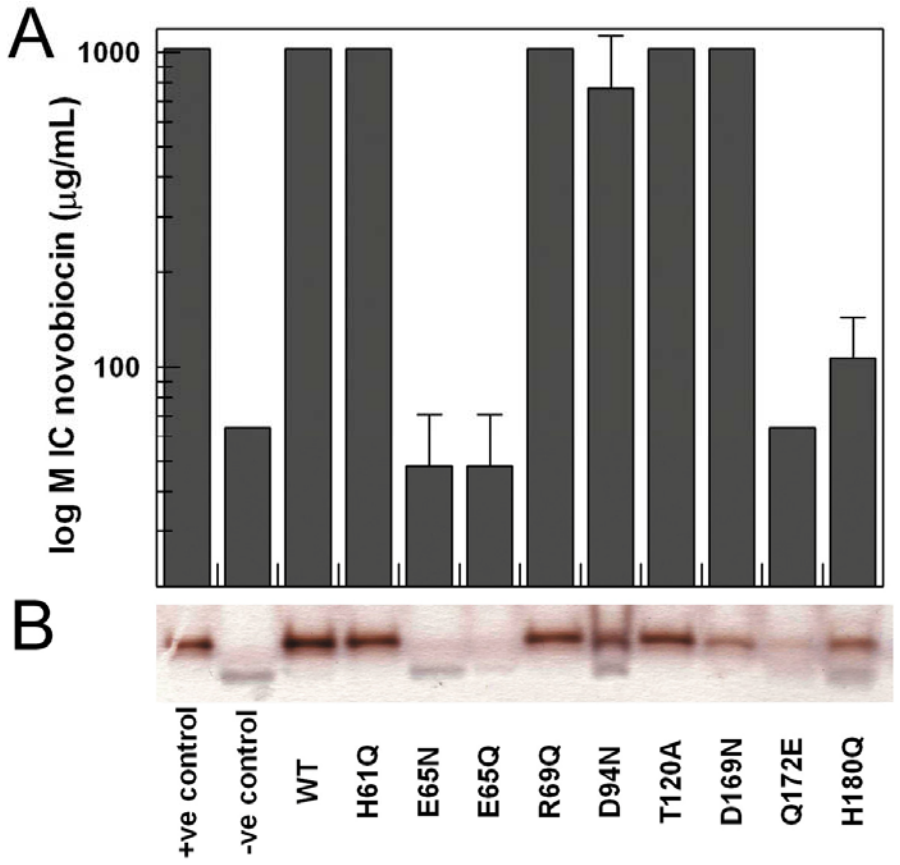

Figure 2-7. Novobiocin MIC and LPS analysis of GmhA mutants. (A) Minimum concentration of novobiocin required to inhibit the growth of *E. coli* BW25113pBAD30 (+ve control), BW25113Δ*gmhA* pBAD30 (-ve control), and BW25113Δ*gmhA* pBAD30*gmhA* mutant strains as described, to 90% of standard growth in the absence of drug (MIC). Strains were grown in M9 minimal media supplemented with 0.2% arabinose and 0 – 1024 µg/mL novobiocin. **(B)** LPS analysis of *E. coli* BW25113Δ*gmhA* pBAD30*gmhA* mutants by silver stained 10% SDS polyacrylamide gel electrophoresis. LPS was extracted from cultures of the above strains, grown overnight in M9 minimal media + 0.2% arabinose.

Intact LPS was extracted from each of the deleted *gmhA* strains containing the plasmids expressing the GmhA mutant forms and analyzed using silver stained 10% SDS PAGE. When viewed in this manner, truncated LPS can be differentiated from full length LPS based on relative migration distance since truncated LPS migrates much faster through the gel. As depicted in Figure 2-7B, H61Q, R69Q, T120A and D169N GmhA replacements do not affect LPS production, as the *gmhA*-deleted strains containing these proteins produce full length LPS. The remaining five GmhA constructs (E65N/Q, D94N, Q172E and H180Q) resulted in at least partially truncated LPS. The complete truncation due to both E65 mutant-expressing strains was consistent with MIC data, suggesting substantially reduced GmhA activity. Surprising, however, was the partial truncation due to Q172E and H180Q mutations. GmhA containing these mutations appear to be at least partially active *in vivo*. The partial truncation of D94N is also somewhat contradictory to MIC results, although the D94N expressing strain demonstrated decreased novobiocin MIC compared to wild type. Based on these data, it appears that complete LPS truncation is not required to sensitize *E. coli* to novobiocin. Rather, LPS can be partially truncated, as observed in the D94N mutant without compromising the membrane to a threshold limit, beyond which the permeability barrier is breached, as with the Q172E and H180Q mutants.

DISCUSSION

Structural analysis of GmhA. We have determined the 3D structures of GmhA from *E. coli* and the opportunistic bacterial pathogen *P. aeruginosa*, in apo, substrate- and product-bound forms. These structures complement available structures from *C. jejuni* and *V. cholerae* that have recently emerged from structural genomics studies (Seetharaman et al., 2006). The *E. coli* and *C. jejuni* proteins crystallize as tetramers in the asymmetric unit, while the *P. aeruginosa* and *V. cholerae* proteins crystallize as dimers; as is often the case, the contents of the crystallographic asymmetric unit do not necessarily reflect biological units of activity. Analytical ultracentrifugation studies performed in this work further suggest that the biologically active oligomeric state of GmhA is a tetramer. This interpretation is also supported by the extensive total surface areas buried in tetramer formation for apo (8400 $Å^2$), substrate (7550 $Å^2$) and product-bound (10380 $Å^2$) structures.

Of particular note when comparing the available structures of GmhA, is that all 6 available structures can be classified into one of two very distinct forms: an open and a closed form. The open form is characterized by an extended H3-β2 loop, an unstructured H3' region, and a less well-packed dimer-dimer interface. In the closed form the H3' region adopts a helical structure that in turn causes not only repositioning of the H3-β2 loop inward toward the active site cleft by ~20 Å but also permits more extensive dimer-dimer interactions resulting in a more compact tetramer. The open conformation is observed in structures of GmhA in apo and substrate-bound forms from *E. coli* and also in the apo structures from *P. aeruginosa* and *V. cholerae*. The closed conformation is observed in the apo and product-bound structures from *C. jejuni* and *P. aeruginosa*, respectively. The fact that only two conformations are observed despite structures having been determined in different space groups, from multiple organisms, and in three different states of ligand binding, suggests that GmhA is likely to exist in two distinct conformations. The open and closed conformations represent structures most suited for binding substrate and product, respectively. GmhA is an isomerase, and should be able to readily catalyze both forward and reverse reactions, suggesting that both S7P and D-*glycero*-α,β-D-*manno*-heptose 7-phosphate are 'substrates' of GmhA. With this in mind, it is not surprising that the structure of *C. jejuni* GmhA crystallized in the product bound, closed conformation even with no ligand bound.

Determination of GmhA mechanism of action. Results from both *in vivo* and *in vitro* analysis of GmhA mutational studies suggest the importance of residues E65, Q172 and H180 in enzyme activity. Amino acid substitutions at E65, D94, T120, D169, Q172 and H180 residues result in no observable GmhA activity when analyzed *in vitro* using the phosphate detection assay. Diminished activity of these mutants was expected since these residues are all located within the active site. However, it was difficult to elucidate the actual role of these residues in GmhA action from kinetic analysis alone. For this reason, *in vivo* studies were performed. Both *in vitro* and *in vivo* studies suggest that H61 and R69 play no significant role in GmhA activity, as wild type activity was maintained when

each was mutated. Conversely, E65, Q172 and H180 were deemed necessary in maintaining the LPS permeability barrier as illustrated in novobiocin MIC studies and supported by LPS analysis, suggesting these residues are important to GmhA function. The remaining mutated residues, D94, T120 and D169 did not alter the permeability of *E. coli* to novobiocin. This does not imply, however, that D94, T120 and D169 have no role in activity. There are a number of reasons why these mutations show diminished activity *in vitro* and not *in vivo*, specifically the nature of each assay. Kinetic studies were designed to assay the reaction over a limited time period. Furthermore, mutant proteins were over-expressed *in vivo*, which could help to restore protein activity based on the quantity of protein in the cell. With this consideration in mind, over-expression can be advantageous in demonstrating inactivity, as even with an abundance of protein, the activity of E65, Q172 and H180 could not be completely, or in the case of E65, even partially restored. The role of T120 was hypothesized to be involved in substrate-phosphate binding, as previously predicted by analogy to glucose 6-phosphate isomerase (Valvano et al., 2002). It is quite possible that the role of T120 could be partially compensated by surrounding residues, in particular S55, S119, S121 and S124, which are also predicted to function in phosphate binding. The D94 residue was not observed in the active site of the substrate-bound structure; rather, this mutation was designed based on contacts observed in the product-bound structure, between GmhA-D94 and bound product. D94 is unique amongst residues mutated within the active site and is of particular interest since it is donated from the opposing dimer (chain B). Other residues contributing to substrate or product binding originate from the A-D dimer. Sedimentation equilibrium analysis of both the wild type GmhA and GmhA-D94N mutant indicate that the *E. coli* protein exists as a tetramer in solution. Structural and mutational data also support a tetrameric GmhA, as the *E. coli* protein crystallized as a tetramer in the asymmetric unit and mutation of D94 show at least partial inhibition of GmhA activity. Interestingly, T120 (conserved phosphate binding pocket) and D94 (H3' region) belong to regions of GmhA primarily involved in product binding. Results from mutational studies are therefore consistent with the possibility that product stabilization is an important mechanism used by GmhA to establish desired isomerization reaction kinetics.

Given that E65 and H180 were identified as the most critical residues for GmhA activity, a mechanism of action of GmhA can be proposed by analogy to other known aldo-keto isomerases, with E65 and H180 acting as the catalytic residues. Histidine residues are often found involved in isomerase activity, acting most frequently as a catalytic base, facilitating the reaction through proton shuffling (Berrisford et al., 2006; Knowles, 1991). Specifically, the active site of the isomerase domain of glucosamine 6-phosphate (Gln6P) synthase has been shown to rely on His and Glu residues (Milewski et al., 2006; Teplyakov et al., 1998). This enzyme shares the greatest structural similarity to GmhA among currently characterized isomerases (Seetharaman et al., 2006). A structural comparison of the quaternary and active site structures of these two isomerase enzymes is provided in Appendix 6. As expected, a collection of four serine and threonine residues forms a structurally conserved phosphate-binding pocket. The catalytic E65 residue identified in $GmhA_{EC}$ is also structurally conserved. Further similarity exists for H180,

which is replaced by a lysine (K485) in Gln6P synthase, where the catalytic lysine (K603) of Gln6P synthase has no homologous residue in GmhA. The catalytic histidine (H504) of Gln6P is not conserved structurally; however, it does reside close to D94 within GmhA. Unlike Gln6P synthase, though, mutational analysis does not suggest that GmhA requires a third residue for activity, as fulfilled by H504 in Gln6P synthase, suggesting the S7P sugar ring opens non-enzymatically prior to catalysis. Interestingly, although Gln6P synthase exists as a dimer, each monomer contains two structurally related domains (Appendix 6). Each of these domains is homologous to a single monomer of GmhA. Thus, similar to GmhA, the isomerase portion of Gln6P synthase adopts an overall quaternary structure comprised of four structurally equivalent domains. This finding provides additional support for the biological significance of a GmhA tetramer.

A potential mechanism of action for GmhA, based on previous studies of the isomerase domain from Gln6P synthase, is outlined in Figure 2-8. This mechanism proposes that either E65 or H180 could act as the catalytic base, abstracting a proton from C2 of the S7P substrate, while the other residue would act as a catalytic acid, donating a proton to C1 for stabilization. The reaction then proceeds through the resulting *cis*-enediol intermediate resulting in an aldo form, which then cycles non-enzymatically to give the final product, D-*glycero*-α,β-D-*manno*-heptose 7-phosphate. While it is difficult to predict which residue, E65 or H180, performs each catalytic role, based on the complete absence of any activity when E65 is mutated, it can be hypothesized that E65 assumes the critical role of the catalytic base in this mechanism.

Together the crystallographic and mutational studies presented here offer new insight into the structure-function relationship of GmhA, an essential protein in maintaining the permeability barrier of Gram-negative bacteria. GmhA is highly conserved between pathogenic species, both in sequence and structure. As such, knowledge gained from the current studies of GmhA from *E. coli* and *P. aeruginosa* should be readily transferable to other pathogenic Gram-negative species. Inhibition of GmhA, in synergy with known Gram-positive antimicrobial agents, may aid in treatment of Gram-negative infection. An understanding of the structure and mechanism of GmhA are the first steps in exploiting the heptose biosynthetic pathway as a novel Gram-negative antimicrobial target.

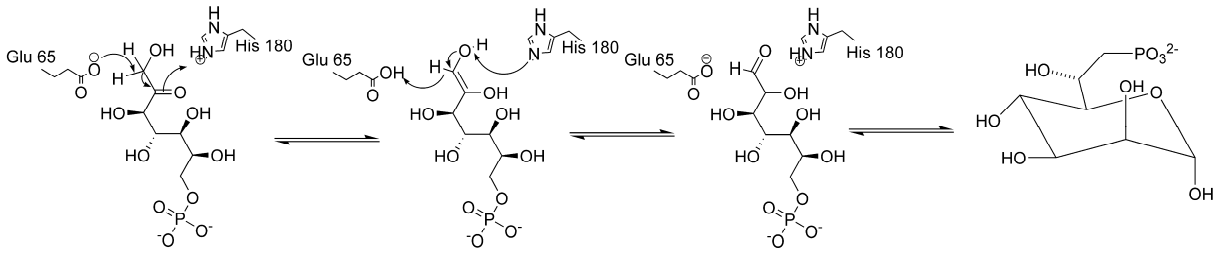

Figure 2-8. Proposed mechanism of GmhA. The GmhA catalyzed conversion of D-sedoheptulose 7-phosphate into D-*glycero*-D-*manno*-heptose 7-phosphate is predicted to proceed through an enediol intermediate, where E65 serves as the catalytic base and H180 serves as the catalytic acid.

REFERENCES

Baba, T., Ara, T., Hasegawa, M., Takai, Y., Okumura, Y., Baba, M., Datsenko, K.A., Tomita, M., Wanner, B.L., and Mori, H. (2006). Construction of *Escherichia coli* K-12 in-frame, single-gene knockout mutants: the Keio collection. Mol Syst Biol *2*, 2006 0008.

Berrisford, J.M., Hounslow, A.M., Akerboom, J., Hagen, W.R., Brouns, S.J., van der Oost, J., Murray, I.A., Michael Blackburn, G., Waltho, J.P., Rice, D.W.*, et al.* (2006). Evidence supporting a cis-enediol-based mechanism for Pyrococcus furiosus phosphoglucose isomerase. J Mol Biol *358*, 1353-1366.

Brooke, J.S., and Valvano, M.A. (1996a). Biosynthesis of inner core lipopolysaccharide in enteric bacteria identification and characterization of a conserved phosphoheptose isomerase. J Biol Chem *271*, 3608-3614.

Brooke, J.S., and Valvano, M.A. (1996b). Molecular cloning of the *Haemophilus influenzae* gmhA (lpcA) gene encoding a phosphoheptose isomerase required for lipooligosaccharide biosynthesis. J Bacteriol *178*, 3339-3341.

Brunger, A.T., Adams, P.D., Clore, G.M., DeLano, W.L., Gros, P., Grosse-Kunstleve, R.W., Jiang, J.S., Kuszewski, J., Nilges, M., Pannu, N.S.*, et al.* (1998). Crystallography & NMR system: A new software suite for macromolecular structure determination. Acta Crystallogr D Biol Crystallogr *54*, 905-921.

De Leon, G.P., Elowe, N.H., Koteva, K.P., Valvano, M.A., and Wright, G.D. (2006). An in vitro screen of bacterial lipopolysaccharide biosynthetic enzymes identifies an inhibitor of ADP-heptose biosynthesis. Chem Biol *13*, 437-441.

Eidels, L., and Osborn, M.J. (1971). Lipopolysaccharide and aldoheptose biosynthesis in transketolase mutants of *Salmonella typhimurium*. Proc Natl Acad Sci U S A *68*, 1673-1677.

Eidels, L., and Osborn, M.J. (1974). Phosphoheptose isomerase, first enzyme in the biosynthesis of aldoheptose in *Salmonella typhimurium*. J Biol Chem *249*, 5642-5648.

Emsley, P., and Cowtan, K. (2004). Coot: model-building tools for molecular graphics. Acta Crystallogr D Biol Crystallogr *60*, 2126-2132.

Fraternali, F., and Cavallo, L. (2002). Parameter optimized surfaces (POPS): analysis of key interactions and conformational changes in the ribosome. Nucleic Acids Res *30*, 2950-2960.

Fukui, K., Momoi, K., Watanabe, F., and Miyake, Y. (1988). In vivo and in vitro expression of porcine D-amino acid oxidase: in vitro system for the synthesis of a functional enzyme. Biochemistry *27*, 6693-6697.

Grossman, T.H., Kawasaki, E.S., Punreddy, S.R., and Osburne, M.S. (1998). Spontaneous cAMP-dependent derepression of gene expression in stationary phase plays a role in recombinant expression instability. Gene *209*, 95-103.

Jones, T.A., Zou, J.Y., Cowan, S.W., and Kjeldgaard, M. (1991). Improved methods for building protein models in electron density maps and the location of errors in these models. Acta Crystallogr A *47 (Pt 2)*, 110-119.

Kneidinger, B., Graninger, M., Puchberger, M., Kosma, P., and Messner, P. (2001). Biosynthesis of nucleotide-activated D-glycero-D-manno-heptose. J Biol Chem *276*, 20935-20944.

Kneidinger, B., Marolda, C., Graninger, M., Zamyatina, A., McArthur, F., Kosma, P., Valvano, M.A., and Messner, P. (2002). Biosynthesis pathway of ADP-L-glycero-beta-D-manno-heptose in *Escherichia coli*. J Bacteriol *184*, 363-369.

Knowles, J.R. (1991). Enzyme catalysis: not different, just better. Nature *350*, 121-124.

Krissinel, E., and Henrick, K. (2007). Inference of macromolecular assemblies from crystalline state. J Mol Biol *372*, 774-797.

Lee, S., Kirschning, A., Muller, M., Way, C., and Floss, H.G. (1999). Enzymatic synthesis of [7-14C, 7-3H] and [1-13C]sedoheptulose 7-phosphate and [1-13C]ido-heptulose 7-phosphate. J Mol Catal, B Enzym *6*, 369-377.

Loutet, S.A., Flannagan, R.S., Kooi, C., Sokol, P.A., and Valvano, M.A. (2006). A complete lipopolysaccharide inner core oligosaccharide is required for resistance of *Burkholderia cenocepacia* to antimicrobial peptides and bacterial survival in vivo. J Bacteriol *188*, 2073-2080.

Marolda, C.L., Lahiry, P., Vines, E., Saldias, S., and Valvano, M.A. (2006). Micromethods for the characterization of lipid A-core and O-antigen lipopolysaccharide. Methods Mol Biol *347*, 237-252.

McArthur, F., Andersson, C.E., Loutet, S., Mowbray, S.L., and Valvano, M.A. (2005). Functional analysis of the glycero-manno-heptose 7-phosphate kinase domain from the bifunctional HldE protein, which is involved in ADP-L-glycero-D-manno-heptose biosynthesis. J Bacteriol *187*, 5292-5300.

Milewski, S., Janiak, A., and Wojciechowski, M. (2006). Structural analogues of reactive interediates as inhibitors of glucosamine-6-phosphate synthase and phosphoglucose isomerase. Arch Biochem Biophys *450*, 39-49.

Morrison, J.P., and Tanner, M.E. (2007). A two-base mechanism for *Escherichia coli* ADP-L-glycero-D-manno-heptose 6-epimerase. Biochemistry *46*, 3916-3924.

Murshudov, G., Vagin, A., and Dodson, E. (1996). Paper presented at: Abstr Proc Daresbury Study Weekend (SERC, Daresbury Laboratory, Warrington, United Kingdom).

Nikaido, H. (2003). Molecular basis of bacterial outer membrane permeability revisited. Microbiol Mol Biol Rev *67*, 593-656.

Nikaido, H., and Vaara, M. (1985). Molecular basis of bacterial outer membrane permeability. Microbiol Rev *49*, 1-32.

O'Gara, M., Adams, G.M., Gong, W., Kobayashi, R., Blumenthal, R.M., and Cheng, X. (1997). Expression, purification, mass spectrometry, crystallization and multiwavelength anomalous diffraction of selenomethionyl PvuII DNA methyltransferase (cytosine-N4-specific). Eur J Biochem *247*, 1009-1018.

Onishi, H.R., Pelak, B.A., Gerckens, L.S., Silver, L.L., Kahan, F.M., Chen, M.H., Patchett, A.A., Galloway, S.M., Hyland, S.A., Anderson, M.S*., et al.* (1996). Antibacterial agents that inhibit lipid A biosynthesis. Science *274*, 980-982.

Otwinoski, Z., and Minor, W. (1997). Processing of X-ray diffraction data collected in oscillation mode. Methods Enzymol *276*, 307-326.

Pflugrath, J.W. (1999). The finer things in X-ray diffraction data collection. Acta Crystallogr D Biol Crystallogr *55*, 1718-1725.

Qoronfleh, M.W., Ho, T.F., Brake, P.G., Banks, T.M., Pulvino, T.A., Wahl, R.C., Eshraghi, J., Chowdhury, S.K., Ciccarelli, R.B., and Jones, B.N. (1995). Production of selenomethionine-labeled recombinant human neutrophil collagenase in *Escherichia coli.* J Biotechnol *39*, 119-128.

Raetz, C.R., and Whitfield, C. (2002). Lipopolysaccharide endotoxins. Annu Rev Biochem *71*, 635-700.

Seetharaman, J., Rajashankar, K.R., Solorzano, V., Kniewel, R., Lima, C.D., Bonanno, J.B., Burley, S.K., and Swaminathan, S. (2006). Crystal structures of two putative phosphoheptose isomerases. Proteins *63*, 1092-1096.

Sirisena, D.M., MacLachlan, P.R., Liu, S.L., Hessel, A., and Sanderson, K.E. (1994). Molecular analysis of the rfaD gene, for heptose synthesis, and the rfaF gene, for heptose transfer, in lipopolysaccharide synthesis in *Salmonella typhimurium.* J Bacteriol *176*, 2379-2385.

Tamaki, S., Sato, T., and Matsuhashi, M. (1971). Role of lipopolysaccharides in antibiotic resistance and bacteriophage adsorption of *Escherichia coli* K-12. J Bacteriol *105*, 968-975.

Teplyakov, A., Obmolova, G., Badet-Denisot, M.-A., Badet, M., and Polikarpov, B.I. (1998). Involvement of the C terminus in intramolecular nitrogen channeling in glucosamine 6-phosphate synthase: evidence from a 1.6 A structure of the isomerase domain. Structure *6*, 1047-1055.

Terwilliger, T.C. (2000). Maximum-likelihood density modification. Acta Crystallogr D Biol Crystallogr *56*, 965-972.

Terwilliger, T.C., and Berendzen, J. (1999). Automated MAD and MIR structure solution. Acta Crystallogr D Biol Crystallogr *55*, 849-861.

Tsai, C.M., and Frasch, C.E. (1982). A sensitive silver stain for detecting lipopolysaccharides in polyacrylamide gels. Anal Biochem *119*, 115-119.

Vagin, A., and Teplyakov, A. (1997). MOLREP: An automated program for molecular replacement. J Appl Crystallogr *30*, 1022-1025.

Valvano, M.A., Marolda, C.L., Bittner, M., Glaskin-Clay, M., Simon, T.L., and Klena, J.D. (2000). The rfaE gene from *Escherichia coli* encodes a bifunctional protein involved in biosynthesis of the lipopolysaccharide core precursor ADP-L-glycero-D-manno-heptose. J Bacteriol *182*, 488-497.

Valvano, M.A., Messner, P., and Kosma, P. (2002). Novel pathways for biosynthesis of nucleotide-activated glycero-manno-heptose precursors of bacterial glycoproteins and cell surface polysaccharides. Microbiology *148*, 1979-1989.

Wright, G.D., and Sutherland, A.D. (2007). New strategies for combating multidrug-resistant bacteria. Trends Mol Med *13*, 260-267.

Yethon, J.A., and Whitfield, C. (2001). Lipopolysaccharide as a target for the development of novel therapeutics in Gram-negative bacteria. Curr Drug Targets Infect Disord *1*, 91-106.

CHAPTER THREE

STRUCTURAL AND KINETIC CHARACTERIZATION OF THE LPS BIOSYNTHETIC ENZYME D-α,β-D-HEPTOSE-1,7-BISPHOSPHATE PHOSPHATASE (GMHB) FROM *ESCHERICHIA COLI*.

CHAPTER THREE PREFACE

The work presented in this chapter was previously published in:

Taylor, PL, Sugiman-Marangos, S, Zhang, K, Valvano, MA, Wright, GD, and Junop, MS. (2010) Structure and kinetic characterization of the LPS biosynthetic enzyme D-α,β-D-heptose-1,7-bisphosphate phosphatase (GmhB) from *Escherichia coli*. *Biochemistry,* **49**:1033-1041.

I co-authored this work with Dr. M. Junop and Dr. G. Wright. I conducted all substrate synthesis, the enzymatic characterization, mutational analysis, and secondary structure comparison of GmhB, as well as all *in vivo* experimentation.

Acknowledgements:

We would like to thank Leonid Flaks, Alexei Soares, and Robert Sweet for their technical assistance with structural data collection and Raquel Epand for her assistance with circular dichroism experiments. Structural data was collected at the National Synchrotron Light Source, Brookhaven National Laboratories, at Beamlines X8C and X12C.

ABSTRACT

Lipopolysaccharide is a major component of the outer membrane of Gram-negative bacteria and provides a permeability barrier to many commonly used antibiotics. ADP-heptose residues are an integral part of the LPS inner core and mutants deficient in heptose biosynthesis demonstrate increased membrane permeability. The heptose biosynthesis pathway involves phosphorylation and dephosphorylation steps not found in other pathways for the synthesis of nucleotide sugar precursors. Consequently, the heptose biosynthetic pathway has been marked as a novel target for antibiotic adjuvants, which are compounds that facilitate and potentiate antibiotic activity. D-α,β-D-heptose-1,7-bisphosphate phosphatase (GmhB) catalyzes the third essential step of LPS heptose biosynthesis. This study describes the first crystal structure of GmhB and enzymatic analysis of the protein. Structure-guided mutations followed by steady state kinetic analysis, together with established precedent for haloacid dehydrogenase (HAD) phosphatases, suggests that GmhB functions through a phosphoaspartate intermediate. This study provides insight into the structure-function relationship of GmhB, a new target to combat Gram-negative bacterial infection.

INTRODUCTION

The development of antimicrobial agents in the 20th century has resulted in dramatic declines in the number of deaths from infectious disease. The resulting widespread use and misuse of these drugs has provided selective pressure for the emergence of bacteria that are resistant to many commonly used antibiotics. In particular, Gram-negative pathogens resistant to most, if not all, currently available drugs, are proving to be especially concerning.

The Gram-negative outer membrane[1] (OM) provides a potent barrier to many drugs and is also essential for cell viability. OM drug targets, such as lipopolysaccharide (LPS) biosynthesis enzymes, are currently being explored to combat infection caused by Gram-negative pathogens. The outer membrane is an especially attractive target given the large arsenal of antibiotics clinically available to treat Gram-positive bacteria, which are ineffective against Gram-negative bacteria due to low permeability. Agents that could increase the permeability of the Gram-negative OM to such antibiotics may likely be advantageous for combination therapies with otherwise excluded antibiotics (Nikaido, 2001; Poole, 2002; Yethon and Whitfield, 2001).

The OM is an asymmetric bilayer consisting of an inner leaflet rich in phospholipids and an LPS-rich outer leaflet. The LPS component provides an effective permeability barrier to small, hydrophobic molecules. LPS typically consists of three major components: 1) lipid A and inner core oligosaccharide (OS), consisting of 2-keto-3-deoxy-D-*manno*-octulosonic acid (Kdo) and one or more L-*glycero*-D-*manno*-heptose residues; 2) an outer core OS made of various linked sugar residues; and 3) O antigen polysaccharide chains of variable length and composition (reviewed in (Nikaido, 2003; Nikaido and Vaara, 1985; Raetz and Whitfield, 2002; Yethon and Whitfield, 2001)). The lipid A-Kdo domain is highly conserved among most Gram-negative bacteria and is the minimum LPS structure required to maintain OM integrity for bacterial survival. Thus, several lipid A-Kdo biosynthetic steps are essential to bacterial growth and proven targets for antibiotics (Barb et al., 2007; Mdluli et al., 2006). The outer core OS and O antigen are not essential for bacterial growth, but they mediate host-microbe interactions, and contribute significantly to virulence and permeability of the OM to small molecules such as antibiotics (Raetz and Whitfield, 2002).

It is widely accepted that the strength of the diffusion barrier is due to the tight packing of the acylated lipid A and lateral interactions of individual LPS molecules (McArthur et al., 2005). Phosphorylated heptose molecules in the inner core OS bind divalent cations, cross-linking the LPS and further decreasing the permeability of the OM. Mutants in heptose biosynthesis lack this cross linking capability and while capable of survival in a laboratory setting they display markedly reduced antibiotic resistance and pathogenicity (Tamaki et al., 1971; Valvano et al., 2002). The biosynthetic pathway of the L-*glycero*-D-*manno*-heptose molecule in Gram-negative bacteria has been elucidated and is illustrated in Figure 3-1 (Kneidinger et al., 2001; Kneidinger et al., 2002). Starting from sedoheptulose 7-phosphate (S7P), sedoheptulose 7-phosphate isomerase (GmhA) is

the first committed enzyme in the pathway (Brooke and Valvano, 1996; Eidels and Osborn, 1974; Taylor et al., 2008). In *Escherichia coli,* phosphorylation at the 1 position of the resulting D-*glycero*-D-*manno*-heptose 7-phosphate is then catalyzed by the kinase moiety of the bifunctional D-*β*-D-heptose phosphate kinase/ D-β-D-heptose 1-phosphate adenyltransferase (HldE) (Valvano et al., 2000) (McArthur et al., 2005). A bifunctional HldE is present in bacteria such as *E. coli* and *Pseudomonas aeruginosa* based on genomic sequence comparison. However, in some organisms such as *Burkholderia cenocepacia*, a significant pathogen in cystic fibrosis patients, this bifunctional enzyme is replaced by two distinct enzymes, HldA and HldC, which accomplish the respective functions (Loutet et al., 2006). D-α,β-D-heptose-1,7-bisphosphate phosphatase (GmhB) catalyzes the removal of the 7 position phosphate (Kneidinger et al., 2001) (Kneidinger et al., 2002), while the adenyltransferase action of HldE (or HldC) transfers the AMP moiety from ATP giving rise to ADP-D-*glycero*-D-*manno*-heptose. Finally, ADP-D-β-D heptose epimerase (HldE) catalyzes the formation of ADP-L-*glycero*-D-*manno*-heptose, the precursor to the final LPS heptose molecule (Morrison and Tanner, 2007; Sirisena et al., 1994). This study focuses on GmhB, which performs the third conserved step in the ADP-heptose biosynthesis pathway.

Primary amino acid sequence analysis of GmhB has classified the protein within the haloacid dehydrogenase (HAD) family of hydrolyases, part of the large DDDD superfamily of phosphohydrolases, in which phosphatases represent a small component (Valvano et al., 2002). Members of this family, such as histidinol phosphate phosphatase (HisB) (Rangarajan et al., 2006) and β-phosphoglucomutase (Lahiri et al., 2003), have characteristic conserved motifs: motif I, DXDX(T/V), where the first aspartic acid is the attacking nucleophile on the substrate phosphate group, and the second protonates the dephosphorylated leaving group; motif II, S/T, is involved in binding the substrate phosphate; and motif III, (G/S)DXX(N/T)D, which comprises the remainder of the active site to orient the substrate and bind the catalytic divalent cation (Mg^{2+}). The catalytic aspartate, an invariant residue, makes use of the metal ion to attack the phosphorous of the substrate, resulting in cleavage of the phosphoester bond and formation of a phosphoaspartate intermediate. An activated water molecule then attacks the phosphoaspartate, releasing inorganic phosphate (Allen and Dunaway-Mariano, 2004; Lahiri et al., 2003; Lu et al., 2008). In this paper, we report for the first time the 3-D structure of GmhB and demonstrate by enzymatic and mutational analyses that GmhB is a member of the HAD family of phosphohydrolases.

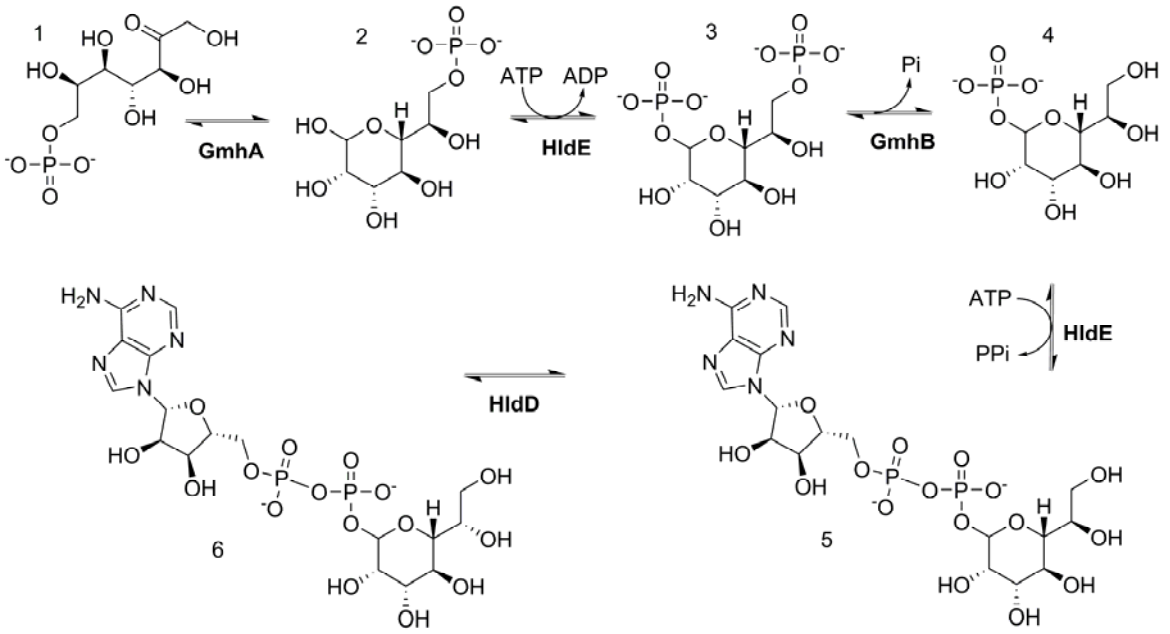

Figure 3-1. Schematic of the ADP-L-*glycero*-D-*manno*-heptose biosynthetic pathway. 1– sedoheptulose 7-phosphate; 2 - D-*glycero*-D-*manno*-heptose 7-phosphate; 3 - D-*glycero*-D-*manno*-heptose 1,7-bisphosphate; 4 - D-*glycero*-D-*manno*-heptose 1-phosphate; 5 - ADP-D-*glycero*-D-*manno*-heptose; 6 - ADP-L-*glycero*-D-*manno*-heptose.

MATERIALS AND METHODS

Expression plasmids. The IPTG inducible pET28a(+) (Novagen) plasmid pET28a(+)*gmhB*, encoding the *E. coli* GmhB with an N-terminal hexa-histidine tag (De Leon et al., 2006), was used for *in vitro* studies. The insert in pET28a(+)*gmhB* was excised between the *Xba*I and *Hind*III sites, purified by agarose gel electrophoresis, and ligated at these sites into a low-copy pBAD30 arabinose-inducible vector. The ligation reaction was conducted overnight at 16ºC using T4 DNA ligase (New England Biolabs) according to the manufacturer's protocol. The resulting plasmid, pBAD30*gmhB*, was used for *in vivo* studies.

Expression strains. *E. coli* BL21(DE3) (F^- *ompT gal dcm lon hsdS*$_B$(r_B^- m_B^-) λ [DE3: *lacI lac*UV5-T7 gene 1 *ind1 sam7 nin5*]) bacteria were transformed with pET28a(+)*gmhB* parental and mutant plasmids and used to overexpress these proteins for purification. A *gmhB* deletion strain (BW25113Δ*gmhB*) was generated by replacing the *gmhB* gene with a kanamycin resistance gene (Kan^R) in *E. coli* BW25113 (*lacI*^{q} *rrnB*$_{T14}$ Δ*lacZ*$_{WJ16}$ *hsdR514* Δ*araBA-D*$_{AH33}$ Δ*rhaBAD*$_{LD78}$), using the protocol described by Datsenko *et al*. (Datsenko and Wanner, 2000). Specific primers were designed with regions homologous to both the Kan^R from source vector pKD4 and the chromosomal *gmhB*: forward: 5'CGATACTAGCGTCACATGCCTTATTAAGGAGCTATAAAAGGTGTAGGCTGG AGCTGCTTC3';
reverse:5'AGCGGAAAAATGCATTTTTATTTCAACCGCTCATCTTTTAACATATG AATATCCTCCTTA 3'. Kan^R was amplified from pKD4 using these dual primers by PCR, digested with *DpnI*, and used to transform electrocompetent *E. coli* BW25113 pKD46. Transformants were grown sequentially on LB agar + 15 μg/mL kanamycin (O/N, 37°C), LB agar (43°C, 2hrs), LB agar + 50 μg/mL kanamycin (O/N 37°C). Loss of the helper plasmid pKD46 was confirmed by lack of growth on LB agar +100 μg/mL ampicillin at 37°C, O/N.

Mutagenesis. Site-directed mutations were generated in the pET28a(+)*gmhB* using QuikChange Site Directed Mutagenesis (Stratagene), according to the manufacturer's protocol. Site-directed mutants and their corresponding primers are described in Appendix 7. Mutations were verified by plasmid DNA sequence analysis (MOBIX, McMaster University) using vector specific sequencing primers (Appendix 7).

GmhB protein purification. Parental and mutant hexa-his-tagged GmhB proteins were over-expressed and purified from their respective *E. coli* BL21(DE3) pET28a(+)*gmhB* strains by immobilized metal affinity chromatography using a 5 mL NiNTA chelating column (Qiagen) and an imidazole gradient (GmhB Buffer A – 50 mM HEPES pH 8.0, 20 mM imidazole; GmhB Buffer B – 50 mM HEPES pH 8.0, 250 mM imidazole), as previously described (De Leon et al., 2006). Fractions containing purified protein were verified using SDS polyacrylamide 15% gel electrophoresis, combined, dialyzed overnight in 20 mM HEPES pH 8.0 and concentrated using Amicon 5 Ultra centrifugation filters (Millipore). Protein concentration was determined by Bradford assay and proteins were stored at -20ºC in 50% (v/v) glycerol. Seleno-methionine (SeMet)-

labeled GmhB for SAD phasing was prepared using a previously described method (Hendrickson et al., 1990) and purified as described above .

3D- Structure Determination of GmhB. GmhB crystals were all grown at 20^{o}C using the hanging-drop vapour diffusion method. Native GmhB (9.6 mg/mL in 3% (v/v) isopropanol) was mixed 1 μL to 1 μL with crystallization solution (25% (w/v) polyethylene glycol (PEG)-3350, 0.1 M Tris pH 8.5, and 0.02 M sodium chloride) and dehydrated against 0.5 mL crystallization solution. GmhB-SeMet (3.8 mg/mL in 3% (v/v) isopropanol) was mixed 4 μL to 2 μL with crystallization solution (25% w/v polyethylene glycol (PEG)-3350, 0.1 M Tris pH 7.8, 0.005 M DTT, 0.025 M sodium chloride, and 11% (v/v) glycerol) and 0.6 μL 0.018 M N-dodecyl-β-D-maltoside and dehydrated against 0.5 mL crystallization solution. Co-crystals of calcium-bound and calcium and phosphate-bound GmhB were obtained by overnight soaking of native GmhB crystals in either 0.005 M calcium chloride, or 0.005 M calcium chloride and 0.005 M sodium phosphate.

Native and SeMet apo datasets were collected at wavelengths of 1.1 and 0.979 Å on X8C and X12C beamlines, respectively of the National Synchrotron Light Source at Brookhaven National Laboratory. Datasets were processed and scaled with d*TREK (Pflugrath, 1999) to 1.5 and 1.85 Å respectively. All 16 of the expected SeMet sites were located using HYSS (Adams et al., 2002; Pflugrath, 1999). Phasing and density modification carried out with CNS was used to generate an experimental map. CNS (Brunger et al., 1998) and Coot (Emsley and Cowtan, 2004) were used to build an initial model using the SeMet data. This model was then refined against the higher resolution native dataset. Calcium and calcium/phosphate-bound datasets were collected at a wavelength of 1.54 Å with an R-AXIS IV image-plate detector using a Rigaku RU300 rotating-anode x-ray generator. Datasets were processed and scaled with d*TREK to 1.7 and 1.95 Å respectively. The structure of apo GmhB was used as an initial search model for molecular replacement. Both GmhB co-crystal structures were solved by molecular replacement using PHASER (McCoy et al., 2007) from the PHENIX software package (Adams et al., 2002). Model building and refinement of all GmhB structures was carried out through multiple iterations of Coot and REFMAC5 (G. Murshudov and Dodson, 1996) until R values and geometry statistics reached suitable ranges (Table 3-1). All protein structures were illustrated using PyMOL Molecular Graphics Systems (DeLano Scientific LLC, http://www.pymol.org).

Computational substrate docking. The X-ray structure of GmhB·Ca·P, PDB ID 3ESR, was used as a starting model. D-*glycero*-D-*manno*-heptose 1,7-bisphosphate (HBP) was built and restraint libraries generated using the monomer library sketcher program included in the CCP4 program suite (Collaborative computational project, 1994). The resulting HBP model was manually docked into the putative active site of GmhB using Coot such that the cleavable phosphate overlapped with the phosphate from the X-ray structure. The molecular modeling program ZMM (ZMM Software Inc., Ontario, Canada) was used to generate a double-shell model of GmhB centered around the coordinates of the phosphate atom with a 5 Å flexible shell and 10 Å rigid shell. Energy calculations were performed by the Monte Carlo Minimization (MCM) method using the AMBER

force field. The HBP substrate molecule was subjected to 2,000 random samplings within the double-shell model of GmhB to determine its optimal position, orientation and conformation within the putative active site. The lowest energy structure was then further MC-minimized until the energy did not decrease following 2,000 minimizations.

D-*glycero*-D-*manno*-heptose 1,7-bisphosphate synthesis. D-*glycero*-D-*manno*-heptose 1,7-bisphosphate (HBP) was synthesized enzymatically from ribose 5-phosphate, D-serine and ATP in two steps. First, sedoheptulose 7-phosphate (S7P) was synthesized enzymatically as previously described (Lee, 1999; Taylor et al., 2008). Enzymes were removed using an Amicon Ultra 5 concentrator (3000 rpm, 4ºC, 30 min) to stop the reaction. The filtrate was then combined in a second 5 mL reaction mixture with 25 mM phosphoenolpyruvate (PEP), 30 mM ATP, 10 mM KCl, 20 units pyruvate kinase (Sigma), and 1 mg HldE. 1.5 mg GmhA was used to initiate the reaction. Twenty µL of sample were removed at 0, 1, 3 and 20 h. Purity of the HBP product was monitored by analytical reverse phase HPLC (Acclaim TM^{20} column, 3 µm 120 Å, 4.6 x 150 mm) using water gradients with 0.05 % formic acid as counter ion. Product identification was verified by liquid chromatography electrospray mass spectrometry (LC/ES-MS) analysis using a QTRAP-LC/MS/MS (Applied Bosystems). After 20 h, the enzymes were again removed using an Amicon Ultra 5 concentrator (3000 rpm, 4ºC, 30 min). The filtrate was applied to a 50 mL Q-Sepharose anion exchange column and the product eluted using a 0-1 M ammonium acetate gradient. Fractions were analyzed by LC/MS and those containing product were combined, lyophilized, washed with water, and lyophilized again. The lyophilized product was stored at -20ºC. HBP product was confirmed after each step by LC/ES-MS and final product was confirmed by ^{13}C, and ^{31}P NMR Both LC/ES-MS and NMR results suggest the presence of minor substrate contaminations in the final product.

GmhB Steady State Kinetic Analysis. The malachite green-phosphomolybdate phosphate detection assay was used in GmhB kinetic studies as previously described (De Leon et al., 2006) with the following modifications. The reaction mixture consisted of 20 mM HEPES pH 8.0, 10 mM $MgCl_2$, 10 mM KCl, and 0.0024 nmol GmhB, in a total volume of 90 µL. Reactions were initiated with 10 µL of HBP product. Reactions were stopped after 10 min, where the reaction remains in the linear range, using 5% trichloroacetic acid. 20 µL of the stopped reaction was diluted to 50 µL with H_2O. Two hundred µL of malachite green phosphomolybdate reagent was added and A_{660nm} was measured after 5 min. Initial rates were fit to (eq 1) describing
Michaelis-Menten kinetics using Grafit 4 software (Erithacus Software, Staines, U.K.).

$$\upsilon = k_{cat}E_t[S]/(K_m + [S]) \text{ (eq. 1)}$$

The same procedure was used to determine the concentration of HBP present in each reaction, except 1 mM ATP and 1.5 µg HldE are added to the reaction mixture and 2 – 500X dilution of the original HBP solution were used to initiate the 60 min reaction.

Secondary structure comparison. Circular dichroism spectra of GmhB and GmhB C107A were collected using an AVIV spectropolarimeter equipped with temperature control. Samples were prepared at a concentration of 14 and 22 μM, respectively, in a buffer containing 5 mM HEPES pH 8.0, 5% glycerol. The background spectrum of this buffer was subtracted from all measurements. A 1-mm-path-length quartz cuvette was used for all analysis. Scans were performed from 260 to 200 nm, every 1.0 nm with 30 s equilibration at each point, at 25°C. The spectra are reported as mean residue molar ellipticity ($[\theta_n]$, ° cm^2 $dmol^{-1}$) as calculated with CDPRO software and equation 2:

$$[\theta_n] = [\theta_n]_{observed} \text{ x } (c \text{ x } \# \text{ residues})^{-1} \quad \text{(eq. 2)}$$

where $[\theta_n]_{observed}$ is the ellipticity measured and c is molar concentration of the protein.

In vivo complementation studies. The low-copy pBAD30*gmhB* was used to transform *E. coli* BW25113Δ*gmhB* cells to create a *gmhB* complemented strain. Positive and negative control strains were created by introducing pBAD30 into BW25113 and BW25113Δ*gmhA* cells, respectively. Bacteria were cultured overnight at 37 ºC in M9 minimal medium + 0.2 % arabinose + 100 μg/mL ampicillin. Minimal inhibitory concentrations (MIC) of novobiocin were determined as follows: Overnight cultures, as described above, were diluted to an optical density of 600 nm (OD_{600}) 0.11 and further diluted 1 in 200. Strains were grown at 37ºC in 96 well plates in the presence of varying concentrations of DMSO dissolved novobiocin (2 to 1024 μg/mL). OD_{600} was measured after 24 h to assay growth.

LPS extraction and detection. *E. coli* BW25113Δ*gmhA* pBAD30*gmhB* and control strains were grown at 37 ºC for 20 h in M9 minimal medium + 0.2 % arabinose + 100 μg/mL ampicillin. LPS was extracted from these cells as previously described (Marolda et al., 2006; Taylor et al., 2008). LPS samples were analyzed by SDS polyacrylamide 10 % gel electrophoresis and detected by silver staining as previously described (Taylor et al., 2008).

RESULTS

GmhB 3D-Structure. The structure of apo GmhB from *E. coli* was solved by SAD phasing and refined to 1.50 Å with R and R_{free} values of 16.0 and 21.0, respectively (Table 3-1). GmhB was crystallized in the space group $P2_12_12_1$ with two monomers in the asymmetric unit that superimpose with an r.m.s.d of 0.77 Å. GmhB·Ca and GmhB·Ca·P crystallized in the space group $P2_12_12$ with one monomer in the asymmetric unit and were solved by molecular replacement using the apo structure as a search model. The final structures were refined to 1.70 Å and 1.95 Å, with R and R_{free} values of 20.0 % and 26.0 %, and 21.0 % and 28.0 %, respectively. The oligomerization state of the protein in solution appears to be monomeric, as suggested by the program PISA, and consistent with gel filtration experiments (data not shown).

The structure of GmhB (Figure 3-2) consists of a single domain with an α/β Rossman fold motif made up a of six parallel β-strands (β6-β5-β4-β1-β2-β3) sandwiched between two sets of three α-helices. A search for structural homologs using a DALI server revealed GmhB to have significant homology only to members of the HAD family of proteins (Z score > 10). Two co-crystal structures were determined in the presence of calcium. However only the GmhB·Ca·P structure is depicted in Figure 3-3A, as the GmhB·Ca structure provided no additional structural insight. Both structures contained a single Ca^{2+} ion situated at the C-terminal end of β1, coordinated by the side chains of residues D11 and D136, the main chain of D13, and three solvent molecules (Figure 3-3A). D11 and D13 fulfill the aspartate requirement of the conserved DXDX(T/V) motif I observed in the HAD family of phosphatases, while D136 is part of conserved motif III. In the structure of GmhB·Ca·P, the O atoms of the phosphate molecule overlay precisely with four well-ordered water molecules in the structure of GmhB·Ca and the phosphate coordinates the Ca^{2+} ion in place of one of the solvent molecules. Binding of a divalent metal ion appears to stabilize the active site, as B-factors associated with residues D11, D13 and D136 are all reduced relative to their average apo values in the presence of the Ca^{2+} ion. The bound phosphate interacts with the side-chains of residues D11, D13, T53, and K111, and the main-chain atoms of R12, D13, and N54, as well as a single contact with the Ca^{2+} ion. T53 corresponds to the requisite S/T from motif II of HAD phosphatases and binds the phosphate moiety as predicted. No major differences are observed in the positions of the main chain atoms between the apo and bound structures, and only relatively minor movements are observed in the side chains of residues in proximity to the Ca^{2+} ion and phosphate molecule. The complete HBP substrate was modeled into the GmhB·Ca·P structure using the position of the bound phosphate observed in this structure, as shown in Figure 3-3B. The substrate was readily modeled into the binding pocket without major changes to the position of the bound phosphate or any of the interacting residues.

Table 3-1. GmhB X-ray data collection and refinement statistics

	Dataset			
	Apo (Selmet)	**Apo (Native)**	**Calcium-bound**	**Calcium and Phosphate-bound**
Data collection				
Space group	$P2_12_12_1$	$P2_12_12_1$	$P2_12_12$	$P2_12_12$
Cell parameters				
a,b,c (Å)	*52.00, 64.87, 103.39*	*51.90, 63.98, 103.32*	*63.90, 50.58, 52.64*	*64.18, 50.45, 52.02*
α, β, γ (°)	*90, 90, 90*	*90, 90, 90*	*90, 90, 90*	*90, 90, 90*
Molecules in ASU	*2*	*2*	*1*	*1*
Resolution (Å)[a,b]	46.46 - 1.85 (1.92 - 1.85)	40.19 - 1.50 (1.55 - 1.50)	40.62 - 1.70 (1.76 - 1.70)	39.65 - 1.95 (2.02 - 1.95)
Unique reflections	57, 709	54, 729	18, 244	11, 271
Redundancy[a]	7.17 (7.06)	5.47 (3.34)	3.64 (2.36)	3.79 (3.33)
Completeness (%)[a]	100.0 (100.0)	99.8 (93.1)	94.2 (80.0)	88.5 (98.2)
$I/\sigma(I)$ [a]	16.8 (4.9)	22.7 (4.4)	13.9 (3.2)	13.5 (3.2)
R_{merge} (%)[a]	5.6 (36.3)	3.1 (25.3)	4.7 (31.3)	5.5 (34)
Model and refinement				
Resolution (Å) [a]		25.00 - 1.50	40.62 - 1.70	39.65 - 1.95
R_{work}/R_{free} (%)		16.0 / 21.0	20.0 / 26.0	21.0 / 28.0
$Reflections_{observed}$		51, 887	17, 299	10, 728
$Reflections_{Rfree}$		2, 761	944	540
No. atoms		3, 617	1, 617	1, 538
R.m.s.d. bond				
Lengths (Å)		0.01	0.02	0.02
Angles (°)		1.38	1.5	1.79
B factor (Å^2)	Protein	21.49	28.35	33.95
	Ligand/ion	20.43	24.92	39.82
	Water	33.08	38.28	39.24
PDB ID code		2GMW	3ESQ	3ESR

[a] Statistics for the highest resolution shell are shown in parentheses.
[b] Data cut-off F>0

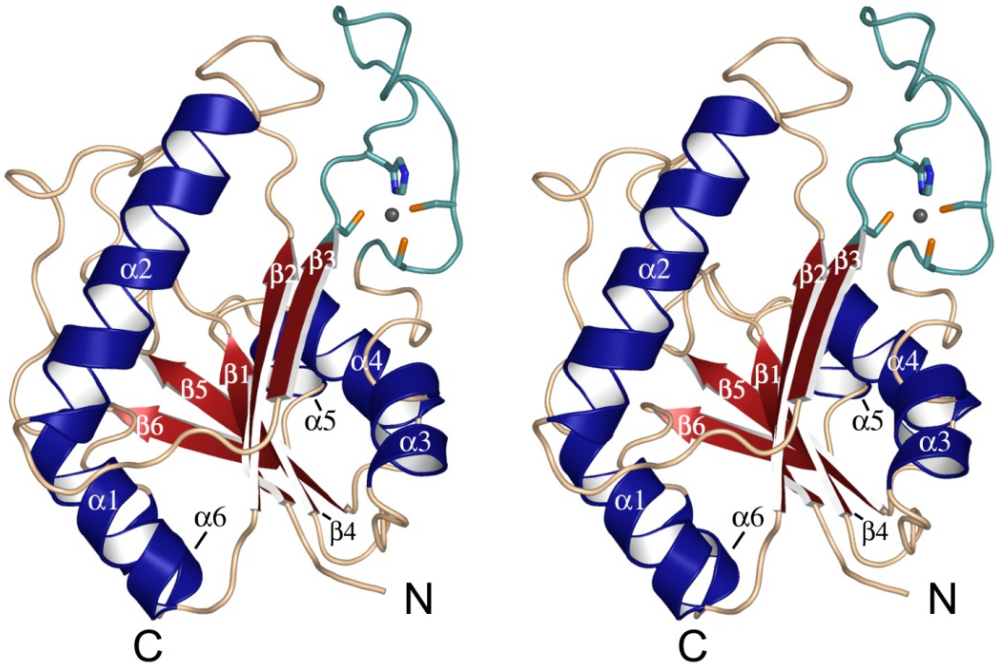

Figure 3-2. Structure of apo GmhB. A stereo ribbon diagram of the GmhB crystal structure. Helices (blue) and beta strands (red) are labeled sequentially according to their primary structure. Residues (C92, H93, C107, and C109) within the β3-α3 loop (cyan) are shown coordinated to a Zn^{2+} ion (grey).

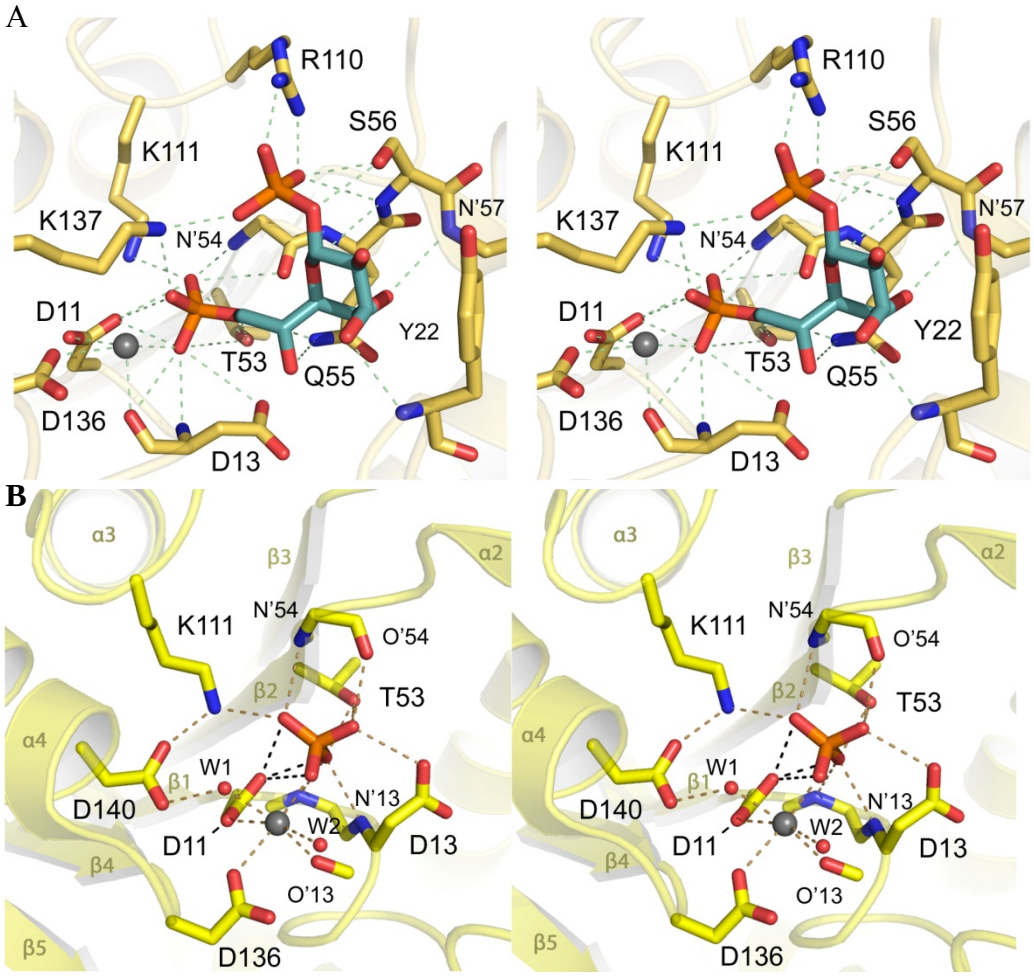

Figure 3-3. GmhB active site. (A) Stereo view of residues and main chain atoms observed to interact with Ca^{2+} (grey) and/or phosphate ions in the GmhB crystal structure. Helices and beta strands are labeled as in Figure 3-2. Two water molecules (red spheres) that coordinate the divalent metal ion are labeled W1 and W2. Metal coordination, hydrogen bonding and ionic interactions are indicated with dashed lines. **(B)** Stereo view of a modeled substrate-bound GmhB structure. The HBP substrate (cyan) was computationally modeled into the active site of GmhB using the phosphate ion coordinates from the GmhB·Ca·P structure as an initial orientation restraint anchor.

A single Zn^{2+} ion is coordinated by the side chains of amino acid residues C92, H93, C107, and C109, and is located at the base of the loop connecting β3 and α3 (Figure 3-2, cyan coloured loop). As no Zn^{2+} was included in the crystallization buffer, the ion likely plays an important role in structural stability and was probably carried over from purification. The described Zn^{2+} binding pocket has no relationship to any of the known motifs described for this family of proteins, further suggesting its role in secondary structural stability of the protein, rather than catalysis.

GmhB mutagenesis and kinetic characterization. GmhB residues were chosen for analysis based on crystallographic data of the *E. coli* enzyme and its similarity to other members of the HAD superfamily (Appendix 8). The predicted catalytic aspartate, D11, and the predicted general acid, D13, were mutated to confirm their predicted essentiality for catalysis based on HAD enzyme precedent and to probe the GmhB mechanism. A predicted catalytic lysine, K111, involved in phosphate binding and stabilization, was also mutated. Finally, to determine the importance of the Zn^{2+} located in the β3-α3 loop, one of the three coordinating cysteines (C107) was selected for mutagenesis.

To monitor GmhB activity directly, we synthesized and purified its substrate, D-*glycero*-D-*manno*-heptose 1,7-bisphosphate (HBP). GmhB activity was measured spectrophotometrically directly through the formation of the inorganic phosphate product, which binds the malachite green/molybdate complex. Using the HBP substrate, activity analysis of purified GmhB wild type and mutant proteins was conducted (Table 3-2). D11N, D13N, and K111A mutants appear to be inactive, with no measurable activity observed from either of these mutants ($k_{cat} < 0.003\ s^{-1}$), compared to wild-type activity levels ($k_{cat}/K_m = 176\ M^{-1}s^{-1}$). These results indicate that, as predicted, D11N, D113N and K111A are all essential for enzyme activity, marking the active site of the protein. Conversely, the Zn^{2+} binding pocket, does not appear to be involved directly in activity, as the creation of a C107A mutant only lowers specificity approximately 5-fold ($k_{cat}/K_m = 26\ M^{-1}s^{-1}$). The role of C107A in structural stability is supported by a significant change to the secondary structure due to the C107A replacement, compared to the wild type enzyme, as observed in the circular dichroism spectra (Appendix 9).

Table 3-2. GmhB kinetic parameters. GmhB wild-type and mutant protein steady state kinetic characterization as determined by the malachite green phosphate detection assay.

Mutant	k_{cat} *(sec^{-1})*	K_m *(mM)*	k_{cat}/K_m *(sec^{-1} mM^{-1})*
WT	36 ± 2	0.20 ± 0.03	176
D11N	< 0.003	-	-
D13N	< 0.003	-	-
C107A	17 ± 4	0.7 ± 0.3	26
K111A	<0.003	-	-

In vitro genetic complementation studies. Deletion of genes encoding most of the enzymes required for ADP-heptose biosynthesis from the *E. coli* chromosome has been shown to cause a detrimental effect on the production of full-length LPS (McArthur et al., 2005) (Brooke and Valvano, 1996). However, Kneidinger *et al.* demonstrated that the deletion of *gmhB* results in a partially truncated, functioning LPS (Kneidinger et al., 2002). To confirm this observation, and test whether or not deleting *gmhB* from the chromosome increases susceptibility to novobiocin, *gmhB* was deleted from the *E. coli* BW25113 chromosome and replaced with a kanamycin resistance gene, using the method described by Datsenko *et al*. (Datsenko and Wanner, 2000). Appendix 9 shows that while deleting *gmhA* from the chromosome results in a 10 fold decrease in MIC of novobiocin, deleting *gmhB* fails to impact the MIC, compared to the parental strain. Similarly, as previously observed, deletion of *gmhB* does not appear to disrupt full-length LPS production (Appendix 10). These observations suggests that another protein present in *E. coli* is able to at least partially compensate for the loss in GmhB activity to maintain LPS integrity, and precluded further *in vivo* experimentation on the GmhB mutants.

DISCUSSION

Based on the protein structural and mutagenic evidence presented here as well as precedent for HAD phosphatases, we propose a mechanism of action for GmhB (Figure 3-5). The structure of GmhB is similar to other phosphatases belonging to the HAD superfamily of enzymes, as demonstrated in Figure 3-4 (*16)*. Members of the HAD superfamily function through nucleophilic attack of the substrate phosphate by a conserved aspartic acid residue, forming a phosphoaspartate enzyme intermediate. The dephosphorylated product is then protonated at the site of attack by a second aspartate serving as a general acid and the product is released from the active site. In the final step, an activated water molecule attacks the phosphoaspartate intermediate, releasing inorganic phosphate and returning the enzyme to its original form (Allen and Dunaway-Mariano, 2004; Lahiri et al., 2003; Lu et al., 2008; Rangarajan et al., 2006). Based on the structural similarity observed, D11 is predicted to be the catalytic aspartic acid of GmhB, essential for forming the phosphoenzyme intermediate by attacking the 7 position phosphate of HBP. In the GmhB·Ca·P structure (Figure 3-3), D11 is perfectly situated to carry out this function, and mutagenesis confirmed its essentiality for catalysis of the deprotonation of HBP. D13, in turn, would function as the active site general acid required to protonate the C7 hydroxyl to form the D-*glycero*-D-*manno* heptose-1-phosphate product, and also to activate a water molecule in the final step to initiate inorganic phosphate release. This residue is positioned appropriately in the GmhB·Ca·P structure to carry out these functions, and was observed to be necessary for GmhB activity with HBP. Based on structural similarity, D13 and D136 would be expected to coordinate the divalent metal ion in the active site, and appear to do so, based on the contacts made with the Ca^{2+} present in the active site of the GmhB·Ca and GmhB·Ca·P structures. Similarly, K111 and T53 are predicted to stabilize the phosphoryl group in the active site. Removal of the functional properties of K111 rendered GmhB inactive, suggesting the importance of this residue to catalysis. As well, both K111 and T53 make strong contacts with the phosphate moiety found within the active site, supporting this prediction. Therefore, as outlined in Figure 3-5, we predict that GmhB converts HBP to H1P via a phosphoaspartate intermediate, utilizing the same mechanism demonstrated for other phosphatases of the HAD super family of enzymes.

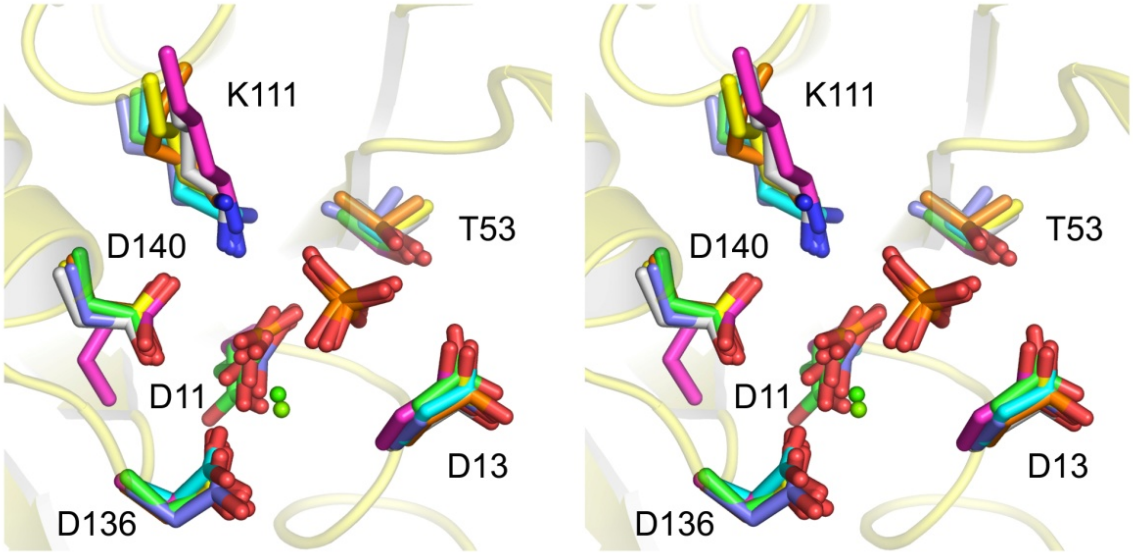

Figure 3-4. Comparison of the active site of HAD family proteins with GmhB. Conserved active site residues from within Motif I and II of HAD family members are shown structurally aligned with analogous residues from GmhB. Residues from different proteins are color coded as follows: phosphoserine phosphatase, green (PDB 1F5S); deoxy-D-mannose-octulosonate 8-phosphate phosphatase, cyan (PDB 1J8D); beta-phosphoglucomutase, purple (PDB 1O03); human polynucleotide kinase-3' phospatase, white (PDB 1YJ5); HAD subclass IIB sugar phosphatase, light blue (PDB 1YMQ); phosphonoacetaldehyde hydrolase, orange (PDB 2AH5); GmhB, yellow (PDB 3ESR). Inorganic phosphate and/or divalent metal ions present in 1F5S, 1YMQ and 3ESR structures are also shown for comparison.

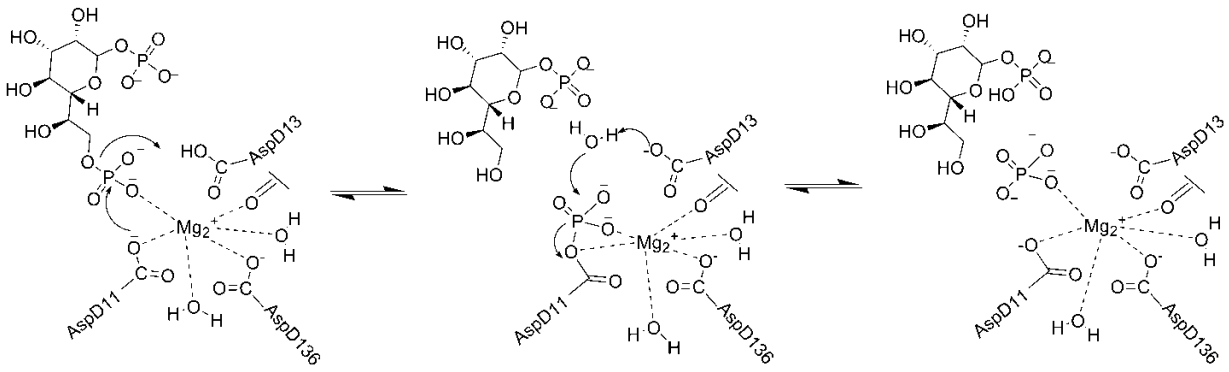

Figure 3-5. GmhB predicted mechanism. The GmhB catalyzed conversion of D-α,β-D-heptose 1,7-bisphosphate to D-α,β-D-heptose 1-phosphate is predicted to proceed through an aspartylphosphate intermediate.

The GmhB structure also features a Zn^{2+} ion that stabilizes the β3-α3 loop region (Figure 3-2). Although, this feature is not observed in most other HAD family member structures, and is not expected to play a role in catalysis, it is absolutely conserved amongst GmhB homologs and the structurally related histidinol phosphate phosphatase (HisB). The residues involved in coordinating the Zn^{2+} ion are situated on either end of this relatively large loop region. A cysteine to alanine substitution at residue 107 resulted in only a slight decrease in GmhB activity, compared to the lack of observable activity when similar analysis was carried out with predicted active site residues (Table 3-2). Therefore, the function of C107 and its bound Zn^{2+} do not appear to be necessary for catalysis. Although distal from the active site, C107 and C109 lay only a couple of residues upstream of the catalytic lysine, K111, and likely confer a measure of stability to this important residue through association with the Zn^{2+} ion. It is not uncommon for enzymes to use a bound Zn^{2+} for stability purposes (Berg and Godwin, 1997).

GmhB displays relatively high sequence similarity (50%) to *E. coli* HisB, a protein involved in histidine biosynthesis. A recent structural study of HisB in complex with a number of ligands have been used as a basis for proposing a unique mechanism for its phosphatase activity (Rangarajan et al., 2006). GmhB and HisB are suggested to be by-products of a gene duplication event of an ancestral HAD family phosphatase with comparatively flexible substrate specificity (Brilli and Fani, 2004). This would suggest that while GmhB and HisB differ in their selection of substrates, they may still share similar modes of catalysis. Despite the evidence from Brilli *et al.* that GmhB and HisB are encoded by paralogous genes (Brilli and Fani, 2004), key structural characteristics of the proposed HisB mechanism are notably absent from the structures of GmhB reported in this study. In both metal-ion bound structures reported, only a single metal binding site was observed in the active site cleft of GmhB despite rigorous inspection of the electron density. Additionally, the key residue (F23) involved in coordinating the second metal ion as described in the HisB mechanism is part of a three-residue insertion in the loop connecting β1 and α1 that is universally absent in GmhB (Appendix 8). Given these significant differences, it would appear that GmhB carries out its function in a manner typical to that described for HAD family phosphatases, and does not mimic the distinct mechanism described for HisB.

GmhB catalyzes a reaction essential to the biosynthesis of ADP-heptose. In the struggle to identify new methods to combat antibiotic resistance, this molecule represents one of the known targets that remains untapped. The appeal to target ADP-heptose biosynthesis is two-fold: 1) the outer core OS and O antigen of Gram-negative bacteria are essential for virulence, and 2) disruption of the OM rescues the effectiveness of numerous clinically useful antibiotics. Unlike the other three enzymes in the ADP-heptose biosynthetic pathway, the deletion of *gmhB* does not induce susceptibility to these antibiotics, specifically novobiocin, nor does it sufficiently truncate LPS in *E. coli*. This finding suggests that one or more other phosphatases may be present in the *E. coli* genome that can compensate for the lack of GmhB activity, and corroborates the findings of Kneidinger *et al.* (Kneidinger et al., 2002). It should be noted, though, that GmhB has been deemed an essential enzyme for OM heptose biosynthesis in other clinically relevant

Gram-negative species such as the causative agent of meningococcal meningitis *Neisseria meningitidis (Shih et al., 2001),* illustrating that not all species necessarily have redundant phosphatases. The dispensability of GmhB has yet to be analyzed in other pathogens suggesting that while not in *E. coli,* GmhB remains a target for antibiotic adjuvants in Gram-negative pathogens. In fact, such differences could be highly exploitable in the development of species-specific antibiotic adjuvant combinations where normal microbial flora could be excluded from killing (e.g. *E. coli*), while selectively targeting pathogens (e.g. *N. meningitidis*).

REFERENCES

Adams, P.D., Grosse-Kunstleve, R.W., Hung, L.W., Ioerger, T.R., McCoy, A.J., Moriarty, N.W., Read, R.J., Sacchettini, J.C., Sauter, N.K., and Terwilliger, T.C. (2002). PHENIX: building new software for automated crystallographic structure determination. Acta Crystallogr D Biol Crystallogr *58*, 1948-1954.

Allen, K.N., and Dunaway-Mariano, D. (2004). Phosphoryl group transfer: evolution of a catalytic scaffold. Trends Biochem Sci *29*, 495-503.

Barb, A.W., McClerren, A.L., Snehelatha, K., Reynolds, C.M., Zhou, P., and Raetz, C.R. (2007). Inhibition of lipid A biosynthesis as the primary mechanism of CHIR-090 antibiotic activity in *Escherichia coli.* Biochemistry *46*, 3793-3802.

Berg, J.M., and Godwin, H.A. (1997). Lessons from zinc-binding peptides. Annu Rev Biophys Biomol Struct *26*, 357-371.

Brilli, M., and Fani, R. (2004). Molecular evolution of hisB genes. J Mol Evol *58*, 225-237.

Brooke, J.S., and Valvano, M.A. (1996). Molecular cloning of the *Haemophilus influenza*e gmhA (lpcA) gene encoding a phosphoheptose isomerase required for lipooligosaccharide biosynthesis. J Bacteriol *178*, 3339-3341.

Brunger, A.T., Adams, P.D., Clore, G.M., DeLano, W.L., Gros, P., Grosse-Kunstleve, R.W., Jiang, J.S., Kuszewski, J., Nilges, M., Pannu, N.S.*, et al.* (1998). Crystallography & NMR system: A new software suite for macromolecular structure determination. Acta Crystallogr D Biol Crystallogr *54*, 905-921.

Collaborative computational project, N. (1994). The CCP4 suite: Programs for protein crystallography. (Acta Cryst D50).

Datsenko, K.A., and Wanner, B.L. (2000). One-step inactivation of chromosomal genes in *Escherichia coli* K-12 using PCR products. Proc Natl Acad Sci U S A *97*, 6640-6645.

De Leon, G.P., Elowe, N.H., Koteva, K.P., Valvano, M.A., and Wright, G.D. (2006). An in vitro screen of bacterial lipopolysaccharide biosynthetic enzymes identifies an inhibitor of ADP-heptose biosynthesis. Chem Biol *13*, 437-441.

Eidels, L., and Osborn, M.J. (1974). Phosphoheptose isomerase, first enzyme in the biosynthesis of aldoheptose in *Salmonella typhimurium*. J Biol Chem *249*, 5642-5648.

Emsley, P., and Cowtan, K. (2004). Coot: model-building tools for molecular graphics. Acta Crystallogr D Biol Crystallogr *60*, 2126-2132.

G. Murshudov, A.V., and E., and Dodson (1996). In Abstr Proc Daresbury Study Weekend (Warrington, UnitedKingdom, SERC, Daresbury Laboratory), pp. 93-104.

Hendrickson, W.A., Horton, J.R., and LeMaster, D.M. (1990). Selenomethionyl proteins produced for analysis by multiwavelength anomalous diffraction (MAD): a vehicle for direct determination of three-dimensional structure. EMBO J *9*, 1665-1672.

Kneidinger, B., Graninger, M., Puchberger, M., Kosma, P., and Messner, P. (2001).

Biosynthesis of nucleotide-activated D-glycero-D-manno-heptose. J Biol Chem *276*, 20935-20944.

Kneidinger, B., Marolda, C., Graninger, M., Zamyatina, A., McArthur, F., Kosma, P., Valvano, M.A., and Messner, P. (2002). Biosynthesis pathway of ADP-L-glycero-beta-D-manno-heptose in *Escherichia coli*. J Bacteriol *184*, 363-369.

Lahiri, S.D., Zhang, G., Dunaway-Mariano, D., and Allen, K.N. (2003). The pentacovalent phosphorus intermediate of a phosphoryl transfer reaction. Science *299*, 2067-2071.

Lee, S., Kirschning, A., Muller, M., Way, C., and Floss, H.G. (1999). Enzymatic synthesis of [7-14C, 7-3H] and [1-13C]sedoheptulose 7-phosphate and [1-13C]ido-heptulose 7-phosphate. J Mol Catal, B Enzym *6*, 369-377.

Loutet, S.A., Flannagan, R.S., Kooi, C., Sokol, P.A., and Valvano, M.A. (2006). A complete lipopolysaccharide inner core oligosaccharide is required for resistance of Burkholderia cenocepacia to antimicrobial peptides and bacterial survival in vivo. J Bacteriol *188*, 2073-2080.

Lu, Z., Dunaway-Mariano, D., and Allen, K.N. (2008). The catalytic scaffold of the haloalkanoic acid dehalogenase enzyme superfamily acts as a mold for the trigonal bipyramidal transition state. Proc Natl Acad Sci U S A *105*, 5687-5692.

Marolda, C.L., Lahiry, P., Vines, E., Saldias, S., and Valvano, M.A. (2006). Micromethods for the characterization of lipid A-core and O-antigen lipopolysaccharide. Methods Mol Biol *347*, 237-252.

McArthur, F., Andersson, C.E., Loutet, S., Mowbray, S.L., and Valvano, M.A. (2005). Functional analysis of the glycero-manno-heptose 7-phosphate kinase domain from the bifunctional HldE protein, which is involved in ADP-L-*glycero*-D-*manno*-heptose biosynthesis. J Bacteriol *187*, 5292-5300.

McCoy, A.J., Grosse-Kunstleve, R.W., Adams, P.D., Winn, M.D., Storoni, L.C., and Read, R.J. (2007). Phaser crystallographic software. J Appl Crystallogr *40*, 658-674.

Mdluli, K.E., Witte, P.R., Kline, T., Barb, A.W., Erwin, A.L., Mansfield, B.E., McClerren, A.L., Pirrung, M.C., Tumey, L.N., Warrener, P*., et al.* (2006). Molecular validation of LpxC as an antibacterial drug target in *Pseudomonas aeruginosa*. Antimicrob Agents Chemother *50*, 2178-2184.

Morrison, J.P., and Tanner, M.E. (2007). A two-base mechanism for *Escherichia coli* ADP-L-*glycero*-D-*manno*-heptose 6-epimerase. Biochemistry *46*, 3916-3924.

Nikaido, H. (2001). Preventing drug access to targets: cell surface permeability barriers and active efflux in bacteria. Semin Cell Dev Biol *12*, 215-223.

Nikaido, H. (2003). Molecular basis of bacterial outer membrane permeability revisited. Microbiol Mol Biol Rev *67*, 593-656.

Nikaido, H., and Vaara, M. (1985). Molecular basis of bacterial outer membrane

permeability. Microbiol Rev *49*, 1-32.

Pflugrath, J.W. (1999). The finer things in X-ray diffraction data collection. Acta Crystallogr D Biol Crystallogr *55*, 1718-1725.

Poole, K. (2002). Outer membranes and efflux: the path to multidrug resistance in Gram-negative bacteria. Curr Pharm Biotechnol *3*, 77-98.

Raetz, C.R., and Whitfield, C. (2002). Lipopolysaccharide endotoxins. Annu Rev Biochem *71*, 635-700.

Rangarajan, E.S., Proteau, A., Wagner, J., Hung, M.N., Matte, A., and Cygler, M. (2006). Structural snapshots of *Escherichia coli* histidinol phosphate phosphatase along the reaction pathway. J Biol Chem *281*, 37930-37941.

Shih, G.C., Kahler, C.M., Carlson, R.W., Rahman, M.M., and Stephens, D.S. (2001). gmhX, a novel gene required for the incorporation of L-*glycero*-D-*manno*-heptose into lipooligosaccharide in *Neisseria meningitidis*. Microbiology *147*, 2367-2377.

Sirisena, D.M., MacLachlan, P.R., Liu, S.L., Hessel, A., and Sanderson, K.E. (1994). Molecular analysis of the rfaD gene, for heptose synthesis, and the rfaF gene, for heptose transfer, in lipopolysaccharide synthesis in *Salmonella typhimurium*. J Bacteriol *176*, 2379-2385.

Tamaki, S., Sato, T., and Matsuhashi, M. (1971). Role of lipopolysaccharides in antibiotic resistance and bacteriophage adsorption of *Escherichia coli* K-12. J Bacteriol *105*, 968-975.

Taylor, P.L., Blakely, K.M., de Leon, G.P., Walker, J.R., McArthur, F., Evdokimova, E., Zhang, K., Valvano, M.A., Wright, G.D., and Junop, M.S. (2008). Structure and function of sedoheptulose-7-phosphate isomerase, a critical enzyme for lipopolysaccharide biosynthesis and a target for antibiotic adjuvants. J Biol Chem *283*, 2835-2845.

Valvano, M.A., Marolda, C.L., Bittner, M., Glaskin-Clay, M., Simon, T.L., and Klena, J.D. (2000). The rfaE gene from *Escherichia coli* encodes a bifunctional protein involved in biosynthesis of the lipopolysaccharide core precursor ADP-L-*glycero*-D-*manno*-heptose. J Bacteriol *182*, 488-497.

Valvano, M.A., Messner, P., and Kosma, P. (2002). Novel pathways for biosynthesis of nucleotide-activated glycero-manno-heptose precursors of bacterial glycoproteins and cell surface polysaccharides. Microbiology *148*, 1979-1989.

Yethon, J.A., and Whitfield, C. (2001). Lipopolysaccharide as a target for the development of novel therapeutics in Gram-negative bacteria. Curr Drug Targets Infect Disord *1*, 91-106.

CHAPTER FOUR
FORWARD CHEMICAL GENETICS SCREEN IDENTIFIES ANTIBIOTIC ADJUVANTS IN *ESCHERICHIA COLI*

CHAPTER FOUR PREFACE

The work presented in the chapter is currently being prepared for publication.

Acknowledgements:

I would like to acknowledge Jan Blanchard, Cecelia Murphy, and Jenny Wang from the McMaster University High-throughput Screening Facility for their invaluable assistance. I would also like to acknowledge Dr. Eric Brown for generously donating *E. coli* strains JA2210 and JA221.

ABSTRACT

Multi-drug resistant nosocomial infections due to Gram-negative pathogens are rapidly increasing, highlighting the need for new chemotherapies. Treating these pathogens is made even more difficult due to the presence of the outer membrane (OM), which acts as a permeability barrier to many antibiotics, including macrolides, rifampins, and coumarins. Agents that increase access of these drugs to traditional Gram-negative targets demonstrate potential for future combination therapies. In this study, a forward chemical genetic screen was designed to identify antibiotic adjuvants in *E. coli*, as well as identify targets in the OM or OM biogenesis that were previously unexplored for combating antibiotic resistance. A wild-type strain of *Escherichia coli* K-12 (BW25113) was screened against a library of 30, 000 small molecules at 10 μM in M9 minimal media. This single point, replicated screen was designed to identify compounds that potentiate novobiocin. Hits were defined as compounds that reduced *E. coli* growth to 60% of control levels and were subsequently validated by checkerboard assay to confirm synergistic properties. The primary screen identified 283 compounds as hits. From these primary hits, four compounds were shown to be synergistic with novobiocin in follow-up studies. These validated hits included A22, a known inhibitor of MreB, which has been shown to alter bacterial cell shape. This screen successfully identified compounds that are able to potentiate novobiocin in *E. coli* and suggests that proteins involved in the maintenance of cell shape are legitimate targets for antibiotic adjuvants. The potential exists to use these compounds as a starting point to develop novel combination therapies for the treatment of Gram-negative infection.

INTRODUCTION

The development of antimicrobial agents in the 20th century has resulted in a dramatic decline in of the burden of disease and death from infectious disease. The resulting widespread use, and misuse, of these drugs however, has led to the selection and emergence of bacteria that are resistant to many commonly used antibiotics. Antibiotic resistance can be classified in two broad categories: acquired and intrinsic. Acquired resistance often occurs as a result of mutations that arise in chromosomal genes or through the uptake of new genes via mobile genetic elements. These mutations or new genetic elements convey a selective advantage in the presence of antibiotics. This mutational advantage is passed on to progeny resulting in the emergence of an antibiotic resistant strain. On the other hand, intrinsic resistance exists independent of antibiotic selection in that all members of the species or group of microbes have equal survival opportunity.

An example of intrinsic antibiotic resistance is offered in the physiology of Gram-negative bacteria. These show remarkable antibiotic resistance due to the permeability barrier presented by the lipopolysaccharide (LPS)-containing outer membrane (OM) in addition to a network of efflux pumps that hinder the uptake and retention of many antibiotics, thereby decreasing drug effectiveness (Hancock, 1984; Nikaido, 2003; Pages and Amaral, 2009). Coupled with this intrinsic resistance, is an increased incidence of acquired resistance in Gram-negative bacteria to current first line drugs such as the β-lactams, tetracyclines, and fluoroquinolones (Lee et al., 2009; Rice, 2009; Roberts, 2005). The result is the emergence of extremely drug resistance pathogens that increasingly defy available therapy. There is no question that novel antibiotics and/or antibiotic alternatives are needed to keep pace with the rapidly increasing level of acquired resistance mechanisms.

The emergence and clinical relevance of multidrug-resistant *Staphylococcus aureus* (MRSA) and vancomycin resistant *Enterococci* (VRE) in the 1980s and 90s has focused much of new antimicrobial discovery toward Gram-positive pathogens. These efforts have yielded three new classes of approved antibiotic drugs over the past decade: the oxazolidinones (linezolid) (Ford et al., 2001; Gravestock, 2005), the lipodepsipeptides (daptomycin) (Robbel and Marahiel, 2010), and the pleuromutilins (retapamulin) (Novak and Shlaes, 2010). However, these compounds have little or no effect on Gram-negative pathogens owing to the challenge of intrinsic resistance. At the same time multidrug-resistant (MDR) Gram-negative pathogens, including *Pseudomonas aeruginosa, Acinetobacter baumannii, Klebsiella pneumoniae,* and Enterobacteriaceae that combine intrinsic and acquired drug resistance are increasing in prevalence (Ho et al., 2010; Kunz and Brook, 2010). These have proven much more challenging for the drug discovery community to address resulting in relatively fewer leads for new Gram-negative-targeted antibiotics in clinical trials.

The growing clinical need has spurred numerous strategies that are currently being explored as a means to combat Gram-negative bacterial infection. These include the development of new antibiotics such as the 3rd generation semi-synthetic tetracycline tigecycline (Fraise, 2006), and the redeployment of old antibiotics, in particular the lipopeptide colistin (Lim et al., 2010; Townsend et al., 2006). In addition, Gram-negative specific targets, such as lipopolysaccharide (LPS) biosynthesis and inhibition of efflux pumps, are currently being explored (Pages et al., 2005; Yethon and Whitfield, 2001). The OM in particular is an attractive target for combating antibiotic resistance. Early steps in LPS biosynthesis are essential to cell growth and unique to these organisms with no orthologues in human biochemistry and thus have the characteristics of classical 'good drug targets'(Raetz and Whitfield, 2002; Yethon and Whitfield, 2001). Furthermore, inactivation of many of the non-essential genes required for LPS biosynthesis and OM integrity confer sensitivity to antibiotics clinically used to treat infections caused by Gram-positive bacteria that are ineffective against Gram-negative bacteria due to intrinsic resistance (Nikaido, 2003; Vaara, 1992). These gene products offer novel targets for antibiotic adjuvants - agents that increase the efficacy of antibiotics when given in combination with drugs.

Such combination therapies represent an untapped potential to repurpose 'old' antibiotics with limited or diminished clinical utility due to intrinsic or acquired resistance. An example of the proof of this concept is the co-administration of amoxicillin, a β-lactam antibiotic, and clavulanic acid, a β-lactam with potent anti-β-lactamase activity to combat amoxicillin resistance (White et al., 2004). This combination and other similar ones have proven highly clinically effective for over 2 decades. Combination therapy need not be limited to inhibition of resistance however, and indeed as noted above there is likely almost limitless potential to exploit non-obvious chemical-genetic interactions by blending antibiotics with other bioactive compounds in pairs and higher order combinations. For example, in a recent study our group showed that loperamide, a common anti-diarrheal drug (Immodium), is able to potentiate the activity minocycline in *P. aeruginosa* and other Gram-negative bacteria, including drug resistant isolates (Ejim et al., 2011).

In this study we systematically explored combinations of the aminocoumarin novobiocin, an antibiotic that has weak anti-Gram-negative activity, with a library of 30,000 small molecules against *Escherichia coli* BW25113 in order to identify pairs that potentiate to increase antimicrobial activity. We identified four non-obvious synergistic combinations that overcome the intrinsic resistance of Gram-negative bacteria to novobiocin demonstrating the power of compound combinations in antibiotic research.

MATERIALS AND METHODS

Bacterial Strains, Reagents, and General Methods. *E. coli* BW25113 (Δ*(araD-araB)567*, Δ*lacZ4787*(::rrnB-3), lambda$^-$, *rph-1*, Δ*(rhaD-rhaB)568*, *hsdR514*) was used for all experiments, unless otherwise noted. Liquid M9 minimal media (M9 salts [4.78 mM Na_2PO_4, 2.2 mM KH_2PO_4, 0.86 mM NaCl, 1.87 mM NH_4Cl], 0.4% glucose, 2 mM $MgSO_4$, 0.1 mM $CaCl_2$) was the growth media for all experiments, unless otherwise noted. The Canadian Compounds Collection (CCC) was used in the screen. This collection of 29,520 small molecules is unique to the McMaster University High-throughput Screening Facility and is compiled from a variety of vendors, including Maybridge (Cornwall, England), ChemBridge (San Diego, CA), MicroSource Discovery Systems, Inc (Gaylordsville, CT), Biomol – Enzo Life Sciences (Farmingdale, NY), and Prestwick Chemical (Illkirch, France). Compounds were dissolved at an average concentration of 1 mM in DMSO and screened at a final concentration of 10 μM.

Minimum Inhibitory Concentration Determination. The minimum inhibitory concentration (MIC) of all antibiotics and compounds of interest were determined to evaluate their inhibitory activity. *E. coli* BW25113 was grown overnight in 5 mL of M9 minimal medium at 37°C with shaking at 250 rpm. The cell culture was then diluted with fresh medium to an optical density of 600 nm (OD_{600}) of 0.1, and further diluted 1:200. In 96-well round bottom plates, 99 μL of diluted cells were mixed with 1 μL of 2-fold serial dilutions of the compounds/antibiotics, in DMSO or water as necessary, with various final concentrations ranging from 0 to 1024 μg/mL, depending on the compound. Growth controls contained 1 μL DMSO or water in place of compound and sterility controls contained 99 μL of non-inoculated media. Plates were incubated at 37°C for 22 h, followed by determination of the OD_{600}. The MIC was determined to be the concentration of the antibiotic at which growth, as determined by OD_{600}, was 10% or less than that of the growth controls, calculated using equation 1, where $\mu OD_{600\ high}$ represents the mean of the growth controls, and $\mu OD_{600\ low}$ represents the mean of the sterility controls.

$$\% \text{ growth} = [(OD_{600} - \mu OD_{600\ low}) / (\mu OD_{600\ high} - \mu OD_{600\ low})] \times 100\ \% \quad \text{(eq. 1)}$$

Novobiocin Combination Screen. To search for compounds that potentiate novobiocin in *E. coli,* a screen of the CCC was conducted. *E. coli* BW25113 was grown and diluted in M9 minimal media as described above. Novobiocin was added at a concentration of 256 μg/mL (¼ MIC). Using a Beckman Biomek FX liquid handler (Beckman Coulter Inc, Fulleron, CA) 2 μL from a 1 mM stock of each compound, dissolved in 100% DMSO, was dispensed into unique wells of a 96-well flat-bottom plate, to achieve final concentration of 10 μM. This was followed by 198 μL of diluted cell culture containing novobiocin. Alternating controls were set in rows 1 and 12 of each plate containing a final concentration of 1.0 μg/mL colistin (positive control) or DMSO (negative control) in place of CCC compounds. All compounds were screened in duplicate. The OD_{600} (initial read) of each plate was read prior to incubation at 37˚C and again (final read) after 22 h incubation. The initial read served as a background absorbance measurement and was

subtracted from the final read to generate net OD_{600} values. Growth controls were used to generate baseline and replicates were plotted against each other to determine hits from the screen. The robustness of the screen was measured by calculating the Z'-score (Zhang et al., 1999). A Z'-score of 0.72 was obtained in this experiment in the presence of ¼ MIC of novobiocin, using equation 2:

$$Z' = 1 - [3(\sigma_p + \sigma_{n)}) / |\mu_p + \mu_n|] \qquad \text{(eq. 2)}$$

where, σ_p and σ_n are the standard deviations of the positive- and negative-controls, respectively and μ_p and μ_n are the means of the positive- and negative-controls, respectively

The hits were defined statistically using 3σ from the mean of the data set (60% growth). Thus, any compounds showing less than 60% growth, calculated using eq. 1, in the presence of ¼ MIC of novobiocin, in duplicate, were determined to be hits. For confirmation and validation, hits were rescreened as described above, in duplicate, in the presence of 0 and 256 μg/mL novobiocin.

Synergy Analysis Using Checkerboards. Once hits were validated, they were analyzed for synergistic activity with novobiocin. Cell cultures were grown and diluted in M9 minimal medium, as described above and added to a 3-point dose matrix, as described previously (Farha and Brown, 2010). This method allowed for identification of synergy in duplicate using minimal reagents. Select combinations were verified using full checkerboards. To evaluate the impact of the compound combinations, fractional inhibitory concentrations (FIC) were calculated using equation 3,

$$FIC = [(FIC_A / MIC_A) + (FIC_B / MIC_B)] \qquad \text{(eq. 3)}$$

where, FIC_A and MIC_A are the fractional inhibitory concentration and minimal inhibitory concentration of compound A and FIC_B and MIC_B are the fractional inhibitory concentration and minimal inhibitory concentration of compound B. Combinations with FIC values > 4 are considered antagonistic, from 0.5 – 4 are considered additive, and < 0.5 are considered synergistic. To test MreB as a target of synergy between A22 and novobiocin, synergy analysis was conducted as described above using A22 resistant (WA221) and sensitive (WA220) strains of *E.* coli (Kruse et al., 2006).

RESULTS AND DISCUSSION

Screen of Compounds that Potentiate Novobiocin in *E. coli* BW25113. A high-throughput screen of approximately 30,000 small molecules was employed to identify bioactive compounds that could potentiate the activity of novobiocin in *E. coli* BW25113. Figure 4-1 summarizes the process used to identify compounds that potentiate and synergize with novobiocin.

Novobiocin is a hydrophobic aminocoumarin antibiotic that binds to the ATP binding site of bacterial DNA gyrase subunit B and blocks DNA supercoiling (Heide, 2009). Novobiocin, and the aminocoumarins in general, show poor antibiotic activity against Gram-negative bacteria. This is due to exclusion by the OM, indeed mutants in OM biosynthesis and integrity have increased sensitivity to novobiocin (Chen and Coleman, 1993; Taylor et al., 2008) (Tamaki et al., 1971). The MIC of novobiocin against *E. coli* BW25113 in M9 minimal medium was determined to be 1024 µg/mL, and the primary screen was performed at ¼ MIC (256 µg/mL) novobiocin to select for robust potentiators of the antibiotic. We defined hits as molecules that were able to inhibit bacterial growth to 60% or less than the growth of the controls resulting in a short list of 283 compounds (0.9% hit rate) (Figure 4-2).

Following the initial screen, the 283 hits were subjected to a secondary screen, where growth inhibitory activity was evaluated in both the presence and the absence of novobiocin. This secondary screen served two purposes: it confirmed the molecules as hits and it eliminated compounds that had intrinsic antibacterial activity against *E. coli* regardless of the presence of novobiocin. As a result, 11 small molecules were identified as hits for further analysis (Figure 4-3).

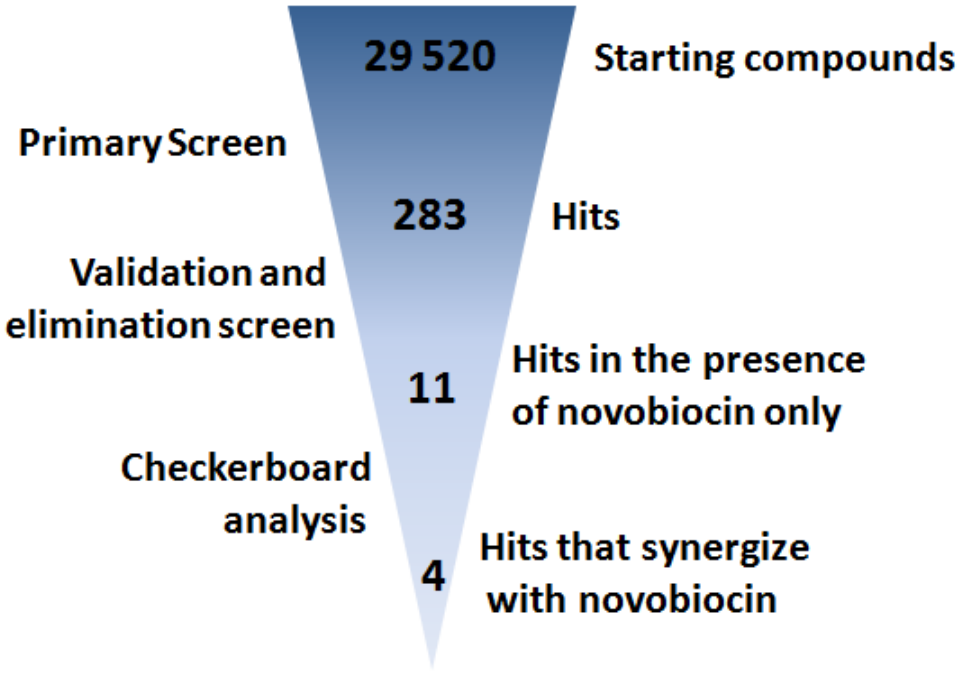

Figure 4-1: Strategy for identifying compounds that synergize with novobiocin to inhibit growth of *E. coli* BW25113.

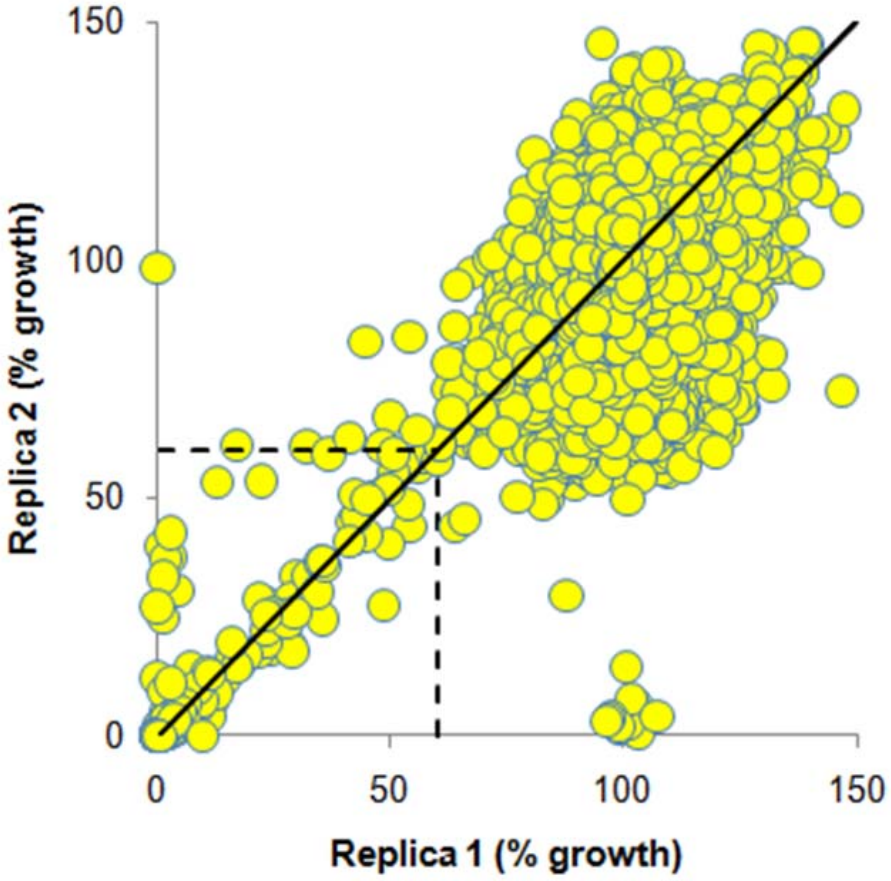

Figure 4-2: Replica plot of primary screening results. Replica plot of *E. coli* BW25113 cells grown in M9 minimal medium for 22 h at 37˚C in the presence 256 µg/mL novobiocin against 29,520 compounds from the Canadian Compound Collection at 10 µM. Solid line – replication line; Dashed line – hit zone, defined as 3σ from the mean of the data.

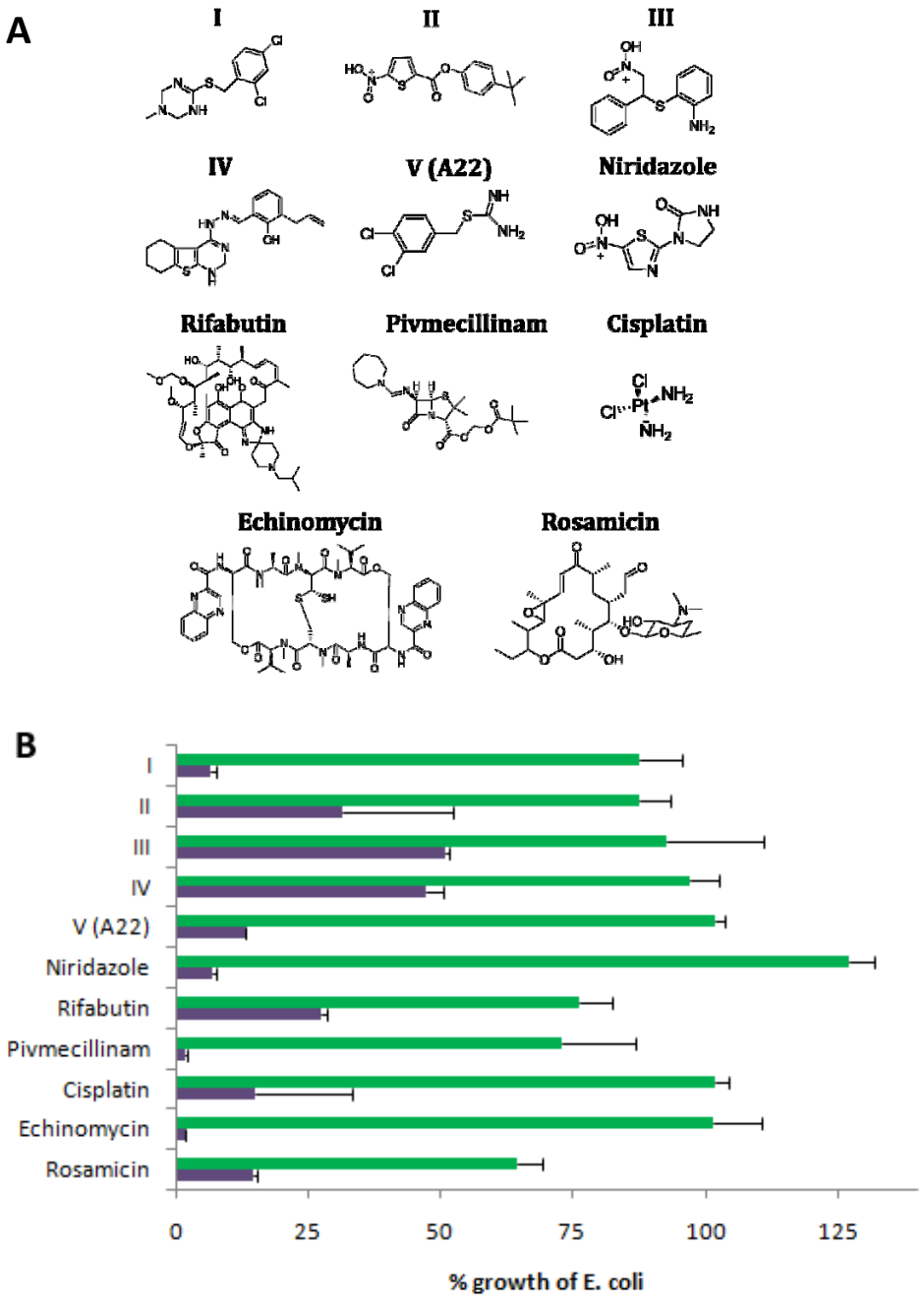

Figure 4-3:Summary of hits. (A) Chemical structures of the 11 compounds that inhibit the growth of *E. coli* BW25113 only in combination with 256 µg/mL novobiocin. (B) Each compound was evaluated for its ability to impair growth of *E. coli* BW25113 in M9 minimal medium in the absence (0 µg/mL – green) and presence (256 µg/mL – purple) of novobiocin.

The hits consisted of molecules with known bioactivity and those of unknown function. Compounds I, II, III and IV could not be attributed to any known function from previous studies. Compound V was a known molecule (A22) that has been characterized as an inhibitor of MreB, a bacterial homolog of actin, required for maintenance of cell shape in rod-shaped bacteria, including *E. coli (Gitai et al., 2005).* For consistency, compound V is referred to as A22 throughout the remainder of this text. Compound I and A22 are related molecules, varying only in chlorine positions on the chlorobenzylthio ring and the presence of a triazine ring on compound I compared to the thiourea on A22.

Cisplatin is an anti-cancer drug that cross-links DNA and is known to inhibit *E. coli* cell division (Rosenberg et al., 1967). Due to the nephrotoxic effects observed when administering cisplatin to patients, limiting downstream applications, no further analysis was performed on this compound (Barabas et al., 2008). Rosamicin, a macrolide antibiotic with improved activity against Gram-negative bacteria (Waitz et al., 1972), was also eliminated from further study due to lack of commercial availability. For comparison, erythromycin was not identified as a hit in this screen. Rifabutin is a member of the RNA polymerase inhibiting rifamycin family of antibiotics and is used in the treatment of tuberculosis (Nahid et al., 2006). Echinomycin has known antibiotic and anti-tumor activity based on its ability to intercalate double-stranded DNA (Foster et al., 1985). Though this molecule has demonstrated toxicity, recent efforts have focused on the development of less toxic analogs (Watanabe et al., 2009). Pivmecillinam is the pro-drug of mecillinam, a β-lactam that specifically binds penicillin binding protein 2 in *E. coli (Canepari et al., 1984)*. Niridazole has broad spectrum antimicrobial activity and can also be used as an anti-parasitic used to treat schistosomiasis, a helmintic disease caused by flatworms (Bannatyne et al., 1986; Hamilton-Miller and Brumfitt, 1976).

Evaluation of Compound Synergies. The nine hits of interest were evaluated for the ability to synergize with novobiocin using a 3-point dose matrix (Farha and Brown, 2010). Using the Fractional Inhibitory Concentration (FIC) index, synergy is achieved when a combination of molecules has an FIC < 0.5. By definition, this is achieved when enhanced activity is observed and both compounds are present at a concentration of ¼ MIC or less. By evaluating each combination at 0 μg/mL, and ¼ and 1/8 MIC, a synergistic effect can accurately be determined using minimal reagents, as compound pairs inhibiting growth at ¼ MIC respectively, can be deemed synergistic, and at 1/8 MIC respectively, highly synergistic. Four of the hits, I, A22, pivmecillinam, and echinomycin are synergistic with novobiocin, while the remainder demonstrated additivity in these conditions (Figure 4-4). While pivmecillinam met the definition of synergy with novobiocin, cell culture grown in the presence of even low concentrations of pivmecillinam do not grow to the same optical density as control cultures (Figure 4-4), suggesting that the compound may be impacting cell growth even in the absence of novobiocin, without completely inhibiting growth. This observation was consistent over numerous trials.

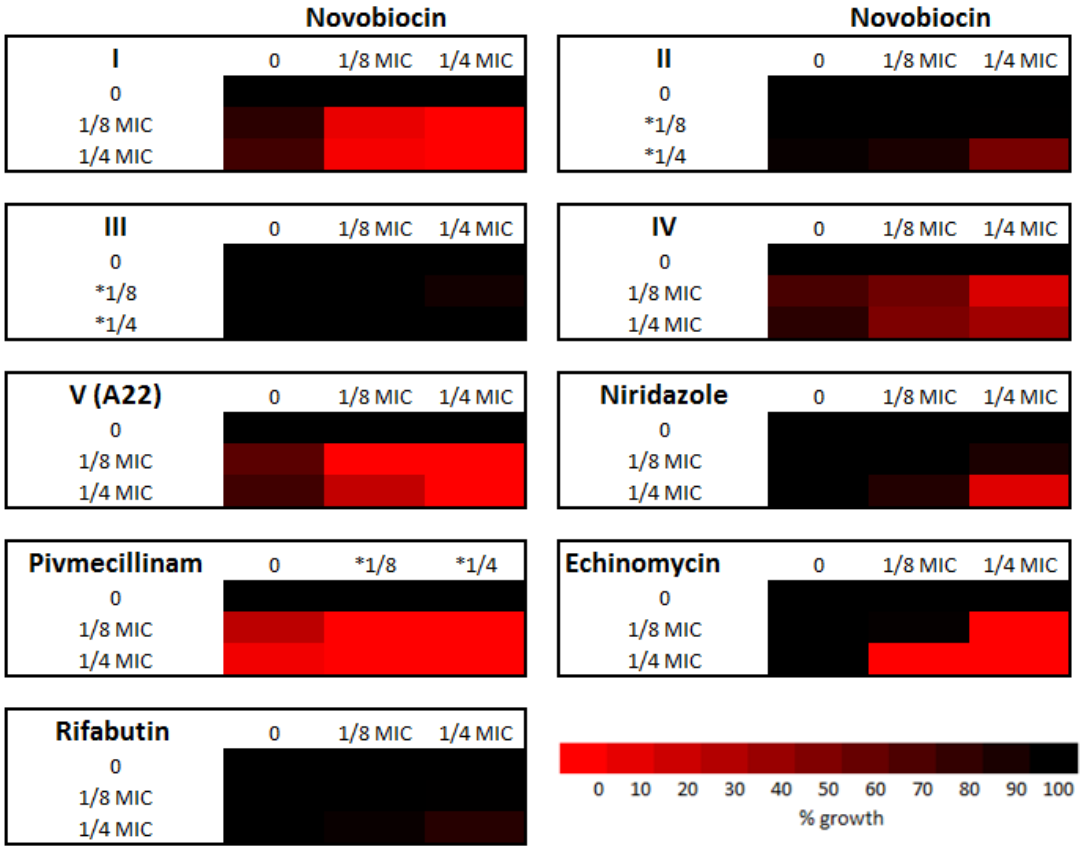

Figure 4-4: Synergy between hits and novobiocin in *E. coli*. 3-point matrix heat plots showing synergistic growth inhibition of *E. coli* BW25113 by novobiocin in combination with hits derived from the primary screen. Compounds I, V (A22), pivmecillinam, and echinomycin each show synergy with novobiocin according to this test, where black represents 100% growth and red represents 0 % growth, normalized to growth controls.

Assessing the spectra of the adjuvants. In order to establish if the synergy observed with these hits was specific to novobiocin, the four synergistic hits, I, A22, pivmecillinam, and echinomycin, as well as compound II and niridazole, which both showed a strong additive action, as indicated by partial growth inhibition in Figure 4-4, were combined with a panel of other antibiotics with known limited activity against Gram-negative bacteria (Figure 4-5). None of the hits demonstrated synergy with the macrolide erythromycin against *E. coli* BW25113. Compound II and lincomycin were selectively synergistic with each other. Rifampin showed a synergy profile similar to novobiocin, with the exception of echinomycin, and vancomycin was only synergistic with pivmecillinam.

The six hits were also tested for synergy with novobiocin in *Pseudomonas aeruginosa* PAO1, to determine if the results were *E. coli* specific (Figure 4-5). Both I and A22 were also synergistic with novobiocin against *P. aeruginosa*, however neither pivmecillinam nor echinomycin had the same effect. Niridazole was synergistic with novobiocin in this organism. Compound I and A22 offered the greatest promise for further study due to their consistent synergy with novobiocin in both *E. coli* and *P. aeruginosa*, as well as their ability to potentiate rifampin (another antibiotic that targets DNA replication).

A22/Novobiocin Synergy is Dependent on MreB: A22, has been previously shown as an inhibitor of the actin homologue MreB (Gitai et al., 2005). This protein can exist as both a monomer and a multi-subunit polymer and its function is essential to the cell. It is involved in maintaining the rod shape of some bacteria and has been show to play a role in chromosome segregation prior to cell division (Kruse and Gerdes, 2005). Gitai *et al* were the first to provide evidence of the involvement of MreB in chromosome segregation by using A22, a small molecule probe that can specifically and reversibly inhibit MreB function (Gitai et al., 2005). Using a strain of *E. coli* that has a single point mutation in the *mreB* gene that renders it resistant to A22 (Kruse et al., 2006), we tested to see if synergy between A22 and novobiocin was maintained against the A22 resistant strain (Figure 4-6). Indeed, while A22 and novobiocin were synergistic in the A22 sensitive strain of *E. coli*, with an FIC of 0.27, synergy was absent in the A22 resistant strain, where the FIC was calculated at 1.0. Similar results were seen for the compound I/novobiocin combination, with FIC values of 0.51 and 1.0 against the sensitive and resistant strains, respectively. The difference in FIC values can possibly be attributed to the structural differences between A22 and compound I. These results indicate that the effect of A22, and to a lesser extent compound I, on the function of MreB promotes the activity of novobiocin.

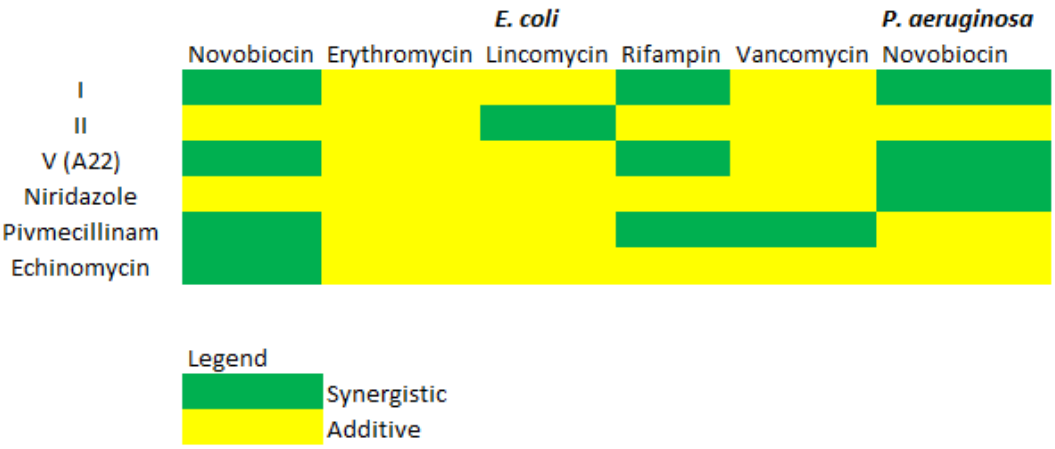

Figure 4-5: Interaction profile of various antibiotics against hits that demonstrated potential to act synergistically against *E. coli* BW25113 or *P. aeruginosa* PA01. Combination were shown to act synergistically (green), or additively (yellow).

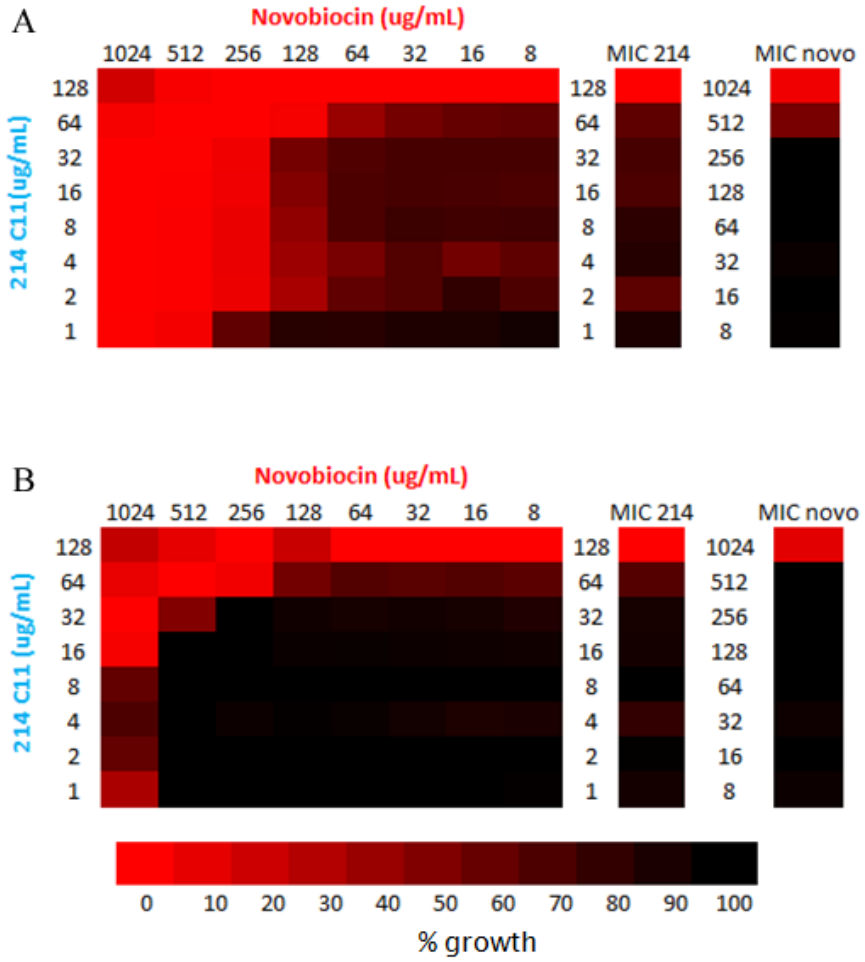

Figure 4-6: Comparing A22/novobiocin synergy in A22 sensitive and resistant *E. coli*. Heat plots showing growth inhibition of *E. coli* expressing *mreB* (A) sensitive and (B) resistant to A22, respectively in the presence of varying concentrations of novobiocin

and A22. Synergy was apparent in the A22 sensitive strain with an FIC of 0.27, compared to an FIC of 0.75 in the resistant strain.

Altering cell shape may potentiate antibiotics in *E. coli.* Bacterial cell shape has been shown to be important in a myriad of cell functions, including the regulation of cell differentiation, attachment, motility, and polar differentiation, among others (Young, 2006). It is agreed that cell shape is determined by the rigid structure of peptidoglycan, a matrix of peptide linked glycan polymers that varies in thickness between species. Disruptions peptidoglycan synthesis can result cell shape abnormalities, such as conversion from rod to spherical shape in *E. coli*, where roughly 80% of the peptidoglycan in the cell wall is contained in a single layer (Huang et al., 2008).

Until recently, little was known about many of the molecular players involved in the synthesis of the peptidoglycan layer, specifically in support of cell shape determination. In 2001, Jones *et al* revealed that MreB formed extended, filamentous, helical polymers that serve to support the cell wall on the inside, serving as a bacterial cytoskeleton homologous in action to actin in eukaryotic cells (Jones et al., 2001). It has also been shown that mutations in MreB can coincide with conversion in shape from rod to sphere, further supporting its role in maintaining cell shape (Osborn and Rothfield, 2007).

Treatment of *E. coli* cells with A22 was shown to induce a spherical phenotype (Iwai et al., 2002), and in 2005, Gitai *et al* demonstrated MreB as its target (Gitai et al., 2005). Based on our study, it would appear that sub-inhibitory concentrations of A22 may be able to affect cell shape sufficiently to potentiate antibiotics in *E. coli*, including novobiocin and rifampin. Interestingly, the *mreB* gene was originally discovered by probing mecillinam-resistant *E. coli* (Wachi et al., 2006). Mecillinam preferentially inhibits penicillin binding protein 2, a transpeptidase involved in the insertion of new polymer strands into the peptidoglycan layer that is also required for maintaining cell shape (Osborn and Rothfield, 2007). In this study, we identified pivmecillinam, the prodrug of mecillinam, as an antibiotic potentiator, offering further evidence that sub-inhibitory concentrations of agents that affect cell shape show promise as antibiotic adjuvants.

CONCLUSIONS

Using a high-throughput, whole-cell screening approach, this study identifies chemical adjuvants of novobiocin and rifampin in *E. coli* and *P. aeruginosa*, two Gram-negative organisms of pressing clinical concern. Specifically, we demonstrate that the bacterial cytoskeleton is a viable target for new antimicrobial combination therapies that is worth future consideration. These results serve to highlight the ability to repurpose molecules of known function as antibiotics, or antibiotic adjuvants.

REFERENCES

Bannatyne, R.M., Jackowski, J., and Grant, R.B. (1986). Antibacterial activity of niridazole against Salmonellae. Antimicrob Agents Chemother *29*, 923-924.

Barabas, K., Milner, R., Lurie, D., and Adin, C. (2008). Cisplatin: a review of toxicities and therapeutic applications. Vet Comp Oncol *6*, 1-18.

Canepari, P., Botta, G., and Satta, G. (1984). Inhibition of lateral wall elongation by mecillinam stimulates cell division in certain cell division conditional mutants of *Escherichia coli*. J Bacteriol *157*, 130-133.

Chen, L., and Coleman, W.G., Jr. (1993). Cloning and characterization of the *Escherichia coli* K-12 rfa-2 (rfaC) gene, a gene required for lipopolysaccharide inner core synthesis. J Bacteriol *175*, 2534-2540.

Ejim, L., Farha, M.A., Falconer, S.B., Wildenhain, J., Coombes, B.K., Tyers, M., Brown, E.D., and Wright, G.D. (2011). Combinations of antibiotics and nonantibiotic drugs enhance antimicrobial efficacy. Nat Chem Biol *7*, 348-350.

Farha, M.A., and Brown, E.D. (2010). Chemical probes of Escherichia coli uncovered through chemical-chemical interaction profiling with compounds of known biological activity. Chem Biol *17*, 852-862.

Ford, C.W., Zurenko, G.E., and Barbachyn, M.R. (2001). The discovery of linezolid, the first oxazolidinone antibacterial agent. Curr Drug Targets Infect Disord *1*, 181-199.

Foster, B.J., Clagett-Carr, K., Shoemaker, D.D., Suffness, M., Plowman, J., Trissel, L.A., Grieshaber, C.K., and Leyland-Jones, B. (1985). Echinomycin: the first bifunctional intercalating agent in clinical trials. Invest New Drugs *3*, 403-410.

Fraise, A.P. (2006). Tigecycline: the answer to beta-lactam and fluoroquinolone resistance? J Infect *53*, 293-300.

Gitai, Z., Dye, N.A., Reisenauer, A., Wachi, M., and Shapiro, L. (2005). MreB actin-mediated segregation of a specific region of a bacterial chromosome. Cell *120*, 329-341.

Gravestock, M.B. (2005). Recent developments in the discovery of novel oxazolidinone antibacterials. Curr Opin Drug Discov Devel *8*, 469-477.

Hamilton-Miller, J.M., and Brumfitt, W. (1976). The versatility of nitro compounds. J Antimicrob Chemother *2*, 5-8.

Hancock, R.E. (1984). Alterations in outer membrane permeability. Annu Rev Microbiol *38*, 237-264.

Heide, L. (2009). The aminocoumarins: biosynthesis and biology. Nat Prod Rep *26*, 1241-1250.

Ho, J., Tambyah, P.A., and Paterson, D.L. (2010). Multiresistant Gram-negative infections: a global perspective. Curr Opin Infect Dis *23*, 546-553.

Huang, K.C., Mukhopadhyay, R., Wen, B., Gitai, Z., and Wingreen, N.S. (2008). Cell shape and cell-wall organization in Gram-negative bacteria. Proc Natl Acad Sci U S A *105*, 19282-19287.

Iwai, N., Nagai, K., and Wachi, M. (2002). Novel S-benzylisothiourea compound that induces spherical cells in *Escherichia coli* probably by acting on a rod-shape-determining protein(s) other than penicillin-binding protein 2. Biosci Biotechnol Biochem *66*, 2658-2662.

Jones, L.J., Carballido-Lopez, R., and Errington, J. (2001). Control of cell shape in bacteria: helical, actin-like filaments in *Bacillus subtilis*. Cell *104*, 913-922.

Kruse, T., Blagoev, B., Lobner-Olesen, A., Wachi, M., Sasaki, K., Iwai, N., Mann, M., and Gerdes, K. (2006). Actin homolog MreB and RNA polymerase interact and are both required for chromosome segregation in *Escherichia coli*. Genes Dev *20*, 113-124.

Kruse, T., and Gerdes, K. (2005). Bacterial DNA segregation by the actin-like MreB protein. Trends Cell Biol *15*, 343-345.

Kunz, A.N., and Brook, I. (2010). Emerging resistant Gram-negative aerobic bacilli in hospital-acquired infections. Chemotherapy *56*, 492-500.

Lee, J.H., Jeong, S.H., Cha, S.S., and Lee, S.H. (2009). New disturbing trend in antimicrobial resistance of gram-negative pathogens. PLoS Pathog *5*, e1000221.

Lim, L.M., Ly, N., Anderson, D., Yang, J.C., Macander, L., Jarkowski, A., 3rd, Forrest, A., Bulitta, J.B., and Tsuji, B.T. (2010). Resurgence of colistin: a review of resistance, toxicity, pharmacodynamics, and dosing. Pharmacotherapy *30*, 1279-1291.

Nahid, P., Pai, M., and Hopewell, P.C. (2006). Advances in the diagnosis and treatment of tuberculosis. Proc Am Thorac Soc *3*, 103-110.

Nikaido, H. (2003). Molecular basis of bacterial outer membrane permeability revisited. Microbiol Mol Biol Rev *67*, 593-656.

Novak, R., and Shlaes, D.M. (2010). The pleuromutilin antibiotics: a new class for human use. Curr Opin Investig Drugs *11*, 182-191.

Osborn, M.J., and Rothfield, L. (2007). Cell shape determination in *Escherichia coli*. Curr Opin Microbiol *10*, 606-610.

Pages, J.M., and Amaral, L. (2009). Mechanisms of drug efflux and strategies to combat them: challenging the efflux pump of Gram-negative bacteria. Biochim Biophys Acta *1794*, 826-833.

Pages, J.M., Masi, M., and Barbe, J. (2005). Inhibitors of efflux pumps in Gram-negative bacteria. Trends Mol Med *11*, 382-389.

Raetz, C.R., and Whitfield, C. (2002). Lipopolysaccharide endotoxins. Annu Rev Biochem *71*, 635-700.

Rice, L.B. (2009). The clinical consequences of antimicrobial resistance. Curr Opin Microbiol *12*, 476-481.

Robbel, L., and Marahiel, M.A. (2010). Daptomycin, a bacterial lipopeptide synthesized by a nonribosomal machinery. J Biol Chem *285*, 27501-27508.

Roberts, M.C. (2005). Update on acquired tetracycline resistance genes. FEMS Microbiol Lett *245*, 195-203.

Rosenberg, B., Van Camp, L., Grimley, E.B., and Thomson, A.J. (1967). The inhibition of growth or cell division in *Escherichia coli* by different ionic species of platinum(IV) complexes. J Biol Chem *242*, 1347-1352.

Tamaki, S., Sato, T., and Matsuhashi, M. (1971). Role of lipopolysaccharides in antibiotic resistance and bacteriophage adsorption of *Escherichia coli* K-12. J Bacteriol *105*, 968-975.

Taylor, P.L., Blakely, K.M., de Leon, G.P., Walker, J.R., McArthur, F., Evdokimova, E., Zhang, K., Valvano, M.A., Wright, G.D., and Junop, M.S. (2008). Structure and function of sedoheptulose-7-phosphate isomerase, a critical enzyme for lipopolysaccharide biosynthesis and a target for antibiotic adjuvants. J Biol Chem *283*, 2835-2845.

Townsend, M.L., Pound, M.W., and Drew, R.H. (2006). Tigecycline: a new glycylcycline antimicrobial. Int J Clin Pract *60*, 1662-1672.

Vaara, M. (1992). Agents that increase the permeability of the outer membrane. Microbiol Rev *56*, 395-411.

Wachi, M., Osaka, K., Kohama, T., Sasaki, K., Ohtsu, I., Iwai, N., Takada, A., and Nagai, K. (2006). Transcriptional analysis of the *Escherichia coli* mreBCD genes responsible for morphogenesis and chromosome segregation. Biosci Biotechnol Biochem *70*, 2712-2719.

Waitz, J.A., Drube, C.G., Moss, E.L., Jr., and Weinstein, M.J. (1972). Biological studies with rosamicin, a new Micromonospora-produced macrolide antibiotic. J Antibiot (Tokyo) *25*, 647-652.

Watanabe, K., Oguri, H., and Oikawa, H. (2009). Diversification of echinomycin molecular structure by way of chemoenzymatic synthesis and heterologous expression of the engineered echinomycin biosynthetic pathway. Curr Opin Chem Biol *13*, 189-196.

White, A.R., Kaye, C., Poupard, J., Pypstra, R., Woodnutt, G., and Wynne, B. (2004). Augmentin (amoxicillin/clavulanate) in the treatment of community-acquired respiratory tract infection: a review of the continuing development of an innovative antimicrobial agent. J Antimicrob Chemother *53 Suppl 1*, i3-20.

Yethon, J.A., and Whitfield, C. (2001). Lipopolysaccharide as a target for the development of novel therapeutics in gram-negative bacteria. Curr Drug Targets Infect Disord *1*, 91-106.

Young, K.D. (2006). The selective value of bacterial shape. Microbiol Mol Biol Rev *70*, 660-703.

Zhang, J.H., Chung, T.D., and Oldenburg, K.R. (1999). A Simple Statistical Parameter for Use in Evaluation and Validation of High Throughput Screening Assays. J Biomol Screen *4*, 67-73.

CHAPTER FIVE
CONCLUSIONS AND ONGOING STUDIES

The threat of infection by Gram-negative bacteria is very real. Hospitals, specifically in ICUs, are a breeding ground for organisms such as *P. aeruginosa, A. baumannii,* and Enterobacteriaceae. Indeed, statistics indicate that approximately 30% of hospital-acquired infections are caused by Gram-negative bacteria (Peleg and Hooper, 2010). Even more concerning is the increasing number of cases where infections are resistant to first line treatment, including carbapenems and β-lactams. Rates of ESBL-producing Enterobacteriaceae and carbapenemase-producing *K. pneumoniae* (KPC) have been steadily increasing in North America for the past decade and outbreaks of KPC have been observed across the U.S. and Europe (Ho et al., 2010). Most distressing of all, are the recent reports of infections caused by infections that are resistant to all available antibiotics, including polymyxin, a last line therapy (Paterson and Lipman, 2007).

There is a distinct lack of new therapies available to treat Gram-negative infection; with the exception of tigecycline and doripenem, no new Gram-negative therapies have been found in the last decade. This situation has led to overuse of available antibiotics, contributing to the development and spread of associated resistance. The difficulty in finding new therapies against Gram-negatives is largely due to their intrinsic resistance mechanisms. The presence of the OM gives these organisms a barrier to molecules that could otherwise be potential therapies. In addition, many Gram-negative pathogens also have a comprehensive system of efflux pumps that can remove foreign molecules prior to action, further limiting therapeutic potential.

The strategy to combating Gram-negative resistance must be two-fold. First, a better understanding of the physiology of Gram-negative bacteria is necessary in order to increase antibiotic efficacy. These unique systems represent potential targets for both antibiotics and antibiotic adjuvants. Second, the discovery of new antibiotics is essential to challenge the current spread of resistance.

UNDERSTANDING ADP-HEPTOSE BIOSYNTHESIS

LPS is crucial to the integrity of the OM permeability barrier. As such, LPS biosynthesis has been identified as a potential target for antibiotic adjuvants. While much work has been done toward understanding the components of lipid A, Kdo, and O antigen biosynthesis (Raetz and Whitfield, 2002), only genetic evidence has been collected to help identify the enzymes involved in ADP-heptose biosynthesis (Valvano et al., 2002), with the exception of the epimerase HldD (Morrison et al., 2005). This work represents the first enzymatic characterization of GmhA and GmhB, which catalyze the first and third steps, respectively, of the ADP-heptose biosynthetic pathway. By analyzing crystallographic data, we were able to identify residues likely to be involved in the active site of each enzyme. Mutational analysis further supported this hypothesis.

Crystallographic data of GmhA from *E. coli, P. aeruginosa, C. jejuni,* and *V. cholera* showed that this enzyme exists in two distinct conformations: an open conformation suited to substrate binding, and a closed conformation that binds the

product (Chapter 2). Additionally, through mutational analysis, we demonstrated that Glu-65 and His-180 were essential to GmhA function. This observation was confirmed by expressing mutant *gmhA* in *E. coli* and evaluating the outcome of both LPS length and susceptibility to novobiocin in the recombinant bacteria, further demonstrating the importance of Glu-65 and His-180 in maintaining LPS integrity. We proposed a mechanism of action of this enzyme using an enediol-intermediate isomerase mechanism, with Glu-65 and His-180 acting as the catalytic base and acid, respectively. Following publication of this work, a similar study was reported on GmhA from *Burkholderia pseudomallei* (Harmer, 2010). This work identified a Zn^{2+} in the active site and suggested that Gln-175 instead acts as the catalytic acid. This study also proposed that Asp-98 acts as both catalytic acid and base in the cyclization of the product. Given the evidence for requirement of both equivalent Gln and Asp residues, and that a Zn^{2+} was not observed in our study, this revised mechanism is also a reasonable hypothesis. Both studies highlight the residues involved in maintaining the active site and provide a sound basis for potential substrate-based inhibitor design for GmhA.

A similar study was performed on GmhB to elucidate its mechanism of action (Chapter 3). This study depicted the first published crystal structure of GmhB. Here, we found catalytic relevance for Asp-11, Asp-13 and Lys-111, leading us to predict a mechanism via an aspartylphosphate intermediate, where Asp-11 acts as the catalytic aspartic acid and Asp-13 acts as the catalytic aspartic base, based on similarity to the HAD family of proteins. A subsequent study on GmhB by Nguyen *et al*. (Nguyen et al., 2010) also found a significant decrease in activity when Asp-13 was mutated, however this group failed to examine the relevance of Asp-11 and Lys-111; instead this paper makes a case for the importance of Arg-110 for catalytic activity, but does not predict a mechanism of action and instead focused on structural comparisons between GmhB and other HAD proteins. The crystal structures in each study highlight the same residues, suggesting comparable crystallographic data but a divergence in focus between the two studies. What is clear in both cases is the importance of Asp-13 to enzyme function. A study by Wang *et al.* (Wang et al., 2010) shows the strict substrate specificity of GmhB, compared to other members of the HAD family of proteins, indicating that minor substrate modifications have the potential to greatly impact activity, making a case for designing inhibitors around the D-*glycero*-D-*manno*-heptose 1,7-biphosphate substrate, however our finding that GmhB may not be essential for complete LPS biosynthesis limits the future viability of such inhibitors for therapeutic use.

Elucidating the active sites of GmhA and GmhB, and providing structural data for these enzymes, nearly completes the characterization of this pathway in *E. coli*. Understanding the role of GmhA and GmhB in LPS biosynthesis is an important first step toward targeting LPS with antibiotic adjuvants. By identifying key residues in the active site, the substrates can be modified as potential inhibitors; realistically given the uncertainty surrounding GmhB essentiality to preserving the OM barrier, only S7P, the GmhA substrate, is amenable to modification for downstream therapeutic potential. Given the stereospecific nature of this substrate and the difficulty observed in its

synthesis, medicinal chemistry on these specific substrates would be very challenging. Since it is unknown whether such molecules would actually inhibit these enzymes, we opted to choose a whole-cell screening approach toward discovering antibiotic adjuvants.

IDENTIFICATION OF NOVEL ANTIBIOTIC ADJUVANTS IN GRAM-NEGATIVE BACTERIA

A whole-cell screen was developed to identify potentiators of novobiocin in *E. coli*. In this manner, we could target all of the LPS biosynthetic enzymes at the same time, as well as any other, possibly unimagined, targets that may alter Gram-negative antibiotic sensitivity (Chapter 4). After validation studies, we found four hits that demonstrated synergy with novobiocin. The most exciting of these hits was A22, a compound previously found to inhibit MreB, an actin-like bacterial cytoskeleton protein. Follow-up studies with an A22 resistant strain of *E. coli* suggested that MreB inhibition by A22 leads to advanced activity by novobiocin. We further hypothesized that alteration of cell shape may potentiate antibiotics in Gram-negative bacteria.

The identification of A22 also served to validate the screen, offering a proof-of-principle that such screening initiatives can be used, with success, to identify antibiotic adjuvants of Gram-negative bacteria. Of particular importance is discovery of not the compound itself, but the pathway it targets. We began this study focused specifically on the OM, hypothesizing that any hits would be directly applicable to OM biogenesis or efflux pump assembly and action. Instead, we identified a molecule that alters cell shape to induce permeability. Recent studies have focused on the understanding of the role of MreB in maintaining cell shape, and also its role in cell division and chromosomal segregation (Kruse et al., 2006) (Gitai et al., 2005; Varma and Young, 2009). This study has identified these pathways as potential targets for antibiotic adjuvants. The greatest success of this screen, therefore, is in demonstrating the potential of alternate cellular components for development of novel combination therapies.

Given the interconnected nature of the living cell, our original hypothesis that disrupting LPS biosynthesis increases the permeability of the Gram-negative OM, can be extrapolated to include disruption of any component of the bacterial surface structure. LPS, phospholipids, efflux pumps, porins, peptidoglycan, and cytoskeleton (including MreB) are all involved in maintaining the structural integrity of the Gram-negative organism, and this is by no means an exhaustive list. The predicted “domino effect” of altering any one of these systems is likely to reverberate throughout the cell, and as such, alteration of cell shape may indeed have a direct effect on the composition, and resulting permeability barrier, of the LPS of interest. Examination of the LPS of cells exposed to A22 could help to identify the effect of cell shape on LPS biosynthesis, and provide evidence to support this theory.

FORWARD CHEMICAL GENETICS VS REVERSE CHEMICAL GENETICS

In many ways this work addresses the ongoing debate as to the best method to search for novel therapeutics. One method, the reverse chemical genetics approach, identifies a target and looks to inhibit it. This was the approach in mind when we initiated study on GmhA and GmhB. However, even with access to structure-function analyses, using these data toward the development of inhibitors would be very challenging. A larger caveat to this approach is that even if the new compounds proved to have inhibitory action *in vitro*, there is no guarantee that the compounds will have *in vivo* activity against the organism of interest. This scenario is especially true when working with Gram-negatives, given the intrinsic resistance described earlier. A previous study demonstrated this point, when *in vitro* inhibitors of HldE were proven ineffective when applied to *E. coli in vivo* (De Leon et al., 2006).

Instead, we opted to follow a forward chemical genetic approach to discovery of antibiotic adjuvants. This method targets the whole cell with prospective compounds, with the general understanding that any potential hits must also be bioactive by virtue of the nature of the screen. We found success in this approach with the identification of A22 as an adjuvant of novobiocin. The challenge in this scenario, though, is determining the specific target within the cell. In screening a library that consists of a variety of compounds with both known and unknown functions, we were able to include compounds that have elucidated targets. Using this approach, we were able to limit downstream target studies and still identify a compound, and target, that would not have been possible using a traditional target-based approach.

This is not to say that the target based approach does not have its merits. For example, substrate-analogue studies focusing on inhibition of LpxC, which catalyzes the first conserved step in the lipid A biosynthetic pathway, have led to the identification of CHIR-090 (Barb and Zhou, 2008; McClerren et al., 2005). This potent LpxC inhibitor is bioactive against both *E. coli* and *P. aeruginosa* and has great antibiotic therapeutic potential. Rather, both whole cell and target-based approaches should be used according the information available in each situation to provide the best potential toward drug discovery.

ONGOING STUDIES

With the structure-function analysis of GmhA and GmhB described in this work, and the thorough examination of HldD undertaken by Tanner *et al*, only the bifunctional HldE remains as the only as yet uncharacterized enzyme in the ADP-heptose pathway. This work is currently ongoing by Dr. Murray Junop at McMaster University.

The discovery of A22 as an antibiotic adjuvant is just the first step in developing this combination as a potential therapy. Microscopy of *E. coli* cells in the presence of the combination would help confirm our theory that a change in cell shape is responsible for the antibiotic susceptibility observed. In addition, the effect of A22 on the DNA gyrase B,

the target of novobiocin, and conversely, of novobiocin on MreB should be analyzed to determine if synergy is instead related to target. This could be accomplished by purification of the respective enzymes and evaluating each as a prospective substrate.

Finally, this screen has been established and validated. Different permutations of this screen can now be applied towards the discovery of new hits. For example, other antibiotics, such as rifampin and erythromycin, could be used as the antibiotic of interest, and other Gram-negative organisms could be examined. Additionally, the Wright lab has access to a substantial library of environmental isolate supernatants that could be screened in combination with any of these antibiotics to identify novel adjuvants. The majority of antibiotics currently in use have their origins as natural products, highlighting the potential in this library.

CONCLUDING REMARKS

As demonstrated throughout this work, the need for novel treatment options against Gram-negative pathogens is paramount to the fight against infectious disease. We have focused our efforts on the hypothesis that combination therapies can be used to disarm the permeability barrier presented by the OM of these organisms. First we examined the structure-function relationships of two non-essential enzymes involved in LPS biosynthesis, offering the first in-depth look at these proteins. We then used a whole cell screening approach to identify potentiators of novobiocin in *E. coli.* This strategy culminated in the identification of A22, a cell shape modifier, as an antibiotic adjuvant. This work highlights the multi-faceted approach that must be taken to both understand bacterial mechanisms and exploit them for therapeutic use. The screen described in this study offers a new methodology for therapeutic discovery via combination therapy to combat the rise of Gram-negative infection.

REFERENCES

Barb, A.W., and Zhou, P. (2008). Mechanism and inhibition of LpxC: an essential zinc-dependent deacetylase of bacterial lipid A synthesis. Curr Pharm Biotechnol *9*, 9-15.

De Leon, G.P., Elowe, N.H., Koteva, K.P., Valvano, M.A., and Wright, G.D. (2006). An in vitro screen of bacterial lipopolysaccharide biosynthetic enzymes identifies an inhibitor of ADP-heptose biosynthesis. Chem Biol *13*, 437-441.

Gitai, Z., Dye, N.A., Reisenauer, A., Wachi, M., and Shapiro, L. (2005). MreB actin-mediated segregation of a specific region of a bacterial chromosome. Cell *120*, 329-341.

Harmer, N.J. (2010). The structure of sedoheptulose-7-phosphate isomerase from *Burkholderia pseudomallei* reveals a zinc binding site at the heart of the active site. J Mol Biol *400*, 379-392.

Ho, J., Tambyah, P.A., and Paterson, D.L. (2010). Multiresistant Gram-negative infections: a global perspective. Curr Opin Infect Dis *23*, 546-553.

Kruse, T., Blagoev, B., Lobner-Olesen, A., Wachi, M., Sasaki, K., Iwai, N., Mann, M., and Gerdes, K. (2006). Actin homolog MreB and RNA polymerase interact and are both required for chromosome segregation in *Escherichia coli*. Genes Dev *20*, 113-124.

McClerren, A.L., Endsley, S., Bowman, J.L., Andersen, N.H., Guan, Z., Rudolph, J., and Raetz, C.R. (2005). A slow, tight-binding inhibitor of the zinc-dependent deacetylase LpxC of lipid A biosynthesis with antibiotic activity comparable to ciprofloxacin. Biochemistry *44*, 16574-16583.

Morrison, J.P., Read, J.A., Coleman, W.G., Jr., and Tanner, M.E. (2005). Dismutase activity of ADP-L-*glycero*-D-*manno*-heptose 6-epimerase: evidence for a direct oxidation/reduction mechanism. Biochemistry *44*, 5907-5915.

Nguyen, H.H., Wang, L., Huang, H., Peisach, E., Dunaway-Mariano, D., and Allen, K.N. (2010). Structural determinants of substrate recognition in the HAD superfamily member D-*glycero*-D-*manno*-heptose-1,7-bisphosphate phosphatase (GmhB). Biochemistry *49*, 1082-1092.

Paterson, D.L., and Lipman, J. (2007). Returning to the pre-antibiotic era in the critically ill: the XDR problem. Crit Care Med *35*, 1789-1791.

Peleg, A.Y., and Hooper, D.C. (2010). Hospital-acquired infections due to gram-negative bacteria. N Engl J Med *362*, 1804-1813.

Raetz, C.R., and Whitfield, C. (2002). Lipopolysaccharide endotoxins. Annu Rev Biochem *71*, 635-700.

Valvano, M.A., Messner, P., and Kosma, P. (2002). Novel pathways for biosynthesis of nucleotide-activated glycero-manno-heptose precursors of bacterial glycoproteins and cell surface polysaccharides. Microbiology *148*, 1979-1989.

Varma, A., and Young, K.D. (2009). In *Escherichia coli*, MreB and FtsZ direct the synthesis of lateral cell wall via independent pathways that require PBP 2. J Bacteriol *191*, 3526-3533.

Wang, L., Huang, H., Nguyen, H.H., Allen, K.N., Mariano, P.S., and Dunaway-Mariano, D. (2010). Divergence of biochemical function in the HAD superfamily: D-*glycero*-D-*manno*-heptose-1,7-bisphosphate phosphatase (GmhB). Biochemistry *49*, 1072-1081.

APPENDICES

APPENDIX 1: GmhA mutagenesis and sequencing primers.
Nucleotides in bold show location of point mutation. Underlined regions indicate codon that will be altered after mutagenesis.

Mutation	**Mutagenesis Primer (5'-3')**
H61Q forward	GGTTCCCATTGCGACGCTATGCA**G**TTTGCCGAAGAGTTG
H61Q reverse	CAACTCTTCGGCAAA**CT**GCATAGCGTCGCAATGGGAACC
E65N forward	CTATGCACTTTGCCGAA**AA**C**T**TGACCGGTCGCTACCGTGAAAAC
E65N reverse	GTTTTCACGGTAGCGACCGGTCAA**GT**T**T**TTCGGCAAAGTGCATAG
E65Q forward	CTATGCACTTTGCCGAA**CAG**TTGACCGGTCGCTACCGTGAAAAC
E65Q reverse	GTTTTCACGGTAGCGACCGGTCAA**CTG**TTCGGCAAAGTGCATAG
R69Q forward	GCCGAAGAGTTGACCGGTC**AG**TACCGTGAAAAC
R69Q reverse	GTTTTCACGGTA**CT**GACCGGTCAACTCTTCGGC
D94N forward	CATATTTCCTGCGTCGGTAAT**AA**TTTCGGTTTCAATGATATTTTC
D94N reverse	GAAAATATCATTGAAACCGAAA**TT**ATTACCGACGCAGGAAATA TG
T120A forward	GTACTGCTGGGGATCTCC**G**CCTCCGGTAACTCTGC
T120A reverse	GCAGAGTTACCGGAGG**C**GGAGATCCCCAGCAGTAC
D169N forward	CGCACTTTGGTTATGCC**AA**CCGCATTCAGGAGATTCAC
D169N reverse	GTGAATCTCCTGAATGCGG**TT**GGCATAACCAAAGTGCG
Q172E forward	CCGCACTTTGGTTATGCCGACCGCATT**G**AGGAGATTCAC
Q172E reverse	GTGAATCTCCT**C**AATGCGGTCGGCATAACCAAAGTGCGC
H180Q forward	GAGATTCACATTAAAGTGATCCA**G**ATCCTGATCCAGTTG
H180Q reverse	CAACTGGATCAGGAT**C**TGGATCACTTTAATGTGAATCTC
Vector	**Sequencing primer (5'-3')**
T7 forward	TAATACGACTCACTATAGGG
T7 reverse	GCTAGTTATTGCTCAGCGG
pBAD30 forward	CCTACCTGACGCTTTTTATCGC
pBAD30 reverse	GGGACCACCGCGCTACTGCCG

APPENDIX 2: Sedimentation equilibrium data for *E. coli* GmhA.
(A) Sedimentationequilibrium analyses for wild type (B) and D94N mutant proteins were consistent with both proteins existing as a tetramer in solution. Data was collected at protein concentrationscorresponding to A280 nm values of 0.1, 0.2, and 0.4 at speeds of 20 000 (1) and 25 000 (2) rpm.

Summary

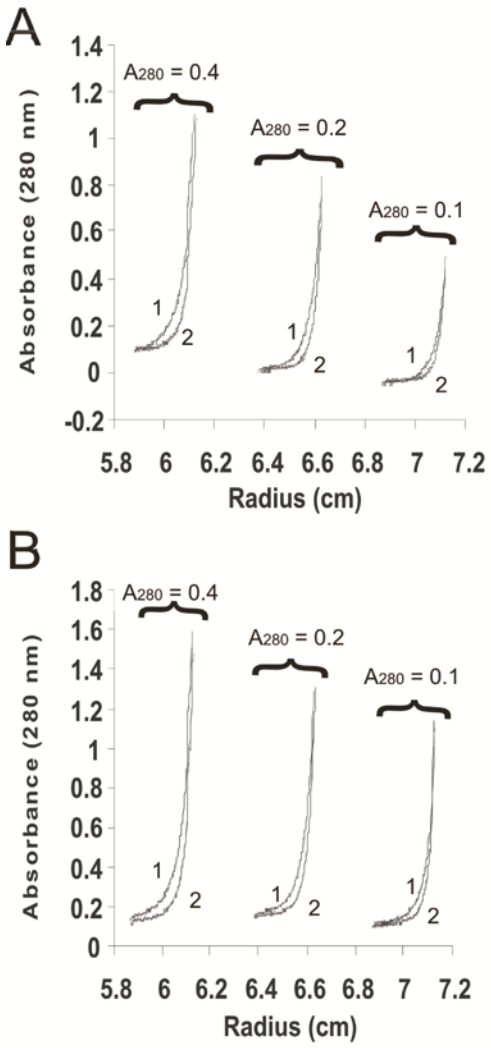

APPENDIX 3: Comparison of GmhA Apo structures from *E. coli* and *P. aeruginosa.* Apo_{EC} and Apo_{PA} are coloured gold and blue, respectively.

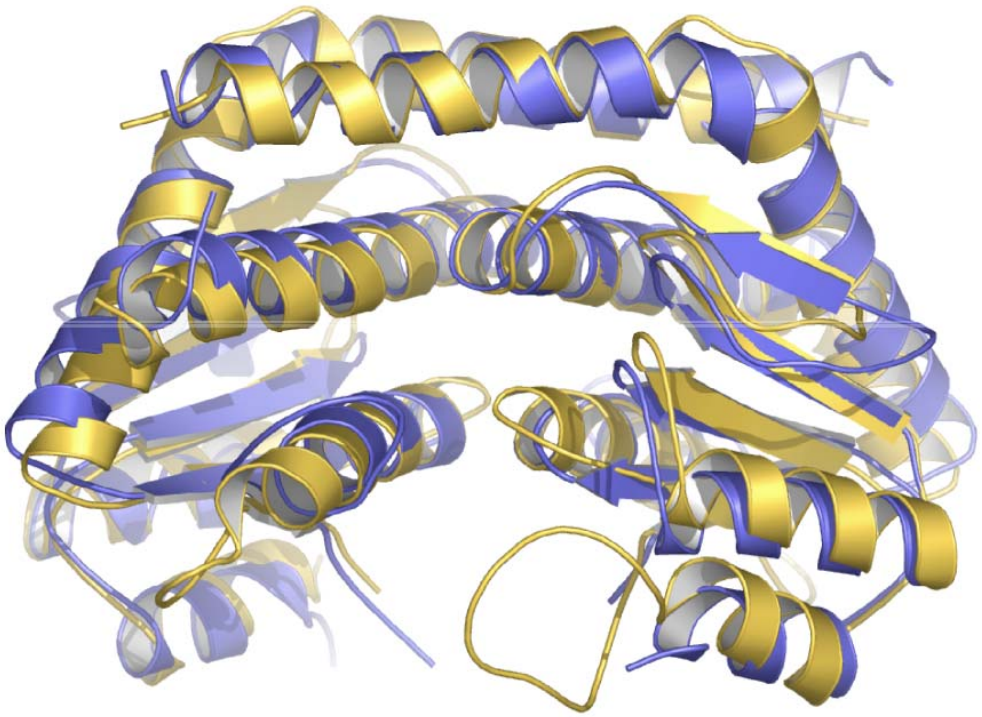

APPENDIX 4: Summary of *E. coli* GmhA mutations and residue-substrate contacts. Contact distances, listed in brackets, are given in Å. R69 and D94 make contact in the *P. aeruginosa* product bound structure only.

Residue	**Mutation**	**Protein Chain**	**Residue position involved in contact**	**Substrate atom involved in contact and distance (Å)**
H61	Q	A	ND1	O1 (2.56), O5 (3.7)
E65	N , Q	A	OE2	O1 (3.54)
R69	Q	A		
D94	N	B		
T120	A	D	OG1	O7 (3.65), O8 (2.53)
D169	N	D	OD1	O3 (3.13)
Q172	E	D	OE1	O2 (2.44)
H180	Q	A	NE2	O2 (2.7)

APPENDIX 5: Anti-histidine immunoblot comparing mutant GmhA expression.
PVDF membrane and anti-histidine immunoblot of *E. coli* BW25113Δ*gmhA* pBAD30*gmhA* mutant lysates, obtained from cultures grown in M9 minimal media and induced with 0.2 % arabinose. Membrane was stained with 0.2 % ponceau's solution in 1 % acetic acid and overlaid with blot photograph. Lysates from the following strains: 1 – BW25113pBAD30 (+ve control); 2 – BW25113Δ*gmhA*pBAD30 (-ve control); 3 – 12 are BW25113Δ*gmhA* pBAD30*gmhA* strain, with mutations as indicated: 3 - wild type; 4 – H61Q; 5 – E65N; 6 - E65Q; 7 – R69Q; 8 – D94N; 9 – T120A; 10 – D169N; 11 – Q172E; 12 – H180Q.

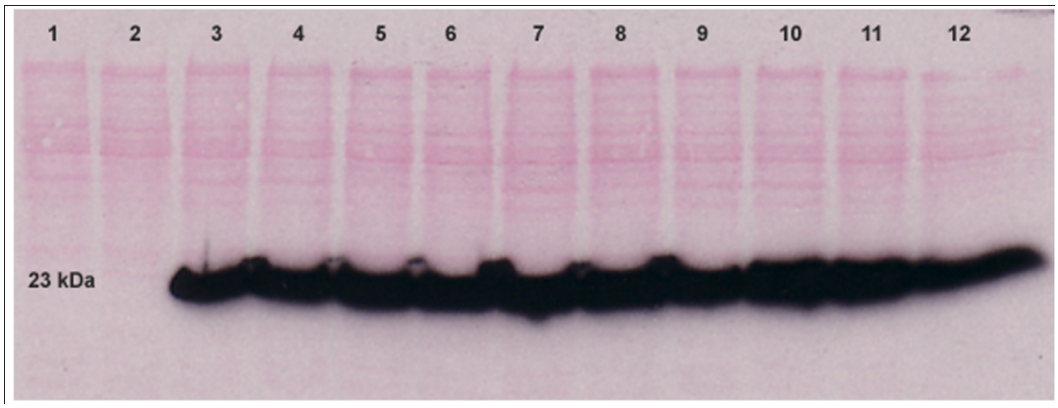

APPENDIX 6: Structural comparison of GmhA and the isomerase domain from glucosamine 6-phosphate synthase. (A) Quaternary structure comparison of GmhA substateEC (gold) and product-bound PA(blue) with the isomerase domain from glucosamine 6-phosphate synthase (purple). The isomerase domain from G6PS is comprised of dimer. Each monomer, however, is structurally equivalent to a dimer of GmhA. (B) Comparison of active site region. Ligands and interacting amino acids are shown in color corresponding to (A).

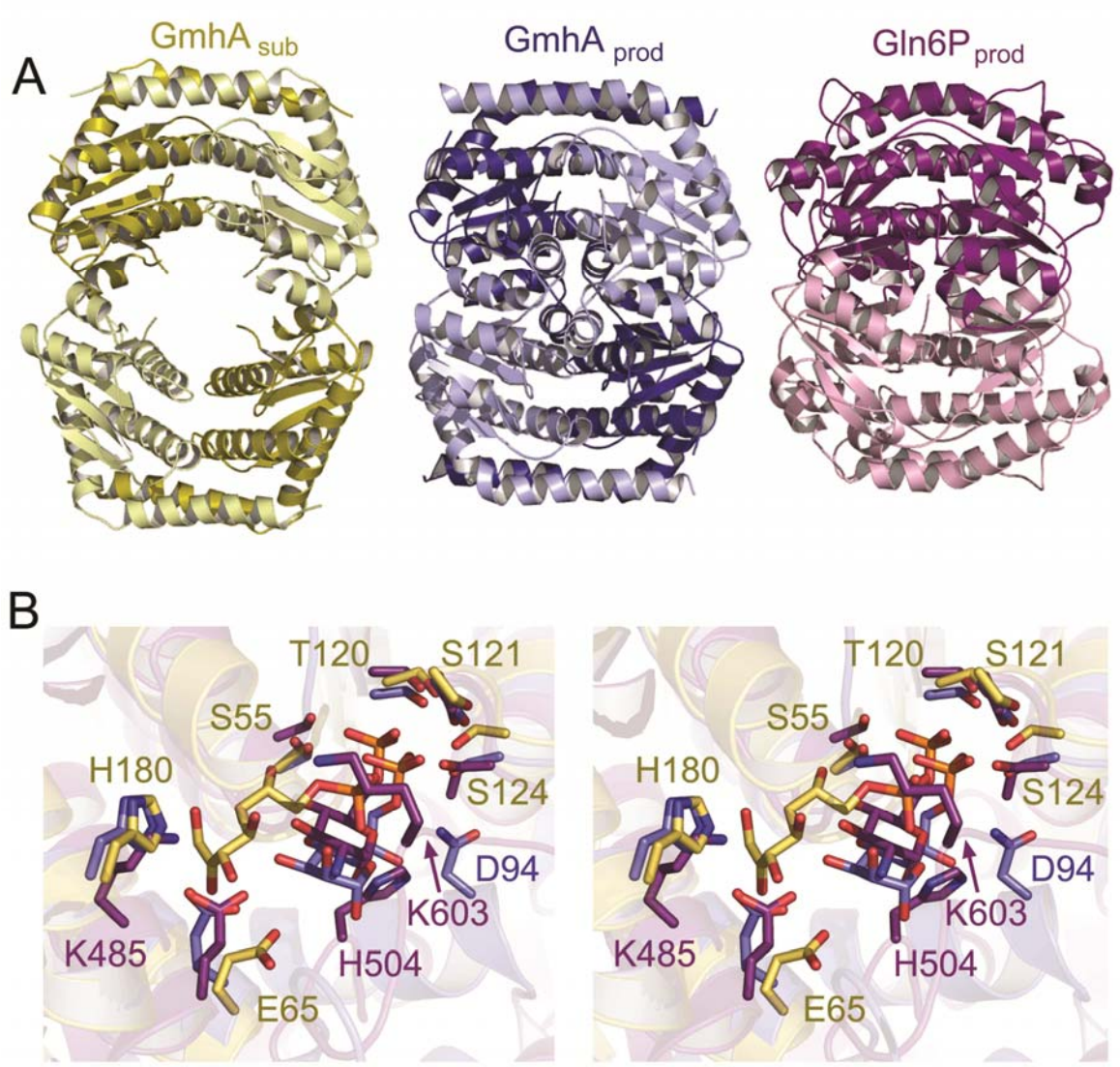

APPENDIX 7: GmhB mutagenesis and sequencing primers. Nucleotides in bold show location of point mutations. Underlined regions indicate codon that will be altered after mutagenesis.

Mutation	**5' Mutagenesis Primer 3'**
D11N forward	CCCGCAATTTTTCTT**A**ACCGTGATGGCACC
Reverse	GGTGCCATCACGGT**T**AAGAAAAATTGCGGG
D13N forward	CCCGCAATTTTTCTTGACCGT**A**ATGGCACC
Reverse	GGTGCCAT**T**ACGGTCAAGAAAAATTGCGGG
C107A forward	GAAGAGTTTCGCCAGGTC**GC**CGATTGCCGCAAACCACATC
Reverse	GATGTGGTTTGCGGCAATCG**GC**GACCTGGCGAAACTCTTC
K111A forward	CAG GTC TGC GAT TGC CGC **GC**A CCA CAT CCG GGG ATG
Reverse	CAT CCC CGG ATG TGG T**GC** GCG GCA ATC GCA GAC CTG
Vector	**Sequencing Primer**
pET28a(+) T7 forward	TAATACGACTCACTATAGGG
reverse	GCTAGTTATTGCTCAGCGG

APPENDIX 8: Structure-based sequence alignment of GmhB and HisB genes from various pathogens. Absolutely conserved residues are indicated by orange triangles; residues involved or predicted to be important for HisB and GmhB substrate interactions are indicated in green and blue triangles, respectively. Residues within the Zn^{2+} stabilized loop are underlined in black. Highly conserved residues are colored as follows: hydrophobic, yellow; negative charge, red; positive charge, blue; proline and glycine, green; threonine and serine, pink; cysteine, light brown; and glutamine and asparagine, purple.

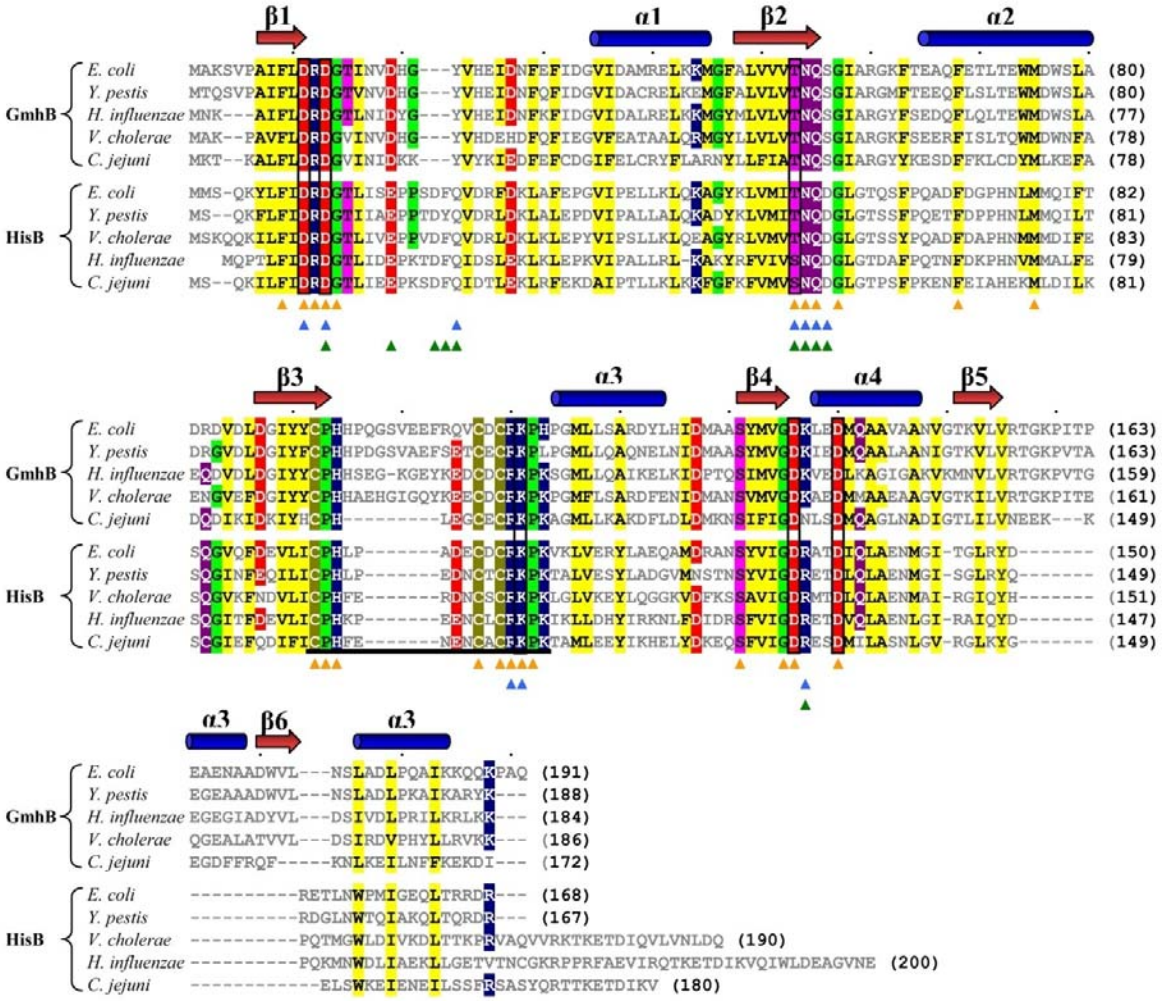

APPENDIX 9: Circular dichroism spectra of GmhB.
CD spectra of GmhB (▲) and GmhB C107A (○) was obtained at 25°, in 5 mM HEPES pH 8 + 5 % (v/v) glycerol. The wavelength scan was measured in mean residue ellipticity units ([θ_n]).

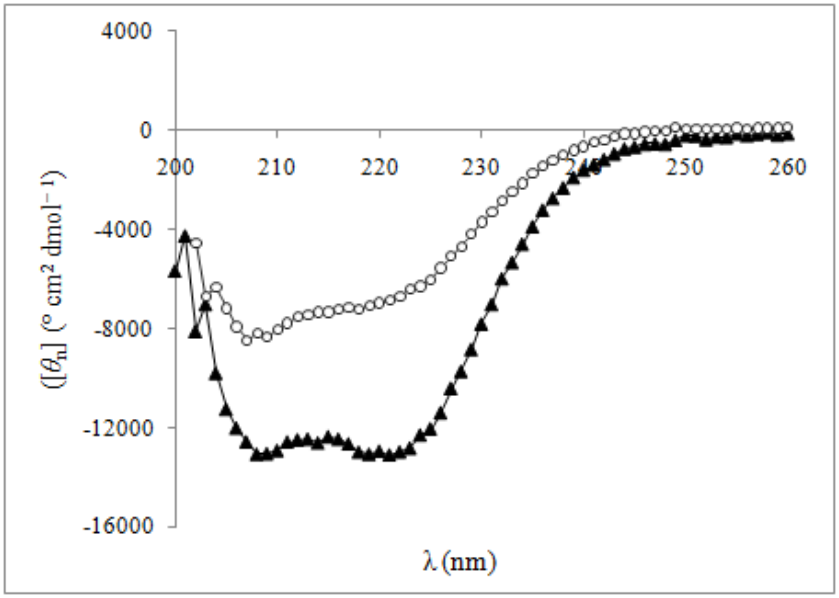

APPENDIX 10: Novobiocin MIC and LPS analysis of GmhB.
(A) Minimum concentration of novobiocin required to inhibit the growth of *E. coli* control strain (+ve control), *gmhA* deletion strain (-ve control), and *gmhB* deletion strains and *gmhB* complement strains (MIC). **(B)** LPS analysis of the above *E. coli* strains by silver stained 10 % SDS polyacrylamide gel electrophoresis. Bands were visualized by silver stain.